CRANFIELD UNIVERSITY

CHARLES HORACE CRAIG

ENHANCED RADIOPACITY AUSTENITIC STAINLESS STEEL FOIL

POSTGRADUATE MEDICAL SCHOOL

PhD THESIS

CRANFIELD UNIVERSITY

POSTGRADUATE MEDICAL SCHOOL

DEPARTMENT OF MATERIALS AND MEDICAL SCIENCES

PhD THESIS

Academic Year 2003-2004

Charles Horace Craig

Enhanced radiopacity austenitic stainless steel foil

Supervisors: Prof CM Friend: Dr MR Edwards

April 2004

ABSTRACT

Austenitic stainless steel designed for implant applications is used to fabricate balloon expandable coronary stents. The alloy was not designed for this purpose but has been found to work well except for relatively low radiopacity in the energy range used for stent deployment, typically 80kV to 100kV. Stents made of more dense elements such as tantalum exhibit high radiopacity in this energy range. Low radiopacity is due to a combination of tubular stents having a thin wall (strut) thickness (less than 0.13mm) and the alloy being comprised of low-density elements, approximately 2/3 iron and 1/3 chromium and nickel. To retain the desired thickness and increase radiopacity, alloy density may be increased by partial substitution with dense element(s). The new alloy must maintain the biocompatibility, corrosion resistance, non-ferromagnetic structure, strength, ductility, and fatigue- and fracture-resistant characteristics that made the original alloy attractive to stent designers. Coronary stents are subject to intensive review by regulatory authorities prior to being approved for human use, thus stent designers are hesitant to depart from accepted standards in selecting new alloys. Revising an existing alloy is the preferred approach to achieve subtle feature changes. A set of criteria was set that maintained chromium, nickel, and molybdenum within prescribed compositional ranges and diminished iron to its minimum level, allowing platinum to be substituted for approximately 1/3 the total elemental weight (wt%). Above 20wt% platinum, undesirable precipitates were found. An alloy containing 20wt% platinum, in the form of foil and at a thickness of 0.127mm, was found to be free of precipitates not found in the base or original alloy and to provide approximately 20% radiopacity increase at 80kV and 15% radiopacity increase at 100kV, exceeding minimum programme goals at 80kV and equaling those at 100kV.

ACKNOWLEDGEMENTS

This research was carried out while an employee of Boston Scientific Corporation's (BSC's) Cardiovascular Group and of Interventional Technologies, Incorporated (IVT), (acquired by BSC in 2001). Thanks go to Dr. Robert Reiss (IVT) and Mr. Matthew Jenusaitis (BSC) for their support of this research, which began in July, 2000. The idea for alloying austenitic stainless steel for fabrication of enhanced radiopacity coronary stents was jointly developed with the writer's supervisor, Mr. Herbert Radisch, Jr., and with Dr. Thomas Trozera, P.E. (consulting engineer). Support in alloy and radiographic development was provided by Mr. Edward Vesely, Jr. and his team at United States Department of Defence's Advanced Materials and Processes Technology Information Analysis Centre. Support in alloy development was provided by: Mr. Paul Turner and his team at United States Department of Energy's Albany Research Centre; Mr. John McEwan and his team at South Africa's Ministry of Minerals and Energy's Mintek research facility. Support in radiographic development was provided by: Mr. Keith Ingram, Centre for Radiographic and Medical Studies, Department of Materials and Medical Sciences, Cranfield University; Mr. Harold Berger and his team at Industrial Quality, Incorporated; Mr. Michael May and his team at Decisive Testing, Incorporated. For serving as academic advisors while studying at George Mason University: Professor Joseph Lieb and Dr. Peter Ceperley, College of Arts and Sciences; Dean *Emeritus* Gustavo Mellander, Graduate School of Education. For serving as academic advisors at Cranfield Postgraduate Medical School: Professor Clifford Friend and Dr. Michael Edwards. For serving as external advisors: Mr. Herbert Radisch, Jr., and Dr. Nev Gokcen. Finally, the writer thanks his wife, Margaret Essig Craig, for her continued love and support for some 27 years, especially during the initial years of postgraduate study at Brunel University, shortly after their marriage, then at Cranfield University, and more recently continued at George Mason University and at Cranfield University, which together has provided an opportunity for and has culminated in this research.

DEDICATION

The writer dedicates this research to the memory of his mother, Edith Freeman Craig, whose premature death due to cardiovascular disease silenced forever her golden voice.

List of contents

List of tables

List of figures

Chapter 1
INTRODUCTION

1.1 Background

Diseases of the heart and circulatory system, or cardiovascular disease, are the leading cause of death in the United Kingdom and also in the United States, where cultures are similar; over one in three deaths (40% and 39%, respectively) are caused by this disease (Petersen *et al*, 2003; American Heart Association, 2003). With a population of almost 60 million, 240,000 died in the United Kingdom in 2001 due to this disease; in the United States, with a population 4.7 times greater, 945,000 died. Over 50% of all cardiovascular deaths in these two nations are due to coronary artery disease. Table 1 shows that while these figures are less than in several nations, they also are more than in some others; miscoding of cause of death, e.g., in Japan, may account for variations of up to 30% in Table 1 data (Lozano *et al*, 2001).

Table 1 Death rates from coronary artery disease for men (left) and women (right) aged 35-74 (1998)(Petersen *et al*, 2003)

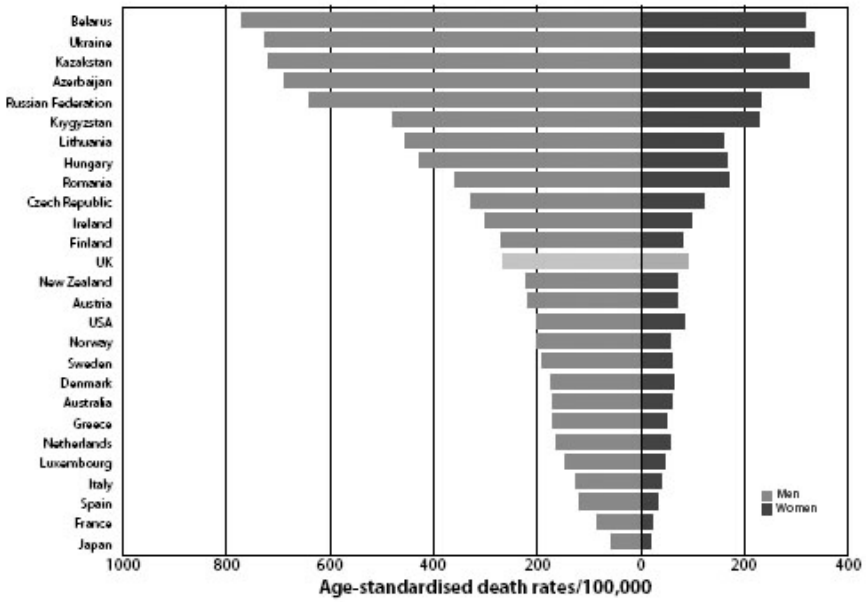

Through the World Health Organisation, governments of most nations are aware of the underlying causes of coronary artery disease. In the United Kingdom, there is a concerted effort, led by government agencies, to reduce the toll of what are known as premature deaths, i.e., deaths of persons under the age of 75 years. Table 2 shows the results achieved since 1970 and the goals for continued reductions in premature deaths.

Table 2 Long-term goals and achievements of a government-led programme in the United Kingdom to reduce deaths by coronary artery disease (Petersen *et al*, 2003)

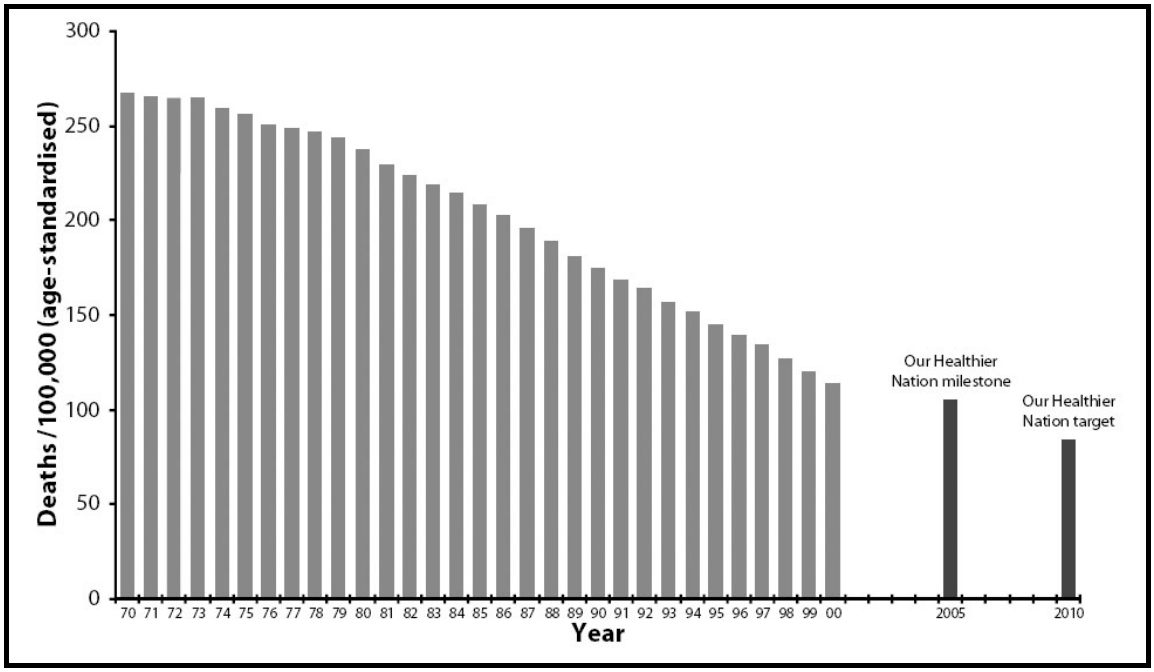

The battle against needless loss of life due to coronary artery disease is fought in many quarters and by persons of many and varied skills. Cardiologists are assisted by other medical specialists, including medical physicists and radiologists, who aid in presenting and interpreting radiographic images, for instance. These images allow visualising the beating human heart to facilitate diagnoses and to aid in its repair. In attendance also are scientists, engineers, designers and fabricators of medical devices, integral team members in identifying or responding to needs for new or improved tools.

1.2 Emergence of radiographically-aided methods of vascular medicine

1.2.1 Angiography

In experiments with the Hittorf-Crooks tube in 1895, Roentgen discovered ionising electromagnetic radiation, later described as Roentgen or x-rays. Within a few weeks, Roentgen used x-rays to produce a 'photograph' of his wife's hand (Abrams, 1997). Also within a few weeks of Roentgen's discovery, Abrams noted, a 'roentgenogram' of an amputated hand was described, which showed that Roentgen's technique could be used to visualise the vascular bed when injected with a contrast agent (e.g., iodine, which, like barium, has a high x-ray absorption coefficient, making it 'radiopaque'). After initial applications only to the study of cadavers, such techniques were applied to patients as a medical diagnostic tool that subsequently became known as angiography.

The emergence of angiography, which began with studies to understand the human vascular system, eventually, according to Abrams, led to angiographic techniques that included studies of the heart. Cope and Baum (1997) noted that angiography requires the use of a catheter and a guidewire to deliver a radiopaque contrast agent to the site being diagnosed to achieve good definition of the 'luminal surface' of the blood vessel. Bettman (1997a) summarised the history and chemistry of contrast agents for angiography and the adverse reactions these may cause; he noted (1997b) that use of iodinated radiopaque contrast agents was preferred for most angiographic applications.

1.2.2 Angioplasty

Becker and Waller (1997) described Gruentzig's balloon angioplasty procedure (or 'intervention'), *circa* 1978, which was used to enlarge a diseased lumen and improve flow beyond the lesion. This was based on the Dotter-Judkins method (Dotter and Judkins, 1964), which used coaxial dilators, whilst continually visualising the

intervention angiographically. The term that emerged to describe such interventions was percutaneous transluminal angioplasty; however, for treatment of coronary artery disease, a complementary term emerged to describe such interventions: percutaneous transluminal coronary angioplasty. Becker and Waller noted that between 1980 and 1987 much research was conducted on the effects of both percutaneous transluminal angioplasty and percutaneous transluminal coronary angioplasty. Myler (1997) has provided an historical perspective on percutaneous transluminal angioplasty (which he simplified to 'peripheral angioplasty') and percutaneous transluminal coronary angioplasty (simplified to 'coronary angioplasty'), noting the 1956 Nobel Prize in Medicine went to Cournand, Forssmann, and Richards for discovery of cardiac catheters and the application of catheterisation to cause pathological change in vascular systems.

Figure 1 shows a typical basic angioplasty equipment and setup. At the centre of

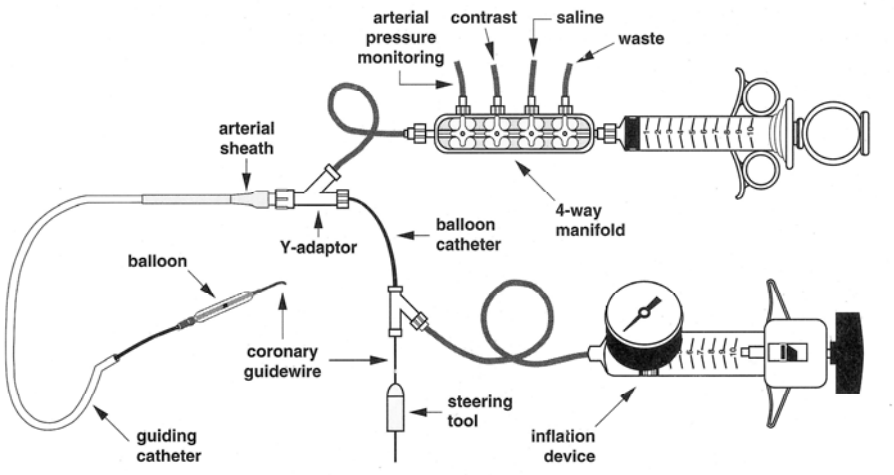

Figure 1 Basic angioplasty equipment and setup (Safian, 1997)

the diagram are two adaptors, typically termed 'Y sites', one horizontal and one vertical. To the left of the horizontal Y site in this diagram are the arterial sheath, guiding catheter and the dilation balloon. The coronary guidewire protruding from the guiding

catheter just beyond the dilation balloon can be seen traversing the two Y sites, ending in a manually-operated steering tool. At the juncture of the horizontal Y site and to the top right can be seen the hand-held manipulator and four-way manifold that is used to inject radiopaque contrast agent or saline solution, monitor blood pressure, and allow for the escape of waste fluids. To the right of the vertical Y site is the inflation tool used to pressurise the dilation balloon.

As summarized by Becker and Waller (1997), various pathophysiologic mechanisms were revealed by use of peripheral angioplasty and coronary angioplasty. The primary concerns that resulted from such use were fracture of the plaque that was the source of the constriction in the blood vessel, and how that fracture manifested itself during the subsequent weeks or months. It was found that while fracture was necessary there was the possibility of too much fracture, termed 'over-injury', which might result in restenosis, which these authors described as regrowth or occlusion in the area where compressional methods were applied to the lumen (from within). Becker and Waller have indicated they consider restenosis to be the principal negative after-effect from the application of either peripheral angioplasty or coronary angioplasty.

1.2.3 Stents

A stent, named after medical devices pioneered by a British family of dentists by that name and re-applied during the past two decades, is a cylindrical device intended to provide mechanical support radially to weak or diseased blood vessels in order that vessel patency is enhanced. Balcon *et* al (1997) and Wong and Schatz (1993) described the history of stent development, noting the term 'stent' was based on work of the 19th century dentist Charles Stent and his two sons, also dentists, who developed a dental apparatus to support misaligned teeth; the term was subsequently applied to any medical

device that supported a body cavity during surgical procedures for skin grafting. According to Balcon *et al*, Charles Dotter, an interventional radiologist, appeared to have used the term 'stent' first for a vascular implant when he reported an early application (Dotter, 1969). Dotter is sometimes referred to as the 'father' of stenting.

The first coronary stent was implanted in a human body in 1986 by Puel, in France (Rousseau *et al,* 1987; Sigwart *et al*, 1987). Figure 2 shows this self-expanding mesh stent, Boston Scientific Corporation's Wallstent®. Originally made of stainless steel, it is made from a cobalt-based alloy wire with a platinum core for enhanced radiopacity. Three views of the Wallstent® are shown in Figure 2 as (a) it is initially mounted on the delivery device, (b) it is partially deployed as the stent begins to expand on being released from its sheath, and (c) it is fully deployed or implanted within the artery.

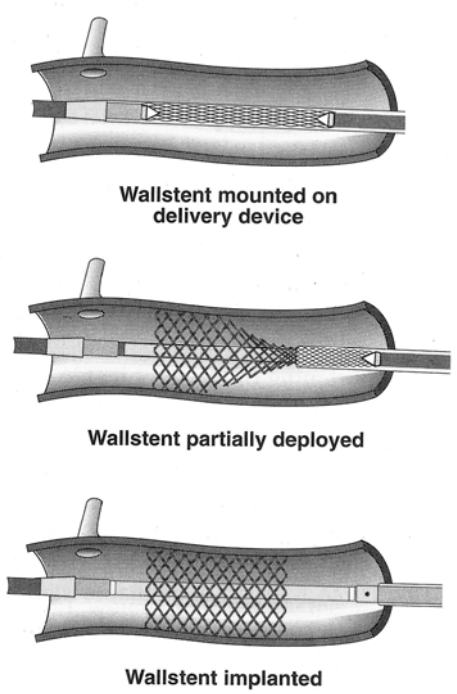

Figure 2 Self-expanding Wallstent® deployment (Safian, 1997)

A first balloon-expandable stent was described by Palmaz *et al* (1985); Figure 3 shows profiles of the undeployed and deployed austenitic stainless steel mesh stent and

part of the deployment apparatus. In Figure 3(a) a section of the compressed stent is portrayed; in Figure 3(b) a comparable section of the fully-expanded (deployed) stent is portrayed. Figure 3(c) portrays the stent mounted on its dilation balloon, along with its guiding catheter and guidewire, here described in a more detailed view as 'leading and trailing retainers'; Figure 3(d) provides a similar view for the deployed stent as it would appear on a fully-inflated dilation balloon.

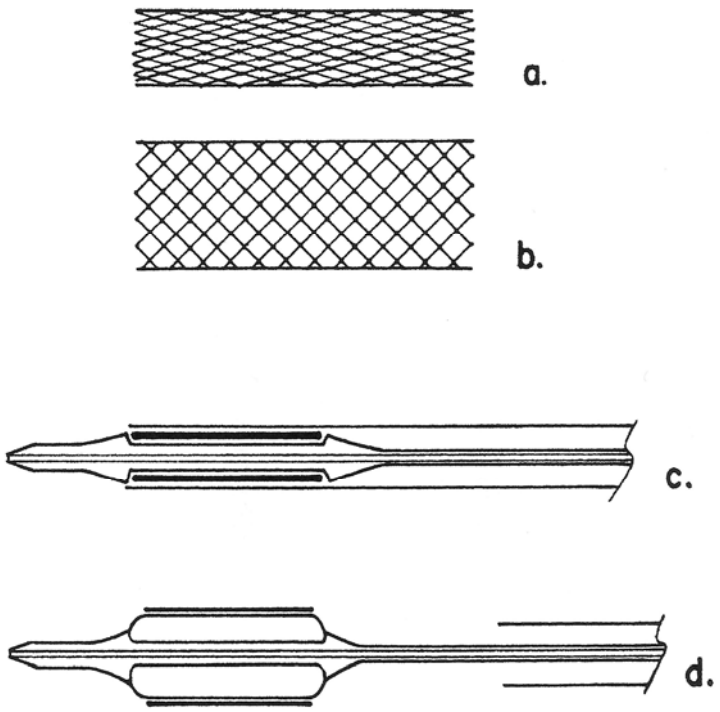

Figure 3 Profile of balloon-expanding Palmaz stent (a) undeployed and (b) deployed; profile of (c) undeployed and (d) deployed Palmaz stent as mounted on balloon along with its leading and trailing retainers (Kutryk and Serruys, 1999)

It was not until the mid-1990s that, according to Balcon *et al* (1997) and Kutryk and Serruys (1999a), results of stents, as compared to results from angioplasty, indicated that stents decreased restenosis and improved patient outcomes. Becker and Waller (1997) noted that in three month follow-up angiograms, use of vascular stents resulted in a greater lumen diameter, even with the onset of restenosis. Kutryk and Serruys

(1999b) have argued that coronary stents may be the most important advance in the field of cardiology since the introduction of coronary angioplasty. The extensive literature reviewed by Balcon *et al* (1997) describes the emergence of a new and important technology that was almost lost because of a misunderstanding of outcomes of early trials and because of an editorial that sensationalised the negative results from the trials.

As inferred above, stents are extremely simple mechanical devices designed to open closed or restricted arteries and keep them from closing again. Stents act as a cylindrical scaffold once they are in place and expanded, or deployed, to the required diameter. Stents may be used in the arteries of the heart, where they are referred to as 'coronary' devices, or elsewhere, where they are referred to as 'peripheral' devices.

A coronary stent is permanently implanted in the native or grafted vasculature of the heart in an attempt to return the flow of blood in an artery to its normal rate at the lesion where the stent is deployed. Such interventions are conducted by an interventional radiologist or an interventional cardiologist; the term 'interventionalist' is often used. Use of stents allows cardiologists to make this intervention in a manner that may obviate the need for performing open heart surgery. Open heart surgery places the patient at greater risk and may subject him to discomfort and to a lengthy hospital stay.

Coronary stents are meant to fit neatly inside the blood vessels as they traverse the sometimes tortuous paths to the desired location. The interventionalist would insert a catheter by inserting a stent, located on a guiding catheter similar to that used for angioplasty, into a blood vessel through the patient's groin and manoeuvre the stent into an appropriate point in his heart and then into a clogged portion of the artery. In either mesh or mesh-like geometries, the stents are initially collapsed, which minimises the diameter and provides flexibility to the interventionalist in negotiating complex

pathways into and through myriad vascular branches within the heart and then to the site of a weakened or diseased coronary artery.

Once at the desired location, either a sheath is removed to allow a self-expanding stent to open or a dilation balloon is inflated via access through the guiding catheter. The mesh or mesh-like geometry of the stent then opens or expands, taking advantage of both the ductility of the metal or alloy selected and a relatively weak structure caused by the finely woven wires of a mesh or their equivalent, struts (when made from tubes). After the stent has been deployed to the desired diameter it retains sufficient strength as a tubular structure to withstand the radial forces on it and maintain its shape without collapsing.

A stent working group report on coronary circulation (Balcon *et al,* 1997) provided a list of tests the group determined both stents and stent materials should be subjected to. For stents, the list included (a) radial strength, (b) fatigue testing, (c) elastic recoil, (d) Magnetic Resonance Imaging testing, (e) expansion (by plastic deformation), and (f) surface characteristics. For stent materials, the list included (a) material analysis, (b) mechanical properties testing, and (c) corrosion testing. Table 3 provides a list of self-expanding and balloon-expandable coronary stents proposed or available for use in Europe *circa* 1997 (Balcon *et al,* 1997).

Table 3 Stents proposed for implantation in Europe *circa* 1997 (Balcon *et al*, 1997)

Stent	Company	Metal	Design	Expanded metallic surface (%)
(A) Self-expanding stents				
Angiomed	Bard	nitinol	wire braid	16–29%
Cardiocoil	In-stent Medtronic	nitinol	spiral coil	8–15%
Radius	Scimed	nitinol	slotted tube, zig-zag design	20%
Wallstent	Schneider	cobalt alloy, platinum core	wire mesh	±15%
(B) Balloon expandable stents				
Act-one	ACT	nitinol	slotted tube	20–25%
Angiostent	Angiodynamics	platinum-iridium	sinusoidal single wire coil, longitudinal spine	9–12%
be-Stent	In-stent Medtronic	stainless steel	slotted tube, serpentine mesh, rotating junctions	11–18%
BioDiv Ysio	Biocompatibles	stainless steel	slotted tube, phosphoryl-choline coating	NA
Cordis	Cordis	tantalum	single helical coil	18%
Cross-flex	Cordis	stainless steel	single helical coil	15%
Crown	JJIS	stainless steel	slotted tube, sinusoidal slot	<20%
Freedom	Global Therapeutics	stainless steel	fishbone, single round wire	11–15%
Gianturco-Roubin II	Cook	stainless steel	flexible coil, single flat wire, longitudinal spine	15–20%
Jo-med	Devon	stainless steel	slotted tube, cellular mesh	NA
Microstent GFX	AVE	stainless steel	connected zig-zag wires, 2 mm long modules	8·5%
Multilink	Guidant-ACS	stainless steel	multiple rings	15%
NIR NIR Royal	Medinol-Scimed	stainless steel gold plated	Multicellular	14–19%
Palmaz-Schatz	JJIS	stainless steel	slotted tube, spiral articulation	<20%
STS	De Scheerder	stainless steel	helical coil	5–15%
Tensum	Biotronik	silicon carbide coated tantalum	slotted tube, 2 articulations	13%
Wiktor-GX	Medtronic	tantalum	helical coil,	7–10%
Wiktor-i	Medtronic	tantalum	single wire	8–9·5%
X-Trode	Bard	stainless steel	connected round wires, longitudinal spine	16–19%

*Several stents are available with heparin coating. Further technical details are available elsewhere[50].

Serruys (1997) carried reviews by various authors of a total of 21 stents in his initial stent 'handbook' (currently in its 4th edition, Serruys and Rensing, 2001). In both these reports, well over half of the balloon-expandable stents were made of stainless steel, while the remaining stents were comprised of a variety of metals, e.g., single elements (tantalum), binary alloys (platinum-iridium; nickel-titanium), and composites (cobalt alloy with platinum core). The stainless steel chosen for the stents reviewed by Balcon *et al* was not reported, but in all cases reported by Serruys (1997), the alloy was a variant of an implant-grade molybdenum-containing austenitic stainless steel, which has a long history of use within the human body. This is because this implant-grade alloy has good biocompatibility, corrosion and pitting resistance, strength and ductility, and, particularly important with coronary stents, it is not ferromagnetic. As noted by Balcon

et al, there is concern about exposure to magnetic resonance imaging. More recently, with the advent of magnetic resonance angiography, remnant ferromagnetism is of concern since high strength magnetic resonance imaging and magnetic resonance angiography fields may displace or remove a deployed coronary stent.

As with contrast agents, the radiopacity of a stent is dependent upon the x-ray mass attenuation coefficient of the element or elements the stent is made from, the density of the element or elements it is made from, and the strut thickness. However, as stents are made thinner they become increasingly less radiopaque and thus less visible radiologically to the interventionalist. As strut size is decreased to make the stent more flexible and more capable of being used in smaller vessels and through more tortuous paths, it becomes a matter of assuring not just flexibility but that sufficient structural strength exists to prevent collapse of the stent under load.

The single through-wall (strut) thickness of the stainless steel stents described in Serruys (1997) varied from a low of approximately 0.070 mm to a high of approximately 0.200 mm. Thus the optimum thickness, from a mechanical point of view, may be about 0.070 mm or, possibly, even less. Extremely thin stainless steel stents are quite difficult to visualise whilst being deployed, most often requiring use of radiopaque markers on the balloons or on the stents themselves. Finding such thin stents after deployment is of concern, as well, since periodic checks are made, particularly in the early weeks after the stent deployment, to be sure it had not somehow moved to another location, leaving the diseased vessel without the required assistance provided by the deployed stent.

1.3 Problem

The interventionalist must be able to visualise continually the stent and its surroundings via real-time radiology both whilst it is being deployed and subsequently. In addition to the radiopaque contrast agent, the interventionalist is often aided by radiopaque marker bands on the dilation balloon that effectively allows the location of the two ends of the stent to be determined; these thin marker bands are typically made of Period 6 elements such as tantalum, platinum, or gold, which have high x-ray mass attenuation coefficients at the x-ray energies typically used and also are quite dense. The stent itself is often invisible or nearly so due to a combination of factors. These factors include: the absorption coefficients and densities of the elements comprising the stent and the surrounding tissue and bone, the thickness of the stent (i.e., wire or strut size) and those of its surroundings, as well as the ability of the x-ray imaging system to detect the transmitted photons and present an image of the stent and its surroundings to the interventionalist. From time to time, the area being imaged may be flooded with a contrast agent to aid in stent visualisation but, as with the radiopaque markers on the dilation balloon, this only occurs during the initial stent deployment stage. If it is necessary to review the condition of the deployed stent or to return to the site of the deployed stent at some later time to either cross over or deploy another stent, it is important to the interventionalist that the precise location and condition of any previously deployed stents be fully determined before attempting such procedures.

Since the tortuous path involved in deploying a stent demands the ultimate in flexibility, the thin structure of the stent must remain largely as presently designed and in effect only the densities and absorption coefficients of the elements used to make the stent lend themselves to change. While stents made from both nickel-titanium shape

memory alloys (typically used for self-expandable stents) and austenitic stainless steels (typically used for balloon-expandable stents) could benefit from increased densities and x-ray absorption coefficients, only austenitic stainless steel will be considered here since the two alloys differ radically in chemical composition and since sponsorship for this research was principally in support of development of new stainless steel stents.

The problem to be addressed, then, is that implant grade austenitic stainless steel, when used as a coronary stent, does not exhibit sufficient radiopacity to allow the stent to be optimally visualised either during or after deployment. The principal elements of austenitic stainless steels are iron, chromium, and nickel, all of which are located in Period 4 of the periodic table of the elements and thus substantially less dense and with much lower x-ray absorption coefficients than, e.g., the elements used for radiopaque markers (tantalum, platinum, or gold). From this analysis, it is clear that the poor radiopacity of stents made from austenitic stainless steel is due to thin sections (struts), to being comprised of low density elements, and to low x-ray absorption coefficients.

1.4 Administrative and economic concerns

The radiopacity of those few austenitic stainless steels that are commercially available for use as surgical implants is not a consideration in most applications of such alloys. Coronary stents are an exception to this rule because their mass is quite small, they are to be embedded in the arteries of the human heart within a closed chest cavity, and the interventional cardiologist treating the patient desires to use radiographic imaging to visualise the area of the diseased artery in need of repair whilst visualising the stent somewhat as a phantom, which should be seen without obscuring the interventionalist's view of the diseased artery. Alternative materials such as the nickel-titanium shape memory alloys are somewhat less radiopaque than stainless steels, while

other alternatives such as tantalum may be overly radiopaque for such an application. Fabrication of stents from composites of radiopaque elements sandwiched in or on alloys made of less-radiopaque elements may create additional design and processing difficulties, e.g., radiopaque coatings tend to be brittle and may spall off when balloon-expandable coronary stents are plastically deformed, as they must be once they are located in the portion of the diseased artery in need of bridging or shoring up in deploying the stent. Radiopaque wires, such as are created by inserting platinum wire in tubes and the two drawn to create a more radiopaque wire, are best for woven stents.

In critical applications of structural alloys where human lives may be endangered, regulatory bodies typically exist, often implementing their own or consensus standards that reflect attempts by both the regulated industry and the regulatory body to support the needs of the application by developing alloy specifications that meet most needs. Subsequent tailoring of a standard alloy to unique needs such as increased radiopacity may depart from the standards and require the proposed user to approach the regulatory body for approval prior to implementing use of the revised alloy in critical applications.

Taking a first-principles approach to designing and developing a radiopaque alloy that also meets the accepted standard for austenitic stainless steel for surgical implants would be an arduous undertaking for a person or entity representing user organisations such as coronary stent designers or fabricators. The emphasis within alloy research and development organisations for such efforts is typically for critical applications where the expected sales volume of the resulting product is sufficient to justify the investment. With the minimal amount of material currently used in manufacture of coronary stents, approximately 0.8 mg/mm of length, as compared, e.g., to hip and knee replacements,

the stent industry has been largely left on its own to devise solutions to the problem of poor radiopacity upon choosing austenitic stainless steel, the issue being addressed here.

Tailoring an existing implant-grade austenitic stainless steel to improve radiopacity while maintaining adherence to the published specifications accepted by the regulatory bodies would be the ideal solution, it would appear. However, the difficulty with such an approach is that the specifications are typically written in such a manner as to prevent the addition of unspecified additional elements, thus causing the alloy to be considered non-compliant. However, submitting details of the modification with its performance characteristics to the regulatory body to gain approval for use may be the solution that has the most near-term viability in addressing the radiopacity problem.

In addition to the important economic and administrative problems that set the scene for a technical solution to a radiopacity problem with implant-grade austenitic stainless steels, defined above, there are technical issues to be addressed. One of the most critical issues is maintaining a non-magnetic alloy because of the dangers inherent in utilising ferromagnetic materials as implants when potentially within the strong fields of magnetic resonance imaging or magnetic resonance angioplasty systems; the risk to the patient is great if the coronary stent shifts or is removed, which could occur if the alloy is not substantially free of ferromagnetic phases at the temperature of the human body. A second issue is multi-pronged but essentially reduces to one of corrosion of the alloy within the environment of the body and one of biocompatibility of the resulting alloy. Many other issues abound; these include strength and ductility and freedom from the deleterious phases and compounds that may change fracture or fatigue characteristics. These issues can be addressed in part by the administrative approach outlined above,

addressing the changes required to increase alloy radiopacity within the context of the very criteria that was applied in developing compliant alloys.

1.5 Objectives

The intrinsic features of the implant grade austenitic stainless steel, e.g., its biocompatibility, corrosion resistance, strength, ductility, and relative freedom from deleterious phases that might contribute to fracture or fatigue failures are such that it is considered quite desirable by stent designers to maintain those features largely as they are. Because of this, only those modifications are considered that affect an increase in overall alloy density and concurrent increase in x-ray absorption coefficient that in turn will lead to the fabrication of a more radiopaque austenitic stainless steel coronary stent.

The approach taken is to add a single high-atomic-number element to a commercially-available implant grade austenitic stainless steel to increase overall alloy density and x-ray absorption coefficient of the resultant enhanced-radiopacity alloy. This is meant to ensure the desirable features of implant grade alloy are retained, to the maximum degree possible, and also that established specification guidelines are met as much as possible; this allows delays in developing, testing, and manufacturing a new or modified alloy to be minimised and, possibly, a shortening of the review and acceptance process of such a new or modified alloy as demanded by regulatory bodies.

The objective is to develop an enhanced radiopacity austenitic stainless steel stent that is approximately 15% greater in radiopacity at 80kV and 100kV radiation than the standard implant grade stainless steel being used for manufacture of coronary stents in the United Kingdom and the United States.

The goal, in short, is to complete the initial proof-of-concept phase required to provide stent designers an austenitic stainless steel that may be viewed as largely

unchanged except that it provides substantially enhanced radiopacity as made into a coronary stent.

1.6 Thesis structure

Chapter 2 is a somewhat more detailed continuation of this introductory chapter, in order for the reader to understand the requirement for, evolution and application of coronary stents made of implant grade austenitic stainless steel. Chapter 3 is focussed on the alloy development process and on both the calculation and quantitative determination of radiopacities. Chapter 4 is focussed on applying the underlying theories and requirements described in Chapter 3 through experimentation to gain results necessary to prove or bring about the required changes described in Chapter 3. Chapter 5 discusses these results, and is followed by Chapter 6, in which conclusions are drawn from the results obtained and recommendations are made as to further work.

1.7 References

American Heart Association. (2003). *Heart disease and stroke statistics – 2003 update.* Dallas, Texas: American Heart Association.

Abrams, HL. (1997). Historical notes. In: Baum, S., and Pentecost, MJ. (eds). *Abrams' angiography: vascular and interventional radiology. (*4th ed). Pages 3-12. New York: Little, Brown.

Balcon, R. (1997), Beyar, R., Chierchia, S., De Scheerder, I., Hugenholtz, PG., Kiemeneij, F., Meier, B., Meyer, J., Monassier, JP., and Wijns, W. Recommendations on stent manufacture, implantation and utilization. *European Heart Journal.* Vol 18. Pages 1536-1547.

Becker, GJ. (1997) and Waller, BF. Mechanisms of balloon angioplasty and restenosis. In: Baum, S., and Pentecost, MJ. (eds). *Abrams' angioplasty: interventional radiology*. (4th ed). Pages 3-23. New York: Little, Brown.

Bettman, MA. (1997a). Radiographic contrast agents: history, chemistry, and variety. In: Baum, S., and Pentecost, MJ. (eds). *Abrams' angiography: vascular and interventional radiology.* (4th ed). Pages 12-21. New York: Little, Brown.

Bettman, MA. (1997b). Physiologic effects and systemic reactions. In: Baum, S., and Pentecost, MJ. (eds). *Abrams' angiography: vascular and interventional radiology* (4th ed). Pages 22-33. New York: Little, Brown.

Cope, C. (1997) and Baum, S. Catheters, methods, and injectors for superselective catheterization. In: Baum, S., and Pentecost, MJ. (eds). *Abrams' angiography: vascular and interventional radiology.* (4th ed). Pages 155-175. New York: Little, Brown.

Dotter, CT. (1964) and Judkins, MP. Transluminal treatment of arteriosclerotic obstructions: description of a new technic and a preliminary report of its application. *Circulation.* Vol 30. Pages 654-670.

Dotter, CT. (1969). Transluminally-placed coilspring endarterial tube grafts: long-term patency in canine popliteal artery. *Investigative Radiology.* Vol 4. Pages 327-322.

Kutryk, MJB. (1999a) and Serruys, PW. Stents: the menu. In: Topol, EJ. (ed). *Textbook of interventional cardiology.* (3rd ed). Pages 533-585. Philadelphia: WB. Saunders.

Kutryk, MJB. (1999b) and Serruys, PW. *Coronary Stenting: Current Perspectives*. Pages 1-15. London: Martin Dunitz.. ISBN: 1-85317-693-1

Lozano, R. (2001), Murray, CJL., Lopez, AD., and Satoh, T. *Miscoding or misclassification of ischaemic heart disease mortality. Global programme on evidence for health policy working paper no. 12.* New York: World Health Organisation. URL: http://www3.who.int/whosis/discussion_papers/pdf/paper12.pdf

Myler, RK. (1997). Coronary and peripheral angioplasty: historical perspective. In: Topol, EJ. (ed). *Textbook of interventional cardiology.* (3rd ed). Pages 127-146. Philadelphia: WB. Saunders.

Palmaz, JC. (1985), Sibbitt, RR., Reuter, SR, Tio, FO., and Rice, WJ. Expandable intraluminal graft: a preliminary study. *Radiology.* Vol 156. Pages 63-77.

Petersen, S. (2003), Rayner, M., and Peto, V. Chapter 1: Mortality. *Coronary Heart Disease Statistics.* London: British Heart Foundation. URL:http://www.heartstats.org

Rousseau, H. (1987), Puel, J., Joffre, F., Sigwart, U., Duboucher, C., and Imbert, C. Self-expanding endovascular prosthesis: an experimental study. *Radiology.* Vol 164. Pages 709-714.

Safian, RD. (1997). Coronary intervention: preparation, equipment & technique. In: Freed, M., Grines, C., and Safian, RD. (eds). *The new manual of interventional cardiology.* Pages 1-63. Birmingham, Michigan: Physician's Press. ISBN: 0963388657

Serruys, PW. (ed). (1997). *Handbook of coronary stents.* London: Martin Dunitz. ISBN: 1853173576

Serruys, PW. (2001) and Rensing, BJ. (eds). *Handbook of coronary stents.* (4th ed). London: Martin Dunitz. ISBN: 1841840939

Sigwart, Ul (1987), Puel, Jl, Mirkovitch, V., Joffre, F., and Kappenberger, L. Intravascular stents to prevent occlusion and restenosis after transluminal angioplasty. *New England Journal of Medicine.* Volume 316:701-706

Wong, S –C. (1993) and Schatz, RA. Developmental background and design of the Palmaz-Schatz coronary stents. In: Herrman, HC. and Hirshfeld, JW., Jr. (eds.). *Clinical use of the Palmaz-Schatz intracoronary stent.* Pages 3-19. Mount Kisco, NY: Futura.

Chapter 2

ALLOY DESIGN

2.1 General

Stainless steel is offered in various sub-categories (grades) that have evolved in order to fit particular applications. Among the available grades are the austenitic alloys, which are face centred cubic and non-magnetic. These alloys are typically made of approximately 2/3 iron to 1/3 chromium and nickel, with minima on chromium and nickel set at 10-11 weight percent (wt%) and 8wt% respectively. Molybdenum in small amounts is sometimes added to iron-chromium-nickel ternary alloys to minimise pitting.

A less-used alternative to produce austenitic stainless steel is to minimise nickel content and use relatively large amounts of manganese and nitrogen. Such alloys exhibit certain advantages, particularly cost, but these advantages are usually accompanied by higher strength and attendant reduced ductility, considered disadvantages for applications such as balloon-expandable coronary stents. Other available grades include ferritic and martensitic stainless steels, which are magnetic. Processing an austenitic stainless steel may result in too much ferrite as it is cooled from the austenite phase or mechanically-induced strains may convert it to martensite.

Typical stainless steels contain up to 0.08wt% carbon, while 'low carbon' alloys are usually limited to 0.03wt% carbon. Low-carbon austenitic stainless steel is often chosen when welding, laser cutting, or using other elevated temperature processes. This is because at higher temperatures carbon combines with chromium and precipitates as carbides onto the grain boundaries, leaving the austenite grains with lowered chromium and the alloy subject to intergranular corrosion.

2.2 Objective, approach and supporting rationale

The objective, as stated in §1.5, is to develop an enhanced radiopacity austenitic stainless steel stent at least 15% greater in radiopacity at 80kV and 100kV radiation than stents made from alloys now available; ideally, radiopacity would be increased by 30%.

In §1.5, it was noted that a multi-pronged approach to alloy design will be taken. To increase radiopacity, the overall density and x-ray absorption coefficient of an existing austenitic stainless steel will be increased. To ensure the resulting alloy retains the desirable features of the base alloy as much as possible, a commercial alloy will be re-melted and a single, high-atomic-number dense element added. Any required elements will be replenished, as necessary, such that the resulting enhanced-radiopacity alloy conforms to the maximum extent possible to the established specification guidelines for the base alloy from which it is derived.

In §1.2, the results of a working group on stents and stent materials were discussed (Balcon, 1997). The list of materials-related issues in the working group report included (a) material analysis, (b) mechanical property testing, and (c) corrosion testing. Stent-specific issues in the working group report indicated concerns about ferromagnetic phases, which must be minimised in austenitic stainless steel, as noted above; the interaction of remnant ferromagnetism with the strong fields of magnetic resonance imaging and magnetic resonance angiography are of concern. The list included (a) hoop strength, (b) fatigue testing, (c) elastic recoil, (d) expansion by plastic deformation, and (e) surface characteristics. Together, and broadly, these features argue for an alloy that exhibits biocompatibility, strength and ductility, and freedom from embrittling phases or inclusions that contribute to fracture, fatigue or corrosion failures.

The small quantities of raw material required for fabricating coronary stents have until now led the medical device industry to utilise available, implant-grade alloys rather than have those tailored to the unique needs of the industry by metal suppliers; with the exception of providing adequate radiopacity, this has worked relatively well. Adding radiopaque coatings to stainless steel has been accomplished but, when compared to the potential to utilise a somewhat similar alloy with greater radiopacity, e.g., implant grade cobalt-based alloys containing high-atomic-number elements, tantalum or tungsten, the engineering mechanics aspects of utilising a single alloy for this application versus a composite argue strongly in favour of the former approach.

In sum, there is the matter of tailoring a general-purpose implantable alloy to the specific needs of coronary stents without losing the key advantages of the base alloy. There are obviously regulatory issues to be concerned with; these must be addressed as the plan is made and, in the long term, brought to fruition. The key technical attributes to be addressed can be summarised as follows:

- Enhanced/increased radiopacity of the component part (stent)
- Absent or fully minimised ferromagnetic phases (ferrite; martensite)
- Absent/minimised potentially embrittling phases (intermetallics, inclusions, etc.)
- Mechanical properties (strength, ductility) comparable to those of current alloys
- Equal/equivalent corrosion properties as determined by standard test methods

2.3 Maintain specification context

Two contextually identical specifications that may be used to govern composition and material properties of implant-grade austenitic stainless steels are those published by International Standards Organisation (ISO 5832-1:1997) and The British Standards Institute (BS 7252-1:1997). These specifications describe an alloy, Composition D,

which while not specially designed for this application, has been widely used for fabricating coronary stents. The former American Society for Testing and Materials (now ASTM International) chairs the International Standards Organisation working group responsible for maintaining ISO 5832-1 but both its recently-balloted equivalent specifications, ASTM F138-03 (bar) and F139-03 (sheet), as well as the earlier F138-00 and F139-00, were published after the International Standards Organisation and British Standards Institute. ASTM F138 and ASTM F139 include minor modifications that have not yet been incorporated into BS 7252-1 or ISO 5832-1. ASTM International does not utilise the 'Composition D' terminology but a somewhat simplified approach that incorporates older systems, which is described in one of its standard practices, ASTM E527-83(1997)E1; this is the 'unified national standard' (UNS) naming scheme. Under ASTM E527, both ASTM F138 and ASTM F139 alloys are alloy UNS S31673, where the 'S' is for stainless steel, the '316' indicates a family of austenitic alloys containing iron, chromium, nickel and molybdenum, and the '73' uniquely identifies the compositional range of alloys described in ASTM F138 and ASTM F139. Any intentional addition of elements not within the scope of the Unified National Standard designation would necessitate application for and eventual issuance of a new UNS S316xx designator, provided that iron remained the primary element and that chromium, molybdenum, nickel, and carbon remained within the scope of the UNS S316xx alloys. New standards specifying composition and properties of such an alloy would be required to be written, vetted, and approved by the issuing authority if the alloy is to be offered commercially. As an example, in the event of presenting the case for a new alloy standard to ASTM International Committee F04 (Medical Devices and Services), Subcommittee F04.12 (metallurgy) would establish a task group to

investigate the need for and, if appropriate, draft the standard for balloting. ASTM International Committee F04 might then propose the newly-approved standard for consideration by International Standards Organisation, which might then be included in ISO 5832-1. ASTM International works closely with the American regulatory authority for medical devices, United States Food and Drug Administration, such that ASTM International Committee F04 consensus standards effectively serve as Federal standards once they have been balloted and approved for use. In the absence of such a new standard, or while preparing such a standard, individual companies may petition regulatory authorities (e.g., United States Food and Drug Administration) for permission to utilise what is termed a 'non-compliant' alloy design, much as companies might petition regulatory agencies for approval of any other design change that does not radically depart from the original design and relates to the risks involved in the proposed human use of a medical device.

UNS S31673 alloys described in ASTM F138 and ASTM F139 are low-carbon, austenitic, molybdenum-containing stainless steels comprised of, at minimum, the interstitial non-metal, carbon (limited to 0.03wt%), and the four substitutional transition metals, chromium (17-19wt%), nickel (13-15wt%), molybdenum (2.25-3.0wt%), and iron (balance). Under ASTM E527, iron must be the predominant element for an alloy to be defined as steel. Other elements, along with their limits, as specified in ASTM F138 and F139, are manganese (2.0wt%), phosphorous (0.025wt%), sulphur (0.010wt%), silicon (0.075wt%), nitrogen (0.10wt%), and copper (0.50wt%).

2.4 Increase overall radiopacity

The desired increases in radiopacity for an implant-grade austenitic stainless steel, here the UNS S31673 alloy, as determined by balloon-expandable coronary stent

developers, are at least a nominally 15 percent increase and, ideally, nominally 30 percent, compared against the existing alloy at 80-100kV at a thickness *t* of 0.127mm.

The adjective, radiopaque, and its noun, radiopacity, are somewhat unfamiliar terms to the metallurgist and industrial radiographer because radiographic methodology in industry developed almost entirely from a technology where transparent-base radiographic film densities were measured and compared to determine quality and sensitivity using image quality indicators (also called radiographic penetration meters, or penetrameters) that are placed on or near the item being inspected (Halmshaw, 1971; Berger, 1985). In industrial radiography, the visibility of what is sometimes referred to as a 'foreign object' such as an inclusion of a particular size may be the objective, thus the ability to distinguish between the transmission density of the penetrameter placed on the surface of the material and the transmission density of the adjacent material, as well as the ability to distinguish between certain wires or holes in the penetrameters, are used for the radiographic film interpreter to gain confidence in his ability to locate and identify the inclusion, if present. Considering the human body as a composite material, the visibility of the stent, a 'foreign object' within its surroundings, is here the objective.

Transmission film density (D), or light absorbance, is typically determined with a calibrated densitometer that takes the common logarithm of the ratio of the intensity of light entering (I_e) the radiographic film versus the intensity of light exiting (I_t) the film, shown in the following equation (American Society for Metals, 1976):

$$\text{Transmission Film Density} = D = \log (I_e / I_t). \qquad \text{Equation 1}$$

With such film, where visible light is the radiation, the ratio (I_e/I_t) is the film opacity; when x-rays are the radiation impinging on a material, this ratio is termed radiopacity:

$$\text{Radiopacity} = I_e / I_t. \qquad \text{Equation 2}$$

Taking the common logarithm of radiopacity yields the absorbance of the material:

$$\text{Absorbance} = \log(\text{Radiopacity}) = \log(I_e / I_t) \qquad \text{Equation 3}$$

Material absorbance for x-radiation is thus the equivalent of transmission film density.

The inverse of opaque is lucent, thus with x-radiation the inverse of radiopacity is radiolucence; this is also known as transmittance:

$$\text{Radiolucence} = \text{Transmittance} = I_t / I_e \qquad \text{Equation 4}$$

The above relationships are described in the chemical literature for determining the molecular structure by use of electronic spectroscopy (Atkins, 1986) and are usually referred to as either Beer's Law or Beer-Lambert's Law. Beer's Law (Adams, 2003) states: "for a parallel beam of monochromatic radiation passing through homogeneous solutions of equal pathlengths the absorbance is proportional to the concentration." Lambert's Law, according to Adams, states: "For a parallel beam of monochromatic radiation passing through homogeneous solutions of equal concentration the absorbance is proportional to the pathlength."

Hubbell and Seltzer (2003) provide an exponential attenuation equation to determine radiopacity when a narrow beam of monoenergetic photons I_e penetrates a layer of material with a density ρ and a mass thickness x (where $x = \rho\, t$ and t = component thickness), which emerges with intensity I_t, as follows:

$$\text{Radiopacity} = (I_e / I_t) = \exp[(\mu / \rho)(\rho\, t)]. \qquad \text{Equation 5}$$

Here μ is the linear absorption coefficient and μ / ρ is the mass attenuation coefficient; tables of μ / ρ for both elements and compounds are provided by Hubbell and Seltzer. The mass attenuation coefficient is experimentally determined but, as described by Hubbell and Seltzer, relies heavily on and correlates well with the theoretically determined total radiation cross section, including the atomic photoeffect cross section,

both coherent (Rayleigh) and incoherent (Compton) scattering cross sections, the cross sections for electron-positron production in the fields of the nucleus and of the atomic electrons, and the photonuclear cross section. For compounds and mixtures, Hubbell and Seltzer assume that these coefficients may be found by simple addition according to the fraction by weight of each element, i, c_i, which contribute to the compound or mixture:

$$(\mu / \rho)_{\text{compounds \& mixtures}} = \sum_i c_i (\mu / \rho)_i . \qquad \text{Equation 6}$$

Alloy density may be estimated using the following equation (Payling, 1997):

$$\frac{1}{\rho} = \sum_i \left(\frac{c_i}{\rho_i} \right). \qquad \text{Equation 7}$$

As can be seen from examination of Equation 2 and the mass attenuation coefficient tables provided by Hubbell and Selzer, if energy and t are invariant, the material radiopacity may be increased by increasing the overall elemental density. Thus dense elements must be added to the UNS S31673 alloys in order to increase radiopacity.

The constraints on the radiopaque alloy to be developed are that, while it is accepted that the alloy will be a non-compliant alloy, the alloy will closely follow ASTM F 138-00 and ASTM F139-00 in terms of composition, ideally increasing radiopacity of the modified UNS S31673 alloy at t = 0.127mm by nominally 30% at 80kV-100kV.

2.5 Ensure no ferromagnetism

Stainless steels are complex multi-component alloys. They can be air-quenched from approximately 600 °C to form a metastable gamma (face-centred cubic, or austenite) phase at room temperature. The metastable gamma phase may include some ferrite phase, often referred to as delta ferrite (body-centred cubic), which is ferromagnetic at room temperature. UNS S31673 alloys are required to be free of delta

ferrite when viewed at 100X magnification, in accordance with ASTM F138 and ASTM F139. In addition, mechanically working the alloy (Dennis, Craig *et al*, 2003) may transform austenite into the martensite phase (body-centred tetragonal), which also is ferromagnetic. A combination of a careful selection of alloying elements to strengthen the austenitic structure and repeated annealing treatments to reduce the stress level during such mechanical processing is required. This latter will continually return the alloy to the austenitic state.

Many references exist on binary and ternary alloys. These are helpful in developing an understanding of the complex nature of multi-component alloys such as austenitic stainless steel. However, these alloys may react, as described in the preceding paragraph, to both thermal processing and mechanical treatments to change the alloy from what it was meant to be to one that is radically different from that which is desired. Because of the complex nature of multi-component austenitic stainless steel welds, Schaeffler (1949) devised an approach whereby certain of the alloying elements are utilised to display graphically whether the resulting alloy is predominantly austenitic, ferritic, or has the tendency to become martensitic (which may result from stresses due to the weld being constrained by the very structures it joins). Using this approach, certain alloying elements are considered as being either nickel or nickel equivalents or chromium or chromium equivalents, as shown in Figure 4. An alternate version was developed by de Long (1974), which includes the influence of nitrogen on the nickel equivalent. These approaches also work well for stainless steel castings and have been widely adopted for such use. In this study, only the Schaeffler diagram is used since little nitrogen is contained in these alloys; that diagram is thought more illustrative than the de Long, which has been incorporated in standards with a focus on ferrite numbers.

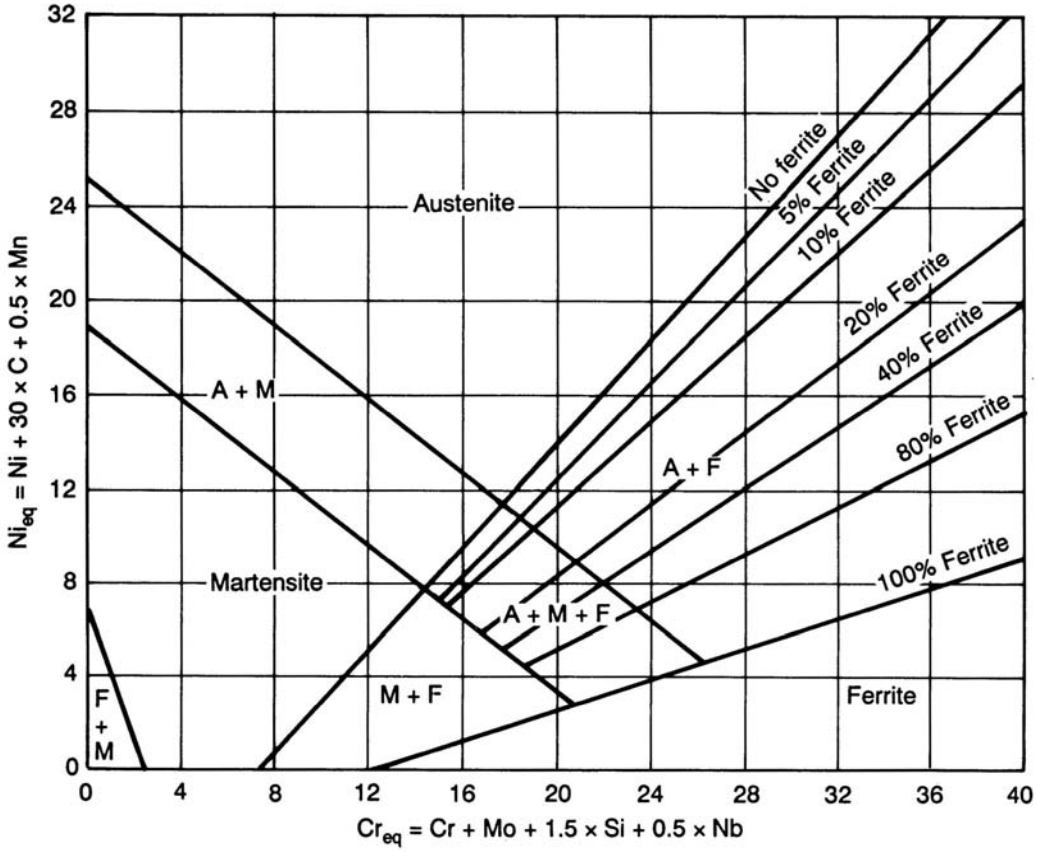

Figure 4 Schaeffler diagram (stainless steel welds) (Schaeffler, 1949)

2.6 Freedom from inclusions or other deleterious phases

The essential requirement that UNS S31673 (or Composition D) alloys have been mandated to meet under British Standards Institute, International Standards Organisation, and ASTM International specifications has been freedom, in the fully annealed state, from such inclusions as would result if refinement through specialised melting practices such as vacuum arc remelting or electroslag melting were not utilised. These inclusions are sulphides, aluminates, silicates, and globular oxides. For microcleanliness, the term used by ASTM International to describe absence of these inclusions, ASTM E45, Method A, is applied, which consists of a 100X optical examination of a polished surface, similar to the test that is applied to determine the presence of ferrite. However, it has long been recognised that phases such as sigma,

Laves, and chi in stainless steels are deleterious for critical applications; the latest versions of the standards referred to above, ASTM F138-03 and ASTM F139-03, include determination of the contents of all these phases.

Although not a specification requirement at the time, the concern at the beginning of this study was upsetting the delicate compositional balance that minimised the potential for σ phase formation whilst in the process of attempting to increase alloy radiopacity. A parallel to the present application of austenitic stainless steels for coronary stents that addressed the deleterious effects of σ phase is in nickel-based superalloy development. Sigma phases tended to appear after long periods of operations at turbine operating temperatures and their presence reduced alloy ductility. Alloys susceptible to sigma phase precipitation were those that had high concentrations of alloying elements in the solid solution gamma phase (which is face-centred cubic). The alloy design methodology known as PHACOMP (for phase composition) emerged from studying that problem (Sims, 1988) and is used to predict the likelihood of sigma formation from a knowledge of the alloy composition. A variant of PHACOMP, termed New PHACOMP, described by its originator, Morinaga (2001), has been applied to a number of superalloys, particularly those where nickel aluminides are utilised, and has also been applied to the *ab initio* design of ferritic steel alloys (Morinaga, 1994). As a design tool, then, New PHACOMP may complement use of Schaeffler or de Long diagrams.

New PHACOMP parallels PHACOMP in one of its two approaches, assigning each transition element a value, in electron volts, which is an average of the components of the crystal field splitting parameter, the d-orbital t_{2g} triplet and the d-orbital e_g doublet (Pearson, 1972). The Md numbers (i.e., d-orbital of element M) are summed to provide the compositional average of Md values in an alloy, Md(avg), defined as follows:

$$Md(avg) = \sum_i x_i (Md)_i. \qquad \text{Equation 8}$$

The first term, x_i, is the atomic fraction of component i of the alloy, and the second term, $(Md)_i$, is the Md value for component i, while the summation of both is over all i.

Morinaga (1994, 2001) thus describes an approach that both parallels the original PHACOMP approach and offers the advantage that it is comprehensive and updated. Further, Morinaga was helpful in this research by determining the Md for elements that had not been previously determined or published, as will be described herein.

This approach also utilises a critical Md, described here as Md(crit), which can serve as an upper limit for the Md(avg) of a particular alloy and may indicate the presence of σ phase or some other deleterious phase. Morinaga offers experiential evidence with other alloys using such an upper limit that has been tied to the presence of such phases but these are not universal in nature and thus serve primarily as alloying guidelines. This relationship, which Morinaga (1985) argues is valid for the γ/γ+σ phase boundary, may be determined by applying the following experimentally-determined formula:

$$Md(crit) = [6.25 \times 10^{-5} T] + 0.834 \qquad \text{Equation 9}$$

Here T is the temperature in kelvins. Thus, if this formula holds for comparable alloys, when Md(avg) is equal to or greater than Md(crit), the σ phase should precipitate out.

2.7 Mechanical properties

The tensile and yield strength and the ductility of the particular form applicable to ASTM F138 (bar and wire) or ASTM F139 (sheet and strip) are determined as proof of compliance. As a design tool, the formula developed by Nordberg (1993) for use with stainless steels may be used to predict tensile and yield strength, as below:

$$\text{Tensile Strength (MPa)} = 470 + 600(N + 0.02) + 14Mo + 1.5\delta + 8d^{-0.5} \quad \text{Equation 10}$$

$$\text{Yield Strength (MPa)} = 120 + 210\sqrt{(N + 0.02)} + 2Cr + 2Mn + 14Mo + 10Cu + \delta(6.15 - 0.054\delta) + [7 + 35(N + 0.02)]d^{-0.5} \quad \text{Equation 11}$$

Here d is the grain size (in mm) and δ is delta ferrite content (in volume %).

Both ASTM F138-00 and ASTM F139-00 require a minimum ultimate tensile strength of 490 MPa and minimum yield strength of 190 MPa for annealed specimens, whether bar or sheet. By adding back chromium, molybdenum, or nickel to an alloy that is diluted by addition of a radiopaque alloy, tensile and yield strength requirements should continue to be met.

2.8 Corrosion

The addition of chromium to steel establishes a unique surface condition that gives rise to these steels being called ‘rust free’ or ‘stainless’ and additions of molybdenum enhance pitting resistance. A pitting resistance equivalent number (PREN) may be determined by various formulae (Sedriks, 1996), which often includes nitrogen, but since nitrogen is allowed but only molybdenum is mandatory in the UNS S31673 alloys, the formula shown in Equation 7 is incorporated into the above specifications:

$$\text{PREN} = [\text{wt\% Cr} + 3.3\ (\text{wt\% Mo})] = 26\ (\text{minimum}). \quad \text{Equation 12}$$

An intergranular corrosion susceptibility test, ASTM A262 Practice E, is required of ASTM F138 and ASTM F139 alloys. Biocompatibility testing of UNS S31673 alloys is not required since those alloys are used as control materials in ASTM F981, but any non-compliant alloy such as may result here would be required to be subjected to a biocompatibility testing regime to determine fitness for human use in a medical device.

2.9 Summary

A design approach has been defined. A single, high-atomic number element will be selected and added to a commercial variant of an implant grade austenitic stainless steel in order to preserve the desirable features of the base alloy and also minimise exception to the governing alloy specification as viewed by regulatory authorities. Modelling of radiopacity, at a thickness comparable to that of coronary stents, is accomplished by use of Beer-Lambert's Law, standardised coefficients of absorption, and single-beam x-radiation that is expected to be a good approximation of actual experimental results. Modelling of the alloy to ascertain its propensity for ferromagnetic phases will be accomplished by use of Schaeffler diagrams, aided by standard binary phase diagrams. Modelling of the alloy to determine its propensity for sigma phase or other embrittling phases will be accomplished by use of a derivative of a superalloy modelling tool, 'PHACOMP', which as 'New PHACOMP' has been in use for well over two decades, although it has not been previously applied to development of austenitic stainless steel. The average of the crystal field splitting parameters, the d-orbital triplet and doublet, and the experimentally-determined critical variant of that parameter, the latter based on success with determining the onset of sigma phase, are used. Mechanical properties, namely tensile and yield strengths, will be modelled by use of the Nordberg equations. Finally, the onset of pitting resistance is identified both in the applicable specification for the base alloy and in the literature as a pitting resistance equivalent number, Equation 12, and is applied to ensure experiences gained with that are capitalised upon.

2.10 References

Adams, DB. (2003). *Beer-Lambert law*. University of Sunderland, Sunderland, UK. URL: http://www.sunderland.ac.uk/~hs0dad/qm/testv2a/beer_lam.htm

American Society for Metals, Committee on Radiographic Inspection. (1976). Radiographic inspection. In: Boyer, HE., and Carnes, WJ. (eds). *Metals Handbook®, 8th ed., vol. 11, nondestructive inspection and quality control*. Pages 105-156. Materials Park, Ohio: ASM International®.

Atkins, PW. (1986). *Physical chemistry*. (3rd ed). Pages 464-467. New York: WH Freeman and Company. ISBN: 0716717492

Balcon, R. (1997), Beyar, R., Chierchia, S., De Scheerder, I., Hugenholtz, PG., Kiemeneij, F., Meier, B., Meyer, J., Monassier, JP., and Wijns, W. Recommendations on stent manufacture, implantation and utilization. *European Heart Journal.* Vol 18. Pages 1536-1547.

Berger, H. (1985). Radiography. In: Boyer, HE., and Gall, TL. (eds). *Metals Handbook®, desk edition*. Pages 155-173. Materials Park, Ohio: ASM International®. ISBN: 087170188X

DeLong, WT. (1974). Ferrite in austenitic stainless steel weld metal. *Welding Journal.* 53(7). Pages 273s-286s.

Dennis, JZ. (2003), Craig, CH., Radisch, HR., Jr., Pannek, EJ., Jr.,Turner, PC., Hicks, AG., Jenusaitis, M., Gokcen, NA., Friend, CM., and Edwards, MR. Processing platinum enhanced radiopaque stainless steels (PERSS®) for use as balloon-expandable coronary stents. In: Winters, GL., and Nutt, MJ. (eds). *Stainless steels for medical and surgical applications*, *ASTM STP 1438*. Pages 61-71. West Conshohocken, PA: ASTM International.

Halmshaw, R. (1971). *Industrial radiology techniques*. Pages 155-173. London: Wykeham Publications. ISBN 0851092101

Hubbell, JH (1997) and Seltzer, SM. *Tables of x-ray mass attenuation coefficients and mass energy-absorption coefficients* (version 1.03). Gaithersburg, MD: National Institute of Standards and Technology. URL: http://physics.nist.gov/xaamdi

Morinaga, M. (1994), Hashizume, R., and Murata, Y. An electronic approach to the design of ferritic steels for power plants. In: Coutsouradis, D., Davidson, JH., Ewald, J., Greenfield, P., Khan, T., Malik, M., Meadowcroft, DB., Regis, V., Scarlin, RB., Schubert, F., and Thornton, DV. (eds). *Materials for advanced power engineering 1994*. Vol 1. Pages 319-328. Dordrecht: Kluwer. ISBN 079230749

Morinaga, M. (2001), Murata, Y., and Yukawa, H. Recent progress in New PHACOMP approach. In: Zhao, J-C., Fahrmann, M., and Pollock, TM. (eds). *Materials design approaches and experiences*. Pages 15-27. Warrendale, PA: The Metals Society, ISBN 0873395034

Morinaga, M. (1985), Yukawa, N., and Ezaki, H. Solid solubilities in transition-metal-based fcc alloys. *Philosophical magazine, A.* 51(2). Pages 223-246.

Nordberg, H. (1993). Mechanical properties of austenitic and duplex stainless steels. *Conference Proceedings, Innovation Stainless Steel.* Florence 11-14 October. Vol. 2. Pages 2.217 – 2.229. Also in: La metallurgia Italiana, 85 (3). 1994 Pages 147-154.

Payling, R. (1997). *Glow discharge optical emission spectrometry*. Pages 287-291. Chichester: John Wiley & Sons. ISBN: 0471966835
URL: http://www.glow-discharge.com/density.htm

Pearson, WB. (1972). *The crystal chemistry and physics of metals and alloys.* Pages 268-286. Chichester: John Wiley & Sons. ISBN 0471675407

Schaeffler, AL. (1994) Constitution diagram for stainless steel weld metal. *Metal progress*, 56(11). Pages 680-680b. In: Davis, JR. (ed). *Stainless steels*. Page 340. Materials Park, OH: ASM International. ISBN: 0871705036

Sedriks, AJ. (1996). *Corrosion of stainless steels* (2nd ed). Pages 111-112. John Wiley & Sons, Chichester. ISBN: 0471007927

Sims, CT. (1988). Prediction of phase composition. In: Sims, CT., Stoloff, NS., and Hagel, WC. (eds). *Superalloys II*. Pages 217-240. Chichester: John Wiley & Sons.

Chapter 3

EXPERIMENTAL DESIGN AND RESULTS

3.1 General

The approach being used here was described in Craig *et al* (2003), wherein the UNS S31673 alloy is first reduced to a quaternary of required elements, in accordance with the two ASTM International documents describing either rod or bar stock (ASTM F138) or sheet or foil (ASTM F139). Similar arguments would apply if utilising Composition D of either ISO 5832-1 or BS 7252-1. The austenitic stainless steel has previously been described as comprised of approximately 2/3 iron and the remainder chromium and nickel; here a fourth required element is molybdenum. Since chromium, nickel and molybdenum each have a fixed range (17-19wt% Cr; 13-15wt% Ni; 2.25-3.0wt% Mo) in the alloy, the iron content in the quaternary is considered as offering the greatest opportunity for change since it is described in all the above specifications as 'balance'. Under the Unified National Standard definition of steel, the alloy remains so defined if the predominant element is iron. This means iron could be reduced by half, to 1/3 the total, and a pentanary could be defined in which slightly less than 1/3 the total weight percent of the alloy is comprised of a single, high-atomic-number element.

While the approach described above applies for purposes of design and analysis, i.e., by reducing the specification to an alloy comprised of either a compliant quaternary or a non-compliant pentanary, the experimental approach entails use of a commercial, implant-grade alloy meeting UNS S31673 criteria and the ASTM F138-00 specification (Carpenter Technology's BioDur® 316LS, in bar stock, unless otherwise noted). This

alloy is re-melted with the high-atomic-number element added, along with additions of some or all required elements that would otherwise fall below the specification limits.

3.2 Increase radiopacity

Before investigating the need for additional alloying elements to be added, it would be helpful to estimate the radiopacity of the UNS S31673 alloy. Considering only the four primary substitutional elements that are required of UNS S31673 alloys and utilising the midpoints of the required elemental weight percentages of those elements provides the following: chromium (18wt%), nickel (14wt%), molybdenum (2.5wt%), and iron (65.5wt%). These four elements comprise a quaternary alloy; the radiopacity for this alloy is calculated by applying Equation 2 on a weighted-average basis to the elements of the quaternary; a thickness of 0.127mm (0.005 inches) is utilised, which is typical of the metal film or tubing wall thickness when fabricating coronary stents. The radiopacity results are shown in Table 4 and Table 5 as equal to 1.07 and 1.04 (dimensionless units), respectively, for 80 keV and 100keV (energies well within the spectrum typically used during stent deployment for which data are readily available). Table 6 shows the radiopacities of each element of the quaternary alloy. Achieving a 30% increase in radiopacity at each energy level for the alloy would result in radiopacity units of 1.39 and 1.34 at 80keV and 100keV, respectively, as shown in Table 4 and Table 5.

Table 4 – Quaternary alloy (Q) showing resultant radiopacity at 80keV (density, ρ, and mass attenuation coefficient, μ/ρ, from tables provided by Hubbell and Selzer, 1997)

Z	Element	Density, ρ	μ/ρ 80keV	thickness	wt%	R (alloy)
		g/cm^3	$\mu = cm^{-1}$	cm		@80keV
24	Cr	7.18	0.49	0.0127	18	=
26	Fe	7.87	0.6	0.0127	65.5	1.07
28	Ni	8.9	0.73	0.0127	14	To increase:
42	Mo	10.22	1.96	0.0127	2.5	130% R(Q)
						=
						1.39

Table 5 – Quaternary alloy (Q) showing resultant radiopacity at 100keV (density, ρ, and mass attenuation coefficient, μ/ ρ, from tables provided by Hubbell and Selzer, 1997)

Z	Element	Density, ρ	μ/ρ 100keV	thickness	wt%	R (alloy)
		g/cm^3	$\mu = cm^{-1}$	cm		@100keV
24	Cr	7.18	0.32	0.0127	18	=
26	Fe	7.87	0.37	0.0127	65.5	1.04
28	Ni	8.9	0.44	0.0127	14	To increase:
42	Mo	10.22	1.1	0.0127	2.5	130% R(Q)
						=
						1.35

Table 6 – Calculated radiopacities for primary elements of UNS S31673 (t = 0.127mm)

	Cr	Fe	Ni	Mo
$R_{80\ keV}$	1.046	1.061	1.086	1.290
$R_{100\ keV}$	1.029	1.038	1.051	1.153

Since the physical constants of the elements are fixed, as for these purposes is the thickness, it is impossible for this quaternary alloy to achieve 130% of its radiopacity. This increase can only be accomplished by removing some portion of one or more elements and replacing that portion with a more radiopaque element. Ideally, this would be achieved within the constraints of the governing specifications, but if not, the element should complement existing elements to achieve a stable, biocompatible alloy; the list of acceptable elements does not include high-atomic-number elements.

However, as noted above, since the compositions comprised of chromium, nickel, and molybdenum are essentially fixed, iron, shown in the several specifications as 'balance', is the only element that may be changed without going outside the bounds of those specifications. Since iron must be the predominant element for the alloy to be described as a stainless steel when the Unified National Standard designation is applied, as with the ASTM International specifications, iron could be removed to a level of 33wt% and a new element could be added in an amount up to 32.5wt%. While such an addition, one not from the palate of optional elements in the listed specifications, brings the alloy into non-compliance, the concept implemented is to remain compliant on all but this matter.

Selecting a fifth element and adding that to those comprising the quaternary alloy results in a pentanary alloy. Selecting only elements sufficiently radiopaque to increase overall radiopacity to approximately 130% of that of the quaternary at each energy level and well within conservative metallurgical practice for stainless steel, i.e., use of non-allotropic d-block elements exhibiting close packed structures, leads to selection of the seven elements beginning with Z = 73 (tantalum) through Z = 79 (gold). The radiopacities of these elements are shown in Table 7; elemental thickness is 0.127mm.

Table 7 – Calculated radiopacities for radiopaque elements for pentanary alloy (t = 0.127mm)

	Ta	W	Re	Os	Ir	Pt	Au
$R_{80\ keV}$	4.98	6.78	8.62	10.77	11.52	10.79	8.88
$R_{100\ keV}$	2.48	2.97	3.41	3.85	3.99	3.89	3.55

The radiopacities for the pentanary are calculated with each of these elements replacing, in turn, the maximum amount of iron; the results are as shown in Table 8 and in Table 9. All seven elements shown in Table 8 (radiopacities at 80keV) meet the criteria of 130% of that of the quaternary, while none of the elements in Table 9 do.

Table 8 – Pentanary alloy showing resultant radiopacity at 80keV (density, ρ, and mass attenuation coefficient, μ/ ρ, are from tables provided by Hubbell and Selzer, 1997)

Z	Element	Density, ρ	μ/ρ 80keV	thickness	wt%	R (alloy)
		g/cm^3	$\mu = cm^{-1}$	cm		@ 80keV
24	Cr	7.18	0.49	0.0127	18	
26	Fe	7.87	0.6	0.0127	33	
28	Ni	8.9	0.73	0.0127	14	*(130%Q=1.39)*
42	Mo	10.22	1.96	0.0127	2.5	
X	(choose)	(choose)	(choose)	0.0127	32.5	
X = 73	Ta	16.65	7.59	0.0127	32.5	1.42>130%Q
X = 74	W	19.3	7.81	0.0127	32.5	1.45>130%Q
X = 75	Re	21.02	8.07	0.0127	32.5	1.47>130%Q
X = 76	Os	22.57	8.29	0.0127	32.5	1.49>130%Q
X = 77	Ir	22.42	8.59	0.0127	32.5	1.51>130%Q
X = 78	Pt	21.45	8.73	0.0127	32.5	1.51>130%Q
X = 79	Au	19.32	8.9	0.0127	32.5	1.51>130%Q

Table 9 – Pentanary alloy showing resultant radiopacity at 100keV (density, ρ, and mass attenuation coefficient, μ/ ρ, are from tables provided by Hubbell and Selzer, 1997)

Z	Element	Density, ρ	μ/ρ 100keV	thickness	wt%	R(alloy)
		g/cm^3	$\mu = cm^{-1}$	cm		@100keV
24	Cr	7.18	0.32	0.0127	18	
26	Fe	7.87	0.37	0.0127	33	
28	Ni	8.9	0.44	0.0127	14	*(130%Q=1.35)*
42	Mo	10.22	1.1	0.0127	2.5	
X	(choose)	(choose)	(choose)	0.0127	32.5	
X = 73	Ta	16.65	4.3	0.0127	32.5	1.22<130%Q
X = 74	W	19.3	4.44	0.0127	32.5	1.24<130%Q
X = 75	Re	21.02	4.59	0.0127	32.5	1.25<130%Q
X = 76	Os	22.57	4.7	0.0127	32.5	1.26<130%Q
X = 77	Ir	22.42	4.86	0.0127	32.5	1.27<130%Q
X = 78	Pt	21.45	4.99	0.0127	32.5	1.27<130%Q
X = 79	Au	19.32	5.16	0.0127	32.5	1.27<130%Q

3.3 Maintain precipitate free austenitic structure

Maintaining the gamma (γ) or face-centred cubic structure that is known as austenite in steel is a key issue in choosing an alloying element to replace part of the iron from the alloy. Here part of the iron from the quaternary is being replaced to increase radiopacity in the resulting pentanary. The radiopaque elements in Table 7 are defined as follows: tantalum and tungsten are body-centred cubic; rhenium and osmium are hexagonal close-packed; and iridium, platinum, and gold are face-centred cubic.

Binary phase diagrams for iron-tantalum, iron-tungsten, and gold-iron are shown in Figure 5, Figure 6, and Figure 7, respectively. It is seen that the γ loop containing the austenite in each of these is not sufficiently large to sustain approximately 32.5wt% of the radiopaque elements. In addition, the binary for iron-tantalum indicates the presence of both an epsilon (*Structurbericht* C14) and a mu (*Structurbericht* D85) phase that would be incompatible with the desired austenitic phase in the pentanary alloy.

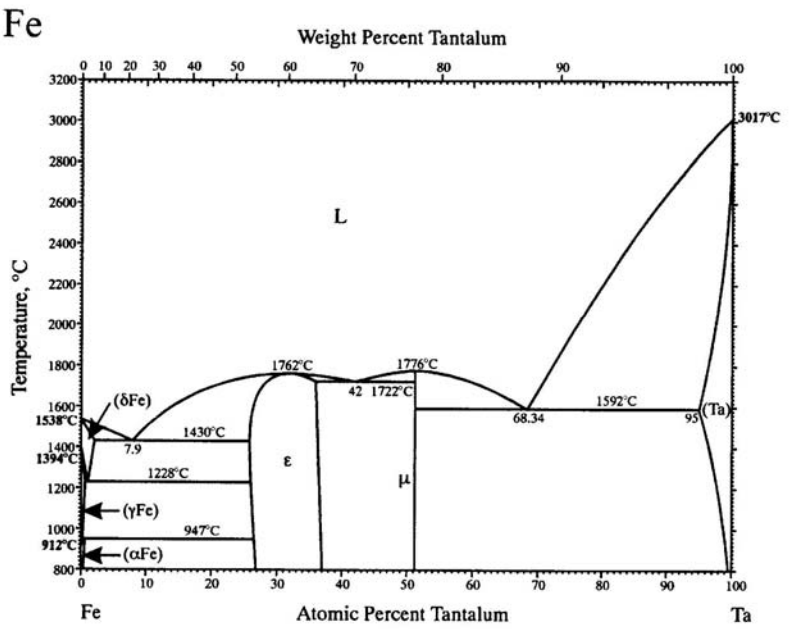

Figure 5 Iron-Tantalum Phase Diagram (Okamoto, 1996)

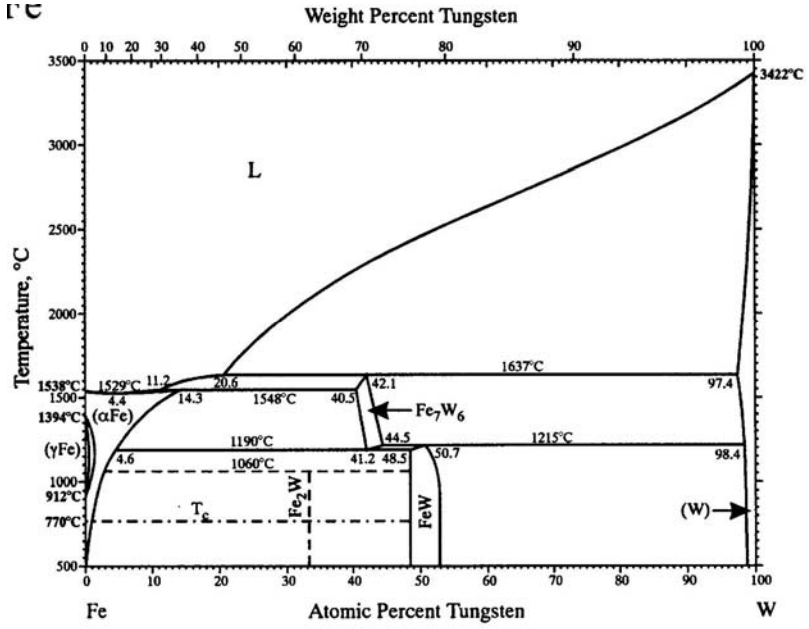

Figure 6 Iron-Tungsten Phase Diagram (Naidu *et al*, 1993)

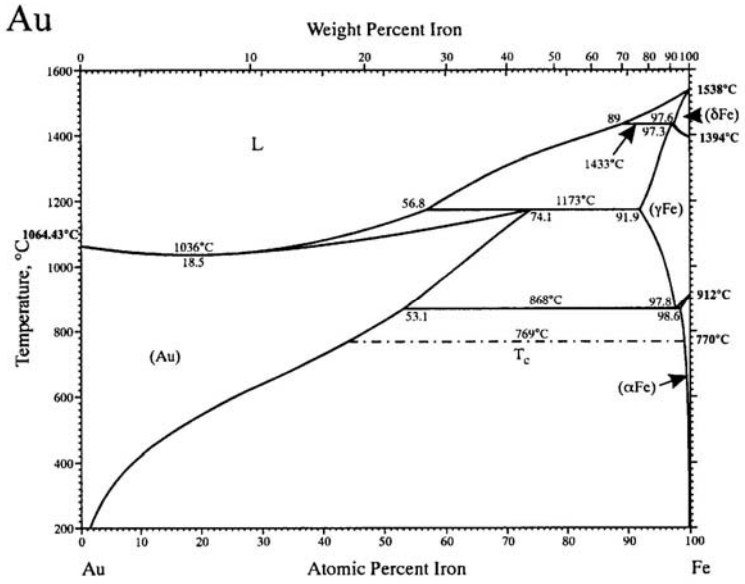

Figure 7 Gold-Iron Phase Diagram (Okamoto *et al*, 1990)

The binary phase diagram for iron-osmium is in Figure 8; the quite large γ field is typical of both iron-osmium and iron-rhenium and is more than sufficient to sustain 32.5wt% of the elements. The remaining two elements are both face centred cubic and have open γ fields, as shown in Figure 9 and Figure 10 for iron-iridium and iron-platinum, respectively.

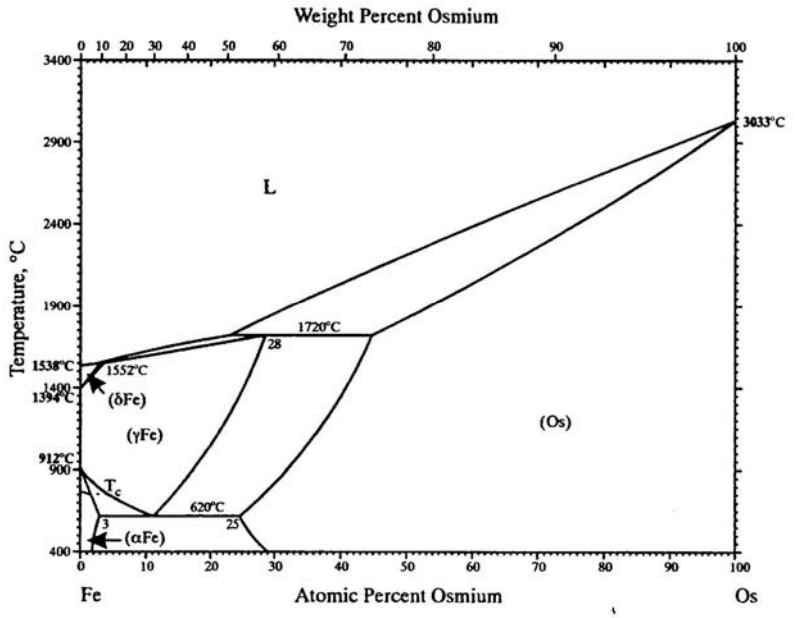

Figure 8 Iron-Osmium Phase Diagram (Swartzendruber and Sundman, 1983)

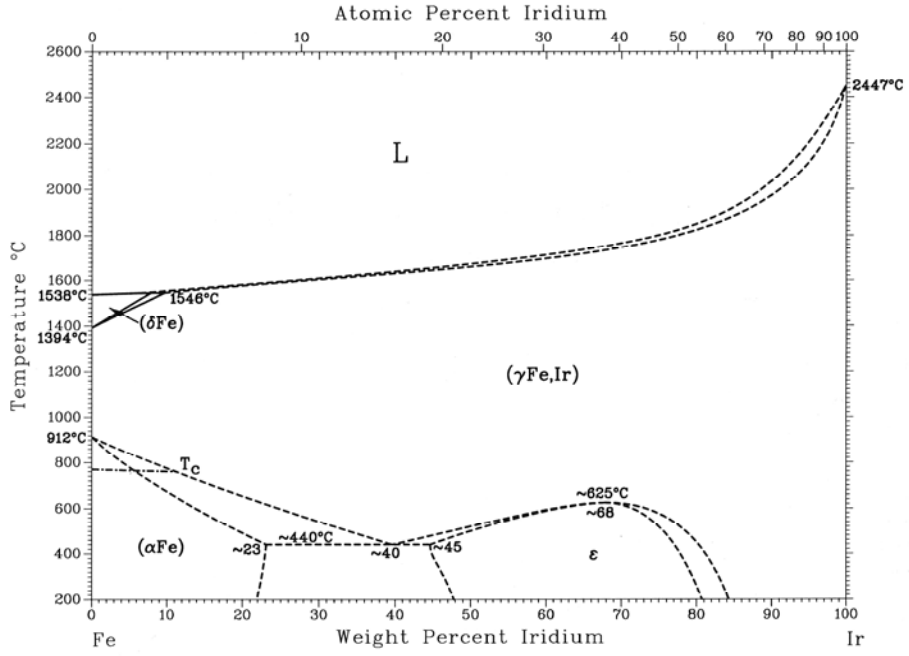

Figure 9 Iron-Iridium Phase Diagram (Swartzendruber, 1990)

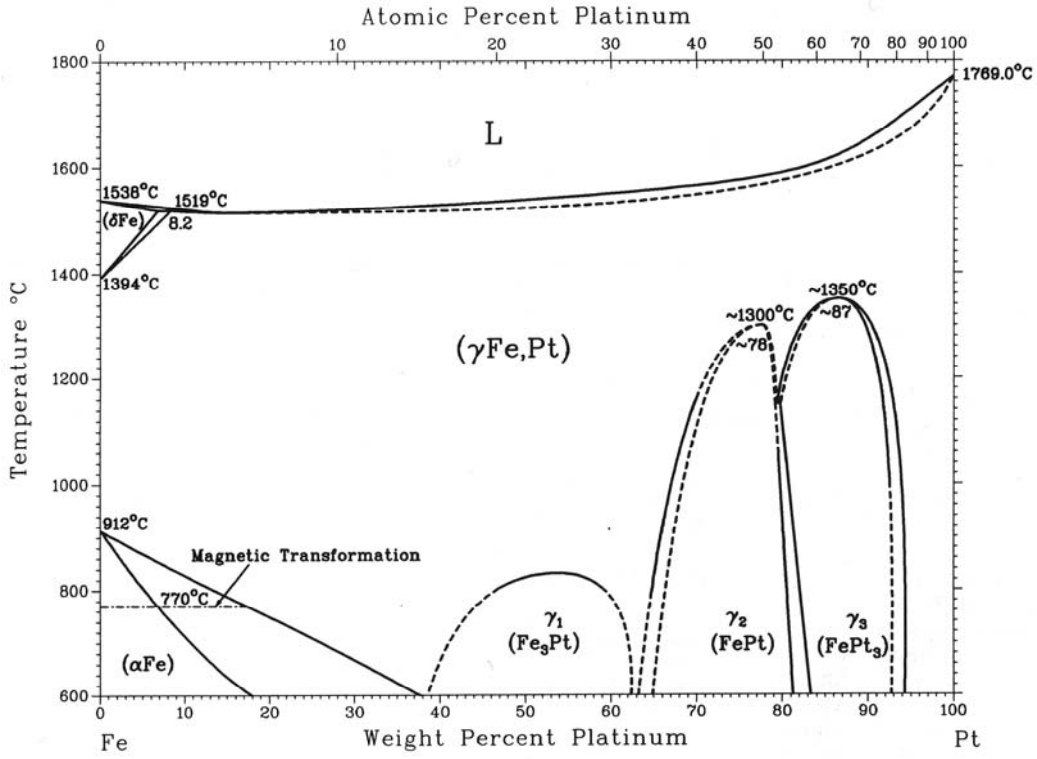

Figure 10 Iron-Platinum Phase Diagram (Okamoto, 1990)

There is the possibility of an epsilon (hexagonally close packed) phase in a binary of iron-iridium with 32.5wt% iridium. No such phase is apparent with iron-platinum and only a somewhat poorly-defined Fe_3Pt phase (*Structurbericht* $L1_2$) exists that appears to begin at approximately 38wt% platinum, well above the 32.5wt% platinum required. Both osmium and rhenium are hexagonally close packed but, as noted above, have a γ field sufficient to accommodate the required increase in density in a binary alloy.

Investigating further the possibility of using platinum as the radiopaque element, it is quite compatible with nickel, Figure 11, as would be expected since both are face centred cubic Group VIIIA elements and in the same column on the periodic table.

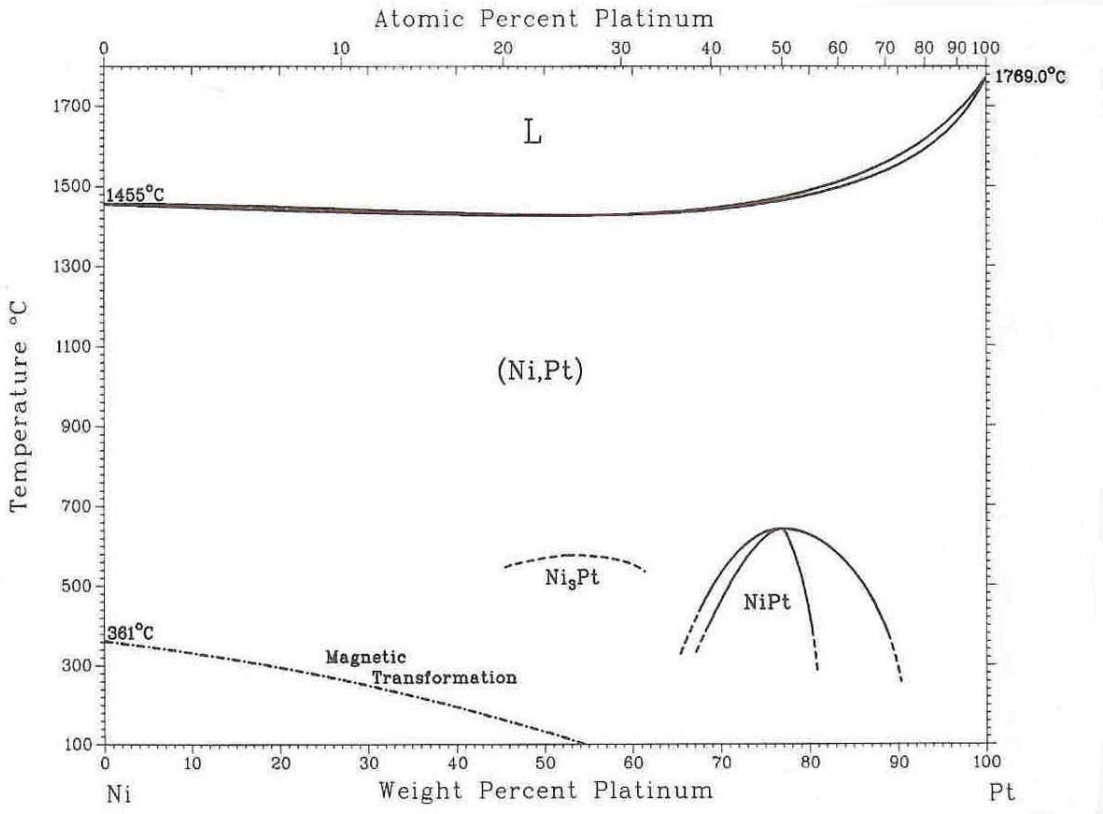

Figure 11 Nickel-Platinum phase diagram (Nash, 1990)

However, face centred cubic platinum is not quite as compatible with body centred cubic chromium, as shown in Figure 12; an intermetallic compound exists in the binary but it is at levels of platinum approximately 10wt% higher than anticipated for use here.

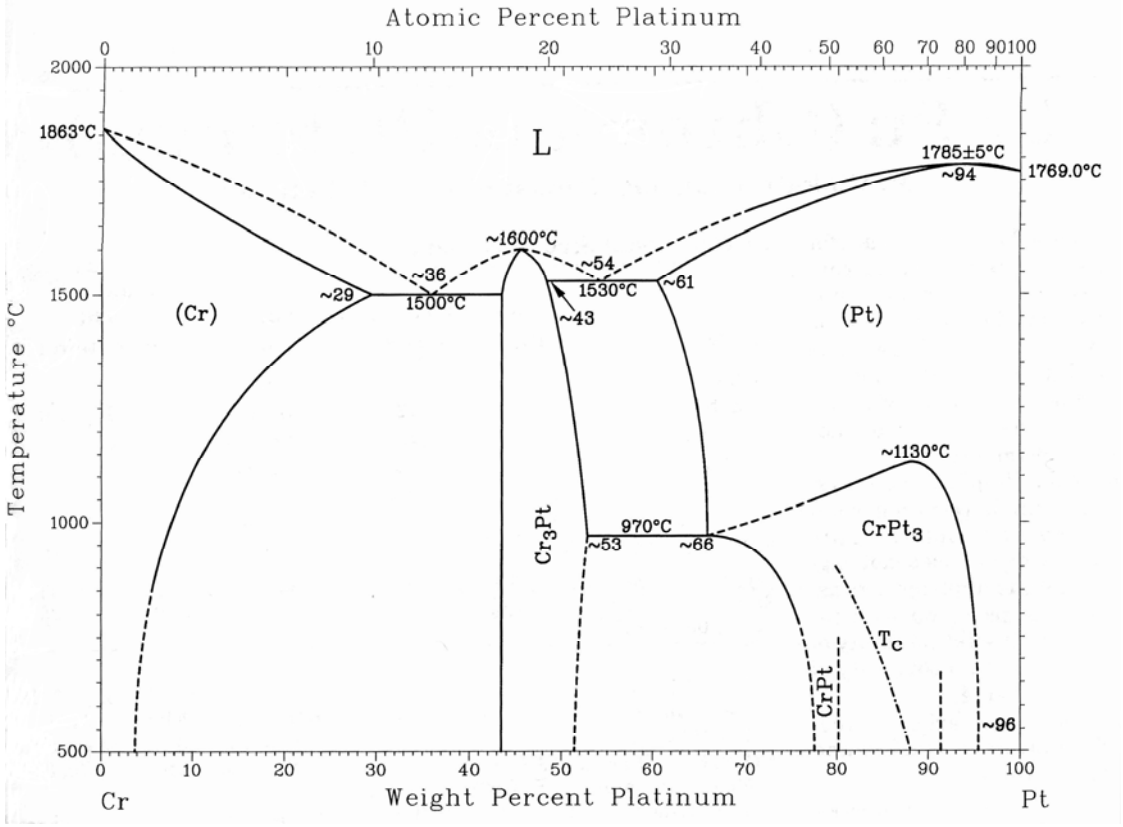

Figure 12 Chromium-Platinum phase diagram (Venkatraman and Neumann, 1990)

The Schaeffler diagram, Figure 4, provides a nickel equivalent for manganese of 0.5 but does not address platinum or iridium. Moema and Paton (2002) determined the nickel equivalent for these elements to be approximately 0.5 for platinum and 0.4 for iridium, thus these can be included on a variant of the Schaeffler diagram. Schaeffler provides a chromium equivalent for molybdenum (1.0) but does not for tungsten, which is also a body-centred cubic Group VIA element. On the premise that body centred cubic tungsten also may have the same equivalency to chromium as molybdenum, also Group VIA, it is assigned such an equivalency (1.0) here. Based on a similar parallelism with the platinum-iridium equivalency determinations (where platinum was determined to have a nickel equivalency of 0.5 and iridium 0.4), tantalum, in Group VA, is arbitrarily assigned an equivalency (0.8) since, like iridium is to platinum, it is in

an adjacent column to the left and has a smaller atomic radius. In this case, the tantalum parallelism is to that of chromium-molybdenum-tungsten, which has unity equivalence with chromium. The resulting Schaeffler diagram, Figure 13, shows the quaternary alloy lies just outside the austenite 'V' at 14wt% nickel and 18wt% chromium with perhaps 1-2% ferrite. Figure 13 shows the pentanary alloys containing 32.5wt% tantalum, tungsten, iridium, and platinum; rhenium and osmium are not shown since they are both hexagonal close packed and have no apparent equivalency to either nickel or chromium.

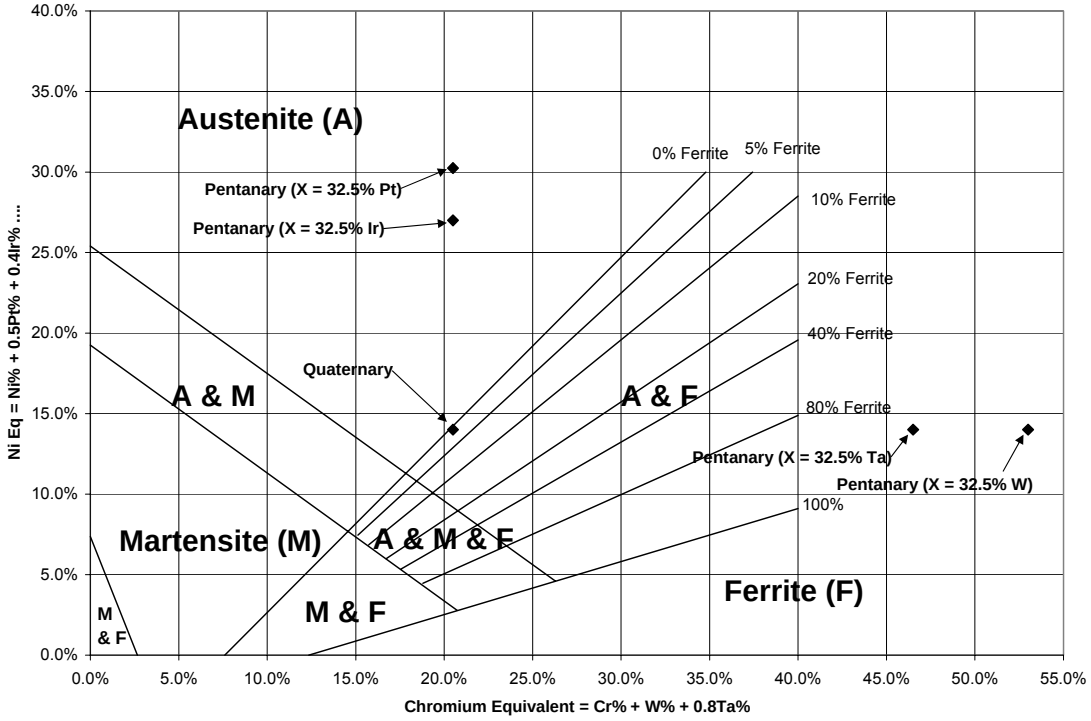

Figure 13 – Schaeffler diagram showing platinum and iridium as nickel equivalents and tungsten and tantalum as chromium equivalents in pentanary, versus quaternary

The tantalum and tungsten pentanary alloys are predominantly ferritic, as would be expected on adding such large amounts of body centred cubic elements to a face centred cubic structure such as the quaternary; this would appear to be true whether or not the assumptions about their chromium equivalency described above holds. Similarly, the

iridium and platinum pentanary alloys are clearly austenitic, again as expected on adding face centred cubic elements with broad solubility to the austenitic quaternary.

In determining the two New PHACOMP parameters, Md(avg) and Md(crit), described in §2.6, Equation 8 and Equation 9, the Md numbers provided in Morinaga (2001a; 2001b) are required, Table 10. Note Md numbers are only provided for metals.

Table 10 New PHACOMP Md numbers (Morinaga, 2001a; 2001b)

Element	Cr	Mn	Fe	Co	Ni	Cu	Mo
Z	24	25	26	27	28	29	42
Md (eV)	1.142	0.957	0.858	0.777	0.717	0.615	1.550
Element	Ta	W	Re	Os	Ir	Pt	Au
Z	73	74	75	76	77	78	79
Md (eV)	2.224	1.655	1.267	1.063	0.907	0.764	0.627

The Md(crit) value utilised in the development of a ferritic stainless steel, 1100 °C, is used here (Morinaga *et al*, 1994); the concern there, as here, is with the sigma phase that is proscribed in the latest variant of standards ASTM F138-03 and ASTM F139-03. Figure 14 is the binary phase diagram for iron-chromium and its intermetallic σ phase; the iron-chromium γ phase that is the underlying basis of stainless steel is also shown.

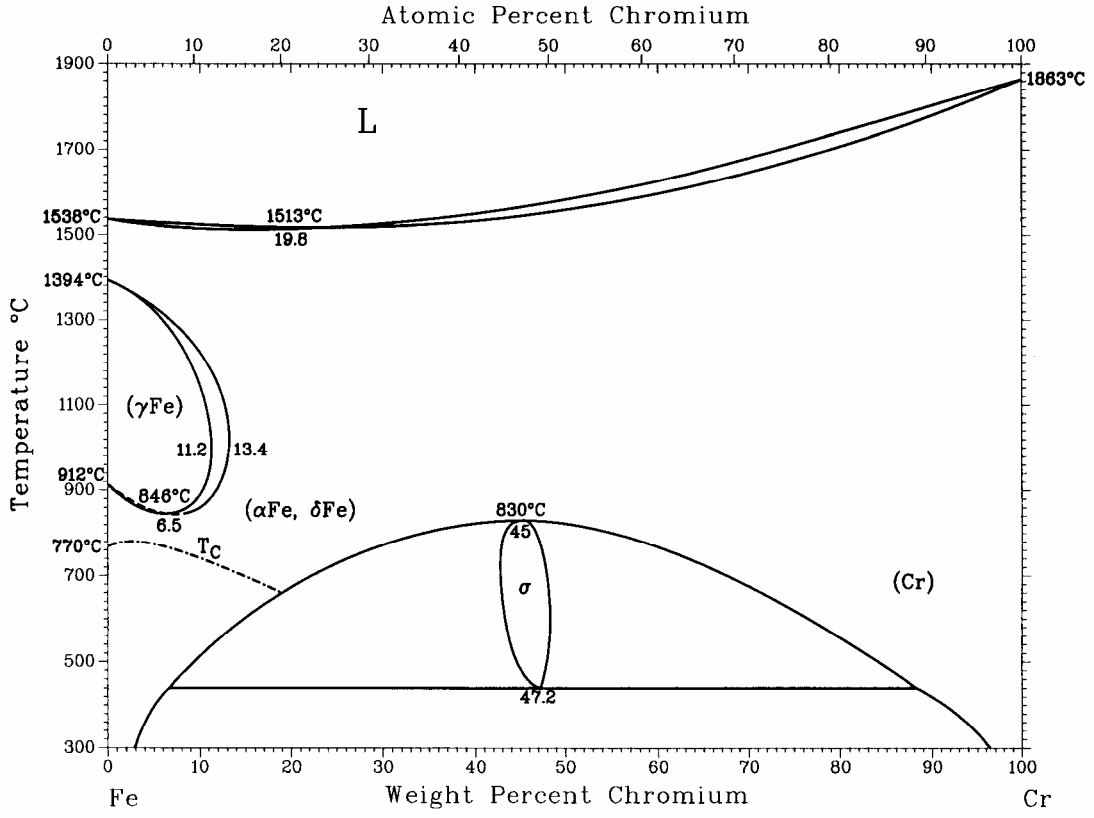

Figure 14 Iron-Chromium binary phase diagram (Massalski, 1990)

Using the pentanary alloys shown as Table 11, the New PHACOMP results are shown for the body centred cubic enhanced alloys (tantalum and tungsten) in Table 12, the hexagonally close packed enhanced alloys (rhenium and osmium), Table 13, and the face centred cubic alloys (iridium, platinum, and gold), Table 14.

Table 11 Pentanary alloys using minimised quaternary plus element "X"

Z	Element	Density, ρ	Md(eV)	wt%
24	Cr	7.18	1.142	18
26	Fe	7.87	0.858	33
28	Ni	8.9	0.717	14
42	Mo	10.22	1.550	2.5
X = 73	Ta	16.65	2.224	32.5
X = 74	W	19.3	1.655	32.5
X = 75	Re	21.02	1.267	32.5
X = 76	Os	22.57	1.067	32.5
X = 77	Ir	22.42	0.907	32.5
X = 78	Pt	21.45	0.764	32.5
X = 79	Au	19.32	0.627	32.5

Table 12 Body centred cubic elements tantalum and tungsten used to enhance radiopacity of quaternary alloy shown in Table 4 and Table 5

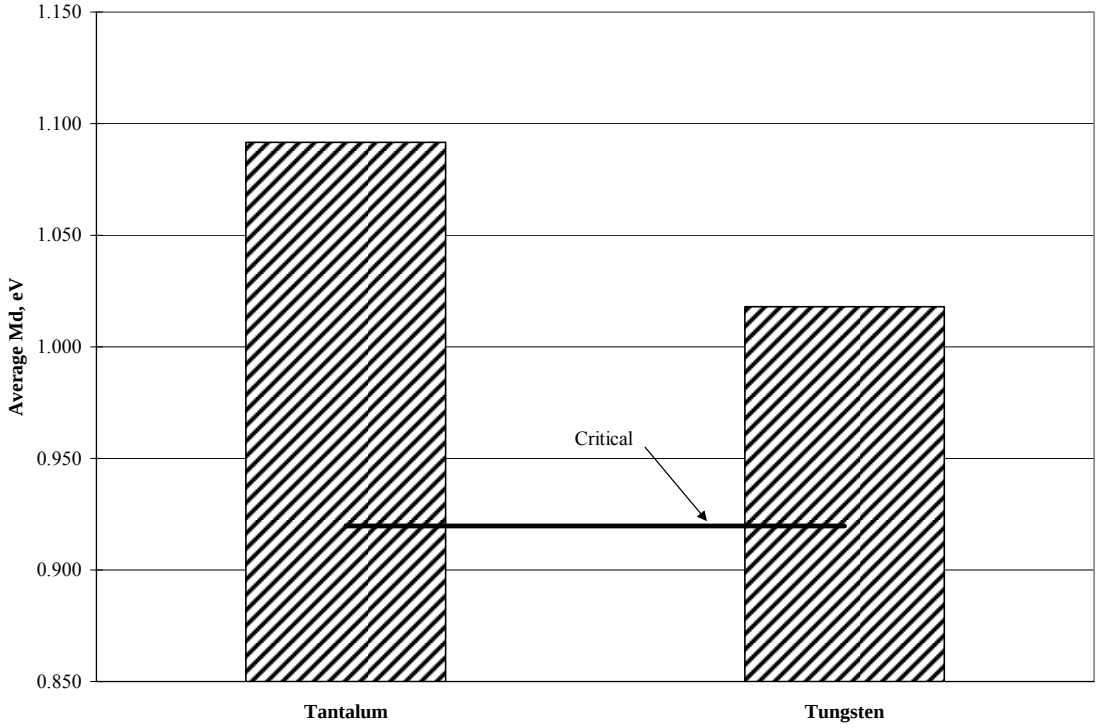

Table 13 Hexagonal close packed elements rhenium and osmium used to enhance radiopacity of quaternary alloy shown in Table 4 and Table 5

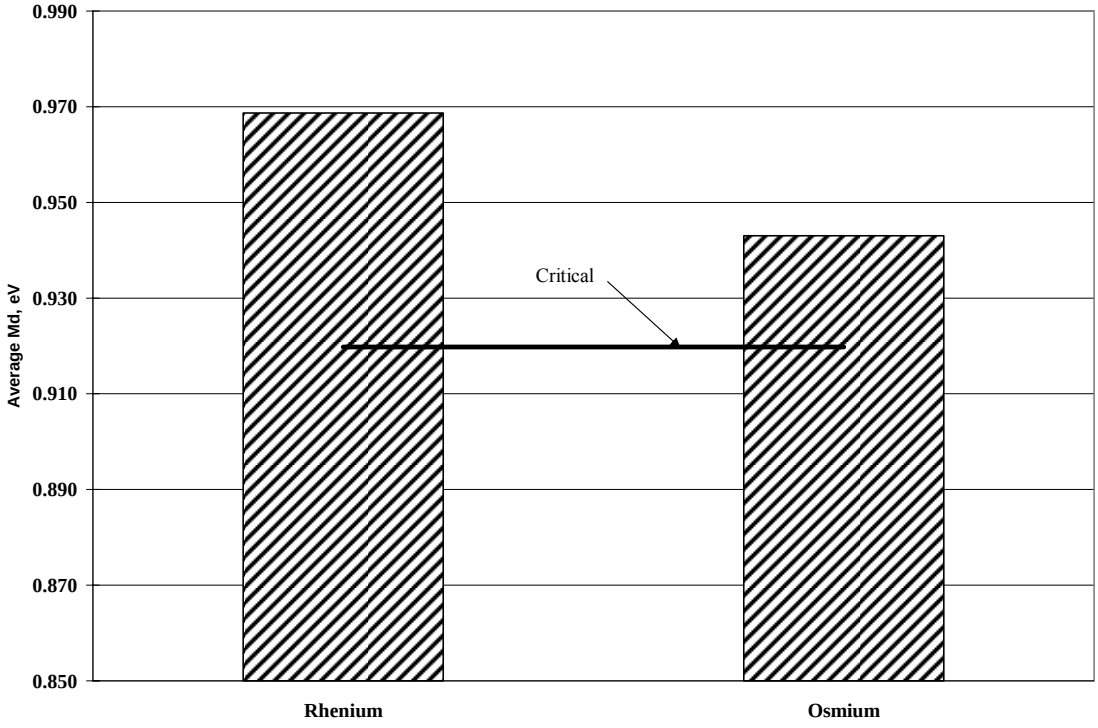

Table 14 Face centred cubic elements iridium, platinum, and gold used to enhance radiopacity of quaternary alloy shown in Table 4 and Table 5

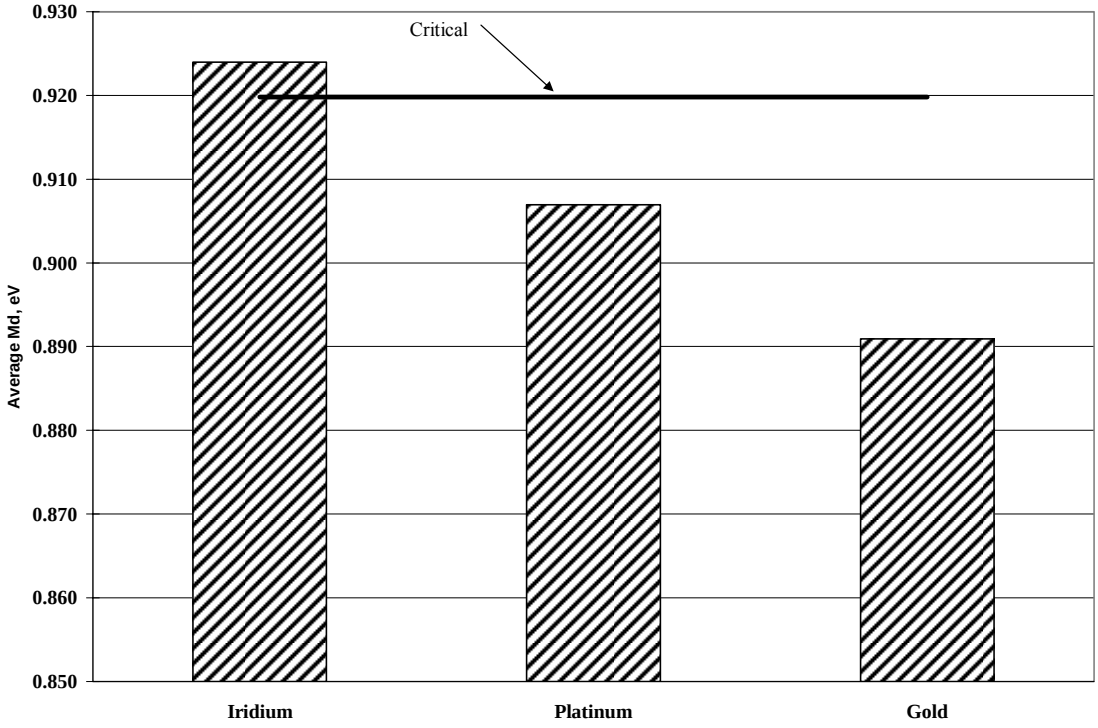

3.4 Strength predictions

Applying the Nordberg equations for tensile and yield strength described in §2.7, Equation 10 (tensile) and Equation 11 (yield), to an alloy meeting ASTM F139 specifications in terms of ferrite content (0wt%) and minimum grain size (0.045mm, or ASTM E112 grain size 5), the result is the same for all pentanary alloys if no consideration is made of the influence of the high-atomic-number alloying elements, i.e., 555MPa tensile strength and 247MPa yield strength. In ASTM F139, the minimum acceptable tensile and yield strength for annealed alloys in either sheet or strip form is shown as 490MPa and 190MPa, respectively.

3.5 Corrosion

Two criteria are applied in ASTM F139-00. Susceptibility to intergranular corrosion is determined by ASTM A262, Practice E, which requires samples to be embedded in copper granules and exposed for 24 hours in equal parts of a boiling solution of hydrated copper sulphate and concentrated sulphuric acid. After exposure, the samples are bent through 180 degrees over a mandrel with a diameter equal to the thickness of the samples, then examined at 20X magnification for cracks indicating sensitisation. For pitting resistance, Equation 12 is applied, thus only chromium and molybdenum contents are considered. For these alloys, with 18wt% chromium and 2.5wt% molybdenum: 18 + 3.3 (2.5) = 26.25, thus the minimum pitting resistance number of 26, as stipulated in ASTM F138 and ASTM F139, is achieved with all the pentanary alloys.

3.6 Results

- Seven high-atomic-number elements were considered for the pentanary element
- All proposed pentanary elements exhibit insufficient radiopacity at 100keV
- Tantalum, tungsten, rhenium, osmium, and iridium exceed the Md(crit) value
- Gold has insufficient solubility in iron to sustain the required level (32.5wt%)
- Platinum meets or exceeds all criteria (except 100 keV radiopacity increase) and is chosen as the alloying element; platinum content is below the level shown in Figure 10 where a secondary phase, Fe_3Pt, may occur in a binary alloy
- Platinum content is well below the level shown in Figure 12 where an intermetallic compound, Cr_3Pt, may occur in a binary alloy
- Strength is adequate; pitting corrosion is acceptable; corrosion testing required

3.7 References

Craig, CH. (2003a), Radisch, HR., Jr., Trozera, TA., Turner, PC., Govier, RD., Vesely, EJ., Jr., Gokcen, NA., Friend, CM., and Edwards, MR. Development of a platinum enhanced radiopaque stainless steel (PERSS®). In: Winters, GL., and Nutt, MJ., *Stainless steels for medical and surgical applications*, *ASTM STP 1438*. Winters, GL., and Nutt, MJ. (eds). Pages 28-38. West Conshohocken, PA: ASTM International. ISBN: 0803134592.

Hubbell, JH. (1997) and Seltzer, SM. *Tables of x-ray mass attenuation coefficients and mass energy-absorption coefficients* (version 1.03). Gaithersburg, MD: National Institute of Standards and Technology. URL: http://physics.nist.gov/xaamdi

Massalski, TD (1990). Cr-Fe (Chromium-Iron). After Kubaschewski. In: Massalski, TB. (ed). *Binary alloy phase diagrams,* (2nd ed). Vol. 2. Pages 1271, 1273. Materials Park, OH: ASM International. ISBN: 0871704048

Moema, JS. (2002) and Paton, R. *The austenitising effect of palladium, platinum and iridium in type 316L stainless steel, Report C3365M.* Randburg, SA: Mintek.

Morinaga, M. (1994), Hashizume, R., and Murata, Y. An electronic approach to the design of ferritic steels for power plants. In: Coutsouradis, D., Davidson, JH., Ewald, J., Greenfield, P., Khan, T., Malik, M., Meadowcroft, DB., Regis, V., Scarlin, RB., Schubert, F., and Thornton, DV. (eds). *Materials for advanced power engineering 1994*. Vol 1. Pages 319-328. Dordrecht: Kluwer. ISBN 079230749

Morinaga, M. (2001a), Murata, Y., and Yukawa, H. Recent progress in New PHACOMP approach. In: Zhao, J-C., Fahrmann, M., and Pollock, TM. (eds). *Materials design approaches and experiences*. Pages 15-27. Warrendale, PA: The Metals Society, ISBN 0873395034

Morinaga, M. (2001b). Personal correspondence. October, 2001.

Nash, P. (1990) and Singleton, MF. Ni-Pt (Nickel-Platinum). In: Massalski, TB. (ed). *Binary alloy phase diagrams,* (2nd ed). Vol. 3. Pages 2841-2845. Materials Park, OH: ASM International. ISBN: 0871704048

Naidu, SVN. (1993), Sriramamurthy, AM., and Rao, PR. Okamoto, H. (eds). *Phase diagrams of binary iron alloys*. Materials Park, OH: ASM International. Pages 444-453. In: Okamoto, H. (ed). (2000). *Desk handbook: phase diagrams for binary alloys*. Page 379. Materials Park, OH: ASM International. ISBN: 0-87170-682-2

Okamoto, H. (1996). *J. Phase Equilibria.* 17(1),. Pages 81-82. In: Okamoto, H. (ed). (2000). *Desk handbook: phase diagrams for binary alloys*. Page 376. Materials Park, OH: ASM International.. ISBN: 0-87170-682-2

Okamoto, H. (1990), Massalski, TB., Swartzendruber, LJ., and Beck, PA. Au-Fe (Gold-Iron). In: Massalski, TB. (ed). *Binary alloy phase diagrams,* (2nd ed). Vol. 1. Pages 367-369. Materials Park, OH: ASM International. ISBN: 0871704048

Okamoto, H. (1990) Fe-Pt (Iron-Platinum). In: Massalski, TB. (ed). *Binary alloy phase diagrams,* (2nd ed). Vol. 2. Pages 1752-1756. Materials Park, OH: ASM International. ISBN: 0871704056

Swartzendruber, LJ. (1990). Fe-Ir (Iron-Iridium). In: Massalski, TB. (ed). *Binary alloy phase diagrams,* (2nd ed). Vol. 2. Pages 1715-1716. Materials Park, OH: ASM International. ISBN: 0871704056

Swartzendruber, LJ. (1983) and Sundman, B. *Bulletin alloy phase diagrams, 4*(4),. Pages 396-399. In: Okamoto, H. (ed). (2000). *Desk handbook: phase diagrams for binary alloys*. Page 369. Materials Park, OH: ASM International. ISBN: 0-87170-682-2

Venkatraman, M. (1990) and Neumann, JP. Cr-Pt (Chromium-Platinum). In: Massalski, TB. (ed). *Binary alloy phase diagrams*, (2nd ed). Vol. 2. Pages 1313-1316. Materials Park, OH: ASM International. ISBN: 0871704056

Chapter 4

EXPERIMENTAL METHODS AND RESULTS

4.1 Introduction

In §3.6, only platinum was identified as meeting all the requirements for use as a single, high-atomic-number substitutional element to maximise the radiopacity of the pentanary when iron is at its minima, as well as meeting several other requirements. Such substitution would potentially increase radiopacity of the pentanary by up to 30%.

As inferred in Chapter 3, a two-pronged experimental approach was devised. The first condition of the research was that a commercial alloy meeting specifications representative of international usage for stainless steel coronary stents would be chosen and that this commercial alloy would be remelted along with a single 'radiopaque' element not previously specified in those, i.e., an element that is not presently allowed. In the second part of the approach, the departure from specification requirements was minimised by allowing the mandatory 'balance' element in the alloy, iron, to decrease, while augmenting the remaining mandatory elements that are diminished upon addition of platinum. The latter condition was possible because iron could be substantially reduced within the constraints of the specification, i.e., under the Unified National Standard adopted by ASTM International and in wide use elsewhere, as long as iron remains the principal element in the resulting alloy, the alloy is considered steel.

The experimental work described below is meant to address the core problem of increasing radiopacity while maintaining substantial adherence to the specification context that represents the technological and historical basis for using austenitic stainless steel as implants, especially fabrication of balloon-expandable coronary stents.

Adherence to internationally-accepted standards for austenitic stainless steel used in fabricating balloon-expandable coronary stents is based on ensuring: (a) no ferromagnetism; (b) freedom from embrittling phases; (c) adequate mechanical properties; and (d) adequate corrosion properties.

The bulk of the research has been carried out using small ingots, typically 100-350g, made in a button furnace. Due to the expense of the raw materials, especially platinum, and the number of ingots required, producing small ingots was the preferred approach. These experiments are described in three stages: (a) a proof-of-concept stage, adding up to 5wt% platinum to a commercial UNS S31673 alloy, (b) a second stage meant to more thoroughly analyse metallurgical and radiological properties of low-radiopacity alloys, adding up to 10wt% platinum to a UNS S31673 alloy, and (c) a third stage focussed on determining if overall radiopacity goals can be met within the resulting microstructures, adding up to 35wt% platinum to a commercial UNS S31673 alloy.

A pilot production effort was also undertaken, with ingot sizes on the order of 50kg, applying manufacturing processes comparable to commercial practice, i.e., vacuum induction and vacuum arc remelt furnaces. As with the 0-10wt% platinum button furnace ingots, the focus was on producing ingots that lead to products that conform to ASTM F139, with the exception of added platinum, which are comparable in quality to commercial UNS S31673 alloys. These ingots could either be made directly into seamless tubing or be rolled into foil that could in turn be made into welded tubing. While this research did not entail making either type of tubing or fabricating stents from those, the rolling processes are ancillary to this research since ASTM F139, which describes wrought products, was the basis of the final testing of these products. These pilot manufacturing efforts culminate in production and comprehensive analysis of

several 5-6wt% platinum alloys and one 30wt% platinum alloy, here described as 'conforming' alloys, to the full spectrum of requirements outlined in ASTM F139-00.

Tubing made from early versions of products of the pilot production effort, a conforming 5wt% platinum alloy and a non-conforming 30wt% platinum alloy, the latter alloy one in which nickel was substantially below the minimum required by ASTM F139, were analysed by transmission electron microscopy and by energy dispersive spectroscopy. No tubing was made from the conforming 30wt% platinum alloy, a small 300g ingot derived from a larger non-conforming 30wt% platinum alloy.

4.2 Conforming, proof-of-concept button melts (1-5wt% platinum)

4.2.1 Introduction and approach

The initial efforts to make a platinum-containing alloy by melting a UNS S31673 alloy, Carpenter Technology's BioDur 316LS, was meant to show that platinum would go into solution with the commercial alloy as a fully austenitic stainless steel and that no unexpected precipitates would form. The New PHACOMP method, binary diagrams and Schaeffler diagrams, and the Nordberg equations were used as modelling tools.

4.2.2 Experiment

Button furnace samples were made by adding nominally 1wt%, 2wt%, 3wt%, 4wt%, and 5wt% platinum to BioDur® 316LS (Table 15).

Table 15 Preliminary alloys containing platinum plus base UNS S31673 alloy (BioDur® 316LS); (all results in wt%)

Target	Cr	Fe	Ni	Mo	Pt
BioDur® 316LS	17.50	62.29	14.71	2.85	
1wt% Pt	17.27	61.76	14.54	2.83	1.06
2wt% Pt	17.17	61.09	14.28	2.81	2.09
3wt% Pt	17.02	60.45	14.14	2.82	2.97
4wt% Pt	16.92	59.86	13.94	2.80	3.96
5wt% Pt	16.74	59.36	13.75	2.75	4.94

BioDur® 316LS rod conforming to ASTM F138-00 was used as the base material. One ingot was remelted without additions of high-atomic-number elements so it could be comparably processed with those samples containing varying amounts of platinum.

The ingots, each approximately 100 grams, were prepared in a vacuum arc button furnace, capable of up to approximately 500 grams, with a non-consumable thoriated tungsten anode and a water-cooled copper hearth, Figure 15. The button furnace was loaded with the raw materials, evacuated, and then backfilled to approximately 0.033 MPa with argon.

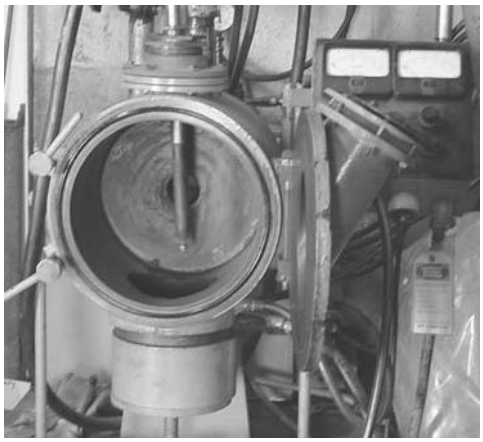

Figure 15 Vacuum arc button furnace used to cast small austenitic stainless steel ingots (United States Department of Energy, Albany Research Centre, Albany, Oregon)

The resulting ingots were milled to produce parallel surfaces in the thickness direction and corners were rounded in preparation for rolling. The samples were placed in a furnace at room temperature and slowly brought to 875°C (2.5 hours), then heated rapidly to a rolling temperature of 1150°C to 1250°C (3.0 hours). The samples were at approximately 1200°C at the commencement of rolling in a two-high mill (Figure 16). From an initial thickness of approximately 8-10mm, the samples were rolled to 3.0mm. The mill settings were reduced 15% for each pass; samples were given a five-minute

reheat between passes. After the final rolling mill pass, all samples were flattened on a forge press, Figure 17, annealed at 1000°C for fifteen minutes, and water quenched.

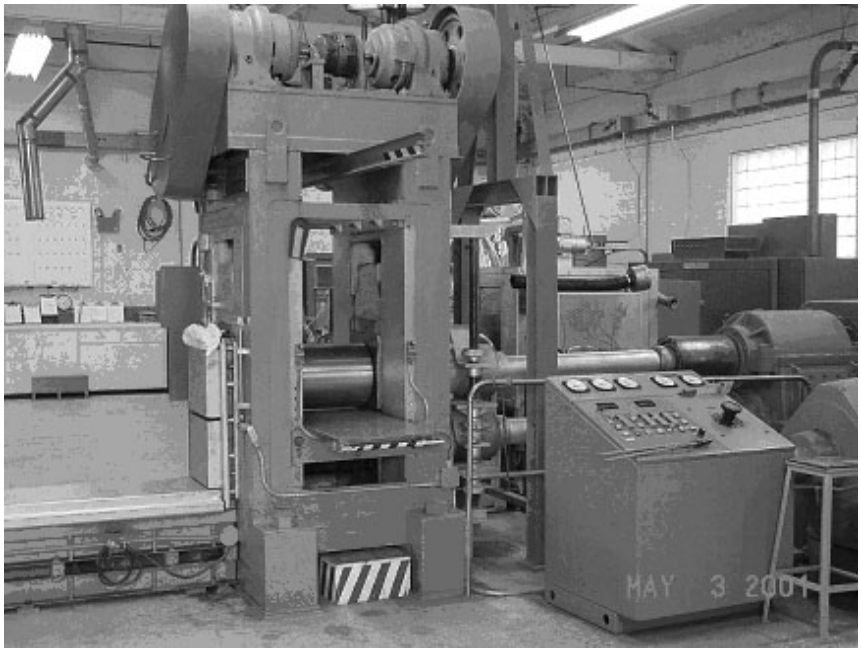

Figure 16 Two-high rolling mill used to hot-roll austenitic stainless steel plate (United States Department of Energy, Albany Research Centre, Albany, Oregon)

Figure 17 Forge used to upset cast austenitic stainless steel ingots
(United States Department of Energy, Albany Research Center, Albany, Oregon)

4.2.3 Results

4.2.3.1 X-ray diffraction

X-ray diffraction measurements using an automated Philips x-ray diffractometer were made on all samples, which were final polished with diamond paste. A copper-anode x-ray tube was used, operated at 45kV and 35mA, using a variable divergence slit, vertical goniometer, diffracted beam monochromator and scintillation counter. Phase content determinations were made from x-ray diffraction step scans collected over a two-theta angular range of 5-80 degrees using a 0.02 degree step size and a counting time of 2 seconds per step. Phase identification was made using x-ray diffraction patterns contained in the International Centre for Diffraction Data® Powder Diffraction File (ICDD, 2000). The resulting chemical composition of the base alloy

and the five alloys containing platinum, shown in Table 15, are included in Table 16, where they are combined with x-ray diffraction results.

Table 16 Preliminary alloys containing platinum plus base UNS S31673 alloy (wt%)

Target	Cr	Fe	Ni	Mo	Pt	XRD
BioDur® 316LS	17.50	62.29	14.71	2.85		fcc only
1wt% Pt	17.27	61.76	14.54	2.83	1.06	fcc only
2wt% Pt	17.17	61.09	14.28	2.81	2.09	fcc only
3wt% Pt	17.02	60.45	14.14	2.82	2.97	fcc only
4wt% Pt	16.92	59.86	13.94	2.80	3.96	fcc only
5wt% Pt	16.74	59.36	13.75	2.75	4.94	fcc only

As shown in Table 16, the primary phase in each alloy remained face centred cubic (fcc). No additional phases were found in either the base UNS S31673 alloy, BioDur® 316LS, or in any of the five alloys having platinum added to the base alloy.

4.2.3.2 Schaeffler diagram

Using the chemical compositions shown in Table 15 and Table 16, Schaeffler diagrams were constructed for the alloys. These diagrams are shown in Figure 18.

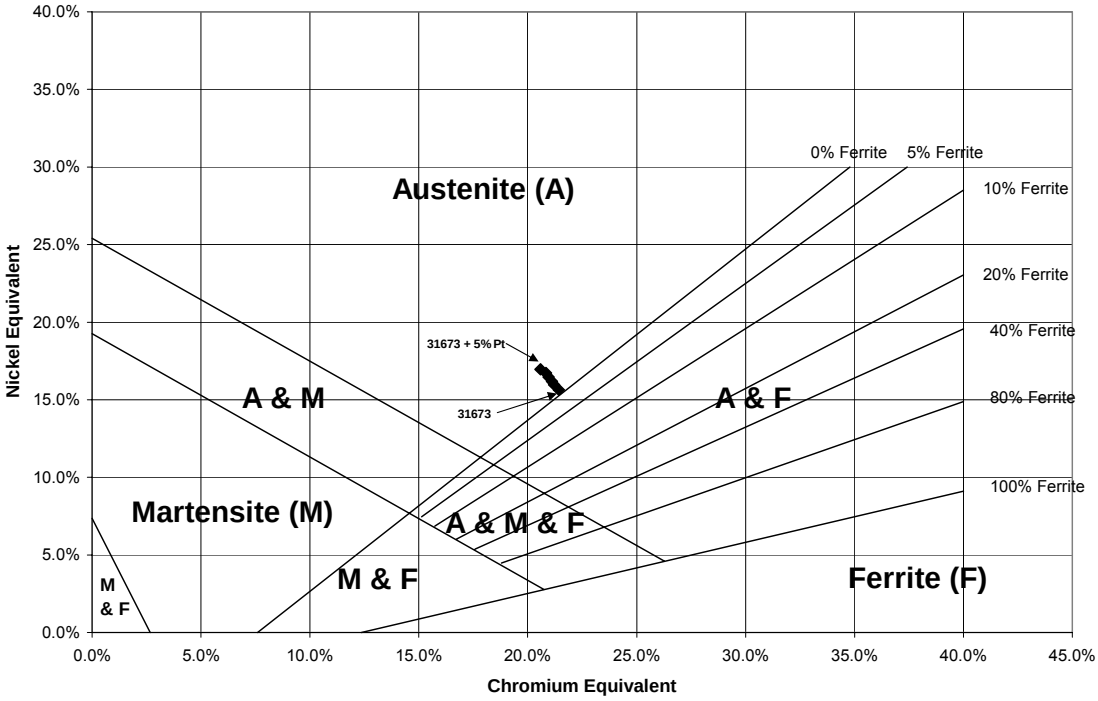

Figure 18 Schaeffler diagram for preliminary alloys containing platinum

The Schaeffler diagram for the face centred cubic alloying element platinum, Figure 18, based on approximately two parts platinum being equivalent to one part nickel, indicates the platinum-containing alloys become more strongly austenitic as platinum is increased from the base UNS S31673.

4.2.3.3 New PHACOMP

Using the chemical compositions shown in Table 15 and Table 16, a New PHACOMP table was constructed for the alloys. This table is shown in Table 17.

Table 17 New PHACOMP results for preliminary alloys containing platinum
(Md critical set at 0.920eV, 1100°C)

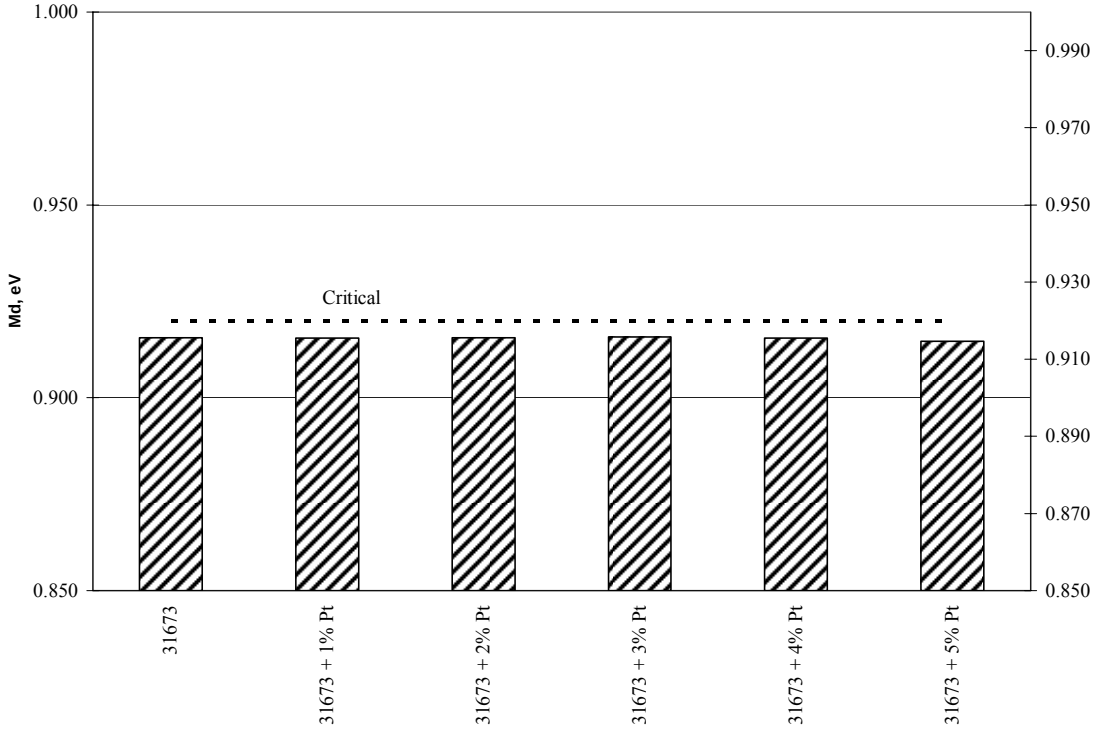

In Table 17, the Md(critical) was set at 0.920eV and does not interact with the alloys from base through 5wt% platinum.

4.2.3.4 Mechanical properties

Both calculated and experimental tensile and yield strength for the base and platinum-containing alloys described in Table 15 are shown in Table 18. The Nordberg equations, Equation 10 (tensile) and Equation 11 (yield), were used to obtain calculated results; carbon was assumed to be 0.016wt%, grain size 0.0449mm, and ferrite nought. Experimental data were obtained using a standard servohydraulic tensile test system (Instron) with a 2500kg load cell, a one-inch (25.4mm) extensometer, and 0.5mm/min crosshead speed. Temperature was 21°C; humidity 0%. Nominal sample width was 0.250in (6.35mm) and nominal thickness 0.100in (2.54mm).

Table 18 Strength calculations for preliminary 0-5wt% platinum in UNS S31673
(C = 0.016wt%; ASTM grain size 6 = 0.0449mm; ferrite = 0wt%)

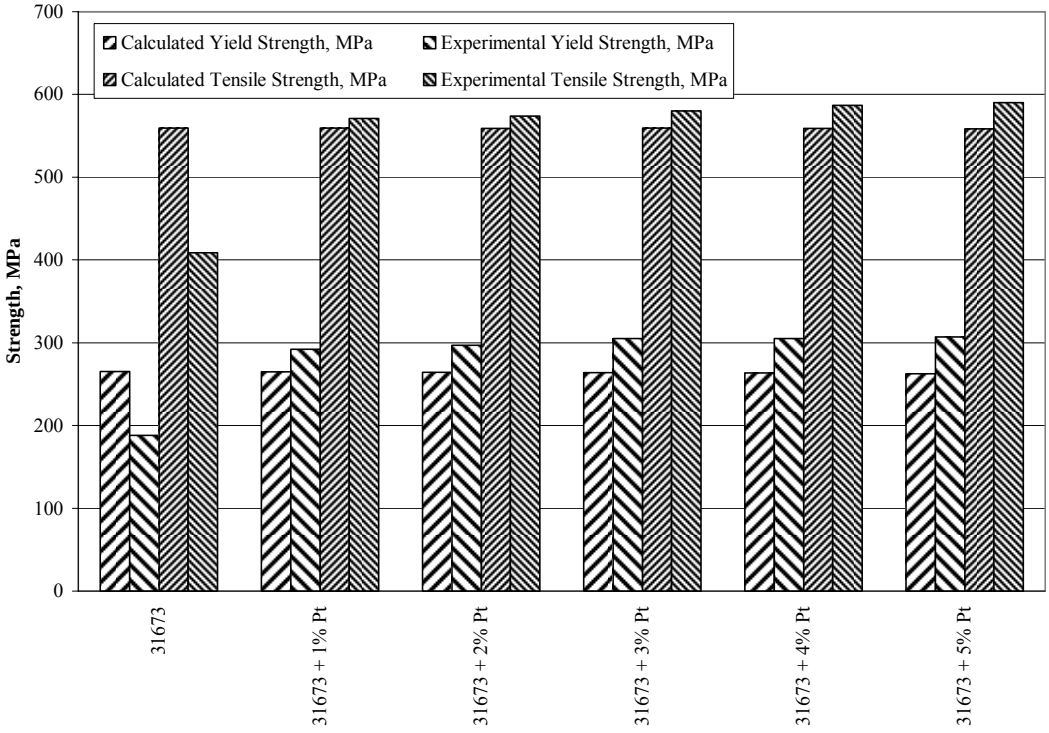

At 409MPa, the tensile strength of the base sample was substantially below the minimum (490Mpa) required by ASTM F139-00; yield strength (188Mpa) was almost equal to the minimum required (190Mpa). However, the calculated and experimental tensile and yield data for all five samples containing platinum corresponded well, with the experimental data slightly greater than found by the Nordberg equations, indicating the addition of platinum increases both tensile and yield strength. Table 19 repeats the experimental tensile and yield strength data and provides elongation and hardness data. Increase in strength with platinum content is further indicated by the hardness increases.

Table 19 Mechanical and physical property data for preliminary 0-5wt% platinum

Sample	ASTM F139-00	Base 31673	1wt% Pt	2wt% Pt	3wt% Pt	4wt%Pt	5wt% Pt
UTS MPa	490	409	571	574	580	587	590
YS MPa	190	188	292	297	305	305	307
Elong-ation %	40 min.	62	62	61	60	63	63
Hardness Rockwell B	95 max.	70.9	76.3	77.8	77.7	77.4	79.2

4.2.3.5 Corrosion

The pitting resistance equivalence number calculations, Equation 12, for the alloys in Table 15 are shown in Table 20. Note all but the 5wt% platinum alloy are acceptable.

Table 20 Pitting resistance equivalence number calculation for 0-5wt% platinum alloys

Target	Equation 12	Result
BioDur® 316LS	Σ (17.50wt% Cr + 3.3 (2.85wt% Mo)	PREN = 26.9 (≥ 26 req. by ASTM F139)
1wt% Pt	Σ (17.27wt% Cr + 3.3 (2.83wt% Mo)	PREN = 26.6 (≥ 26 req. by ASTM F139)
2wt% Pt	Σ (17.17wt% Cr + 3.3 (2.81wt% Mo)	PREN = 26.4 (≥ 26 req. by ASTM F139)
3wt% Pt	Σ (17.02wt% Cr + 3.3 (2.82wt% Mo)	PREN = 26.3 (≥ 26 req. by ASTM F139)
4wt% Pt	Σ (16.92wt% Cr + 3.3 (2.80wt% Mo)	PREN = 26.2 (≥ 26 req. by ASTM F139)
5wt% Pt	Σ (16.74wt% Cr + 3.3 (2.75wt% Mo)	PREN = 25.8 (< 26 req. by ASTM F139)

4.2.4 Summary

The element platinum was used to demonstrate that the concepts derived from the solubility approach are predictable utilising a combination of binary phase diagrams, Schaeffler diagrams, and New PHACOMP. In particular, when x-ray diffraction results

from 1-5wt% of each alloy are compared to New PHACOMP Md(avg) results for each of the alloys, the Md(crit) set at 1100°C where sigma phase in these alloys would be represented was well above the maximum Md(avg) for any of the alloys. This appears to support use of Md(avg) and Md(crit) as valid indicators and thus the utility of New PHACOMP as a predictive method for platinum-containing austenitic stainless steels.

For the platinum-containing alloys, strength measurements for the five samples were in relatively close agreement with the predicted values from the Nordberg equations, discounting the base alloy, which was anomalous. Average calculated yield strength values lagged the average experimental values by approximately 13.5%. Average calculated ultimate tensile strength values lagged the average experimental values by approximately 1.5%.

Discounting the base alloy, experimental data for the 5wt% platinum-containing alloy was found to be approximately 5% greater than the 1wt% platinum alloy for yield strength and approximately 3% greater for ultimate tensile strength. This indicates strength increases with platinum content. As noted above, the hardness values shown in Table 19 confirm this trend, increasing approximately 1% from 1-5wt% platinum.

The pitting resistance equivalent number for the 5wt% platinum alloy was slightly less than required by ASTM F139-00, indicating a need to add chromium and molybdenum to the alloy during the initial melting of the BioDur® 316LS with the platinum so this requirement will be met by all alloys processed in this manner.

4.3 Conforming, low-radiopacity button melts (0-10wt% platinum)

4.3.1 Introduction and approach

Preparing UNS S31673 alloys from elements rather than adding platinum to a commercial UNS S31673 alloy was undertaken in this second phase, also using a button

furnace, similar to that described in §4.2.2. The objectives were to increase radiopacity to the point it could be measured with some certainty and to complete a more thorough analysis of the resulting alloys. This phase has been described in Craig *et al* (2003).

4.3.2 Experiment

Five ingots, four containing added platinum, were prepared in a vacuum button furnace, backfilled at approximately 0.33MPa argon, using a triple-melt procedure wherein the cooled alloy is turned over and remelted so as to increase mixing. The ingots were cleaned, forged, cold-rolled to two thicknesses (1.27mm; 0.127mm), and annealed at 1050°C, followed by a water quench. A commercial UNS S31673 alloy, Sandvik Bioline® 316LVM, was used as a reference alloy; this alloy was remelted in the button furnace to simulate conditions seen by the other alloys. Table 21 provides the full chemical composition of these five alloys, which comply compositionally with ASTM F139-00, with the exception of having added platinum.

Table 21 Chemical composition of UNS S31673 and platinum-containing alloys, 0 - 10wt% (shown in weight percent)(Craig *et al*, 2003)

Element	ASTM F139-00	0wt% Pt	1wt% Pt	3wt% Pt	6wt% Pt	10wt% Pt
Pt	Not allowed	-	1.21	3.04	6.46	10.14
Cr	17-19	19.70	18.20	18.30	18.40	19.20
Ni	13-15	13.57	13.5	13.71	13.52	13.87
Mo	2.25-3.0	2.62	2.55	2.55	3.07	3.01
Mn	2.0 max.	1.38	1.32	1.50	1.55	1.56
Cu	0.5 max.	0.055	<0.005	<0.005	<0.005	<0.005
C	0.030 max.	0.018	0.014	0.013	0.016	0.018
N	0.10 max.	0.028	0.034	0.099	0.037	0.051
Si	0.75 max.	0.25	0.08	0.08	0.08	0.08
P	0.025 max.	<0.001	0.004	0.001	0.001	0.004
S	0.010 max.	0.002	0.003	0.002	0.002	0.004

4.3.3 Results

4.3.3.1 X-ray diffraction

X-ray diffraction was accomplished similar to that described in §4.2.3.1. Only austenite was found; any ferrite may have been masked by the background radiation. These results are shown in Table 22.

Table 22 UNS S31673 and platinum-containing alloys, 0 - 10wt% (Craig *et al*, 2003)

Target	Cr	Fe	Ni	Mo	Pt	XRD
0wt% Pt	19.70	62.38	13.57	2.62	-	fcc only
1wt% Pt	18.20	63.08	13.50	2.55	1.21	fcc only
3wt% Pt	18.30	60.71	13.71	2.55	3.04	fcc only
6wt% Pt	18.40	56.86	13.52	3.07	6.46	fcc only
10wt% Pt	19.20	52.06	13.87	3.01	10.14	fcc only

4.3.3.2 Schaeffler diagram and ferrite measurements

The austenitic nature of the five samples described in Table 21 is shown in the Schaeffler diagram, Figure 19. Only the base alloy is projected to contain ferrite since the austenitising effect of the platinum drives the alloy further into the austenitic range.

Ferrite content was measured in the as-cast, annealed, and cold-rolled conditions for the five samples described in Table 21 using a Fischer Feritscope MP30. This instrument measures the degree of magnetism in the alloy, converting to ferrite content. For the 0wt% platinum alloy, using the Feritscope MP 30, approximately 3.9% ferrite was found in the as-cast condition, compared with approximately 4% ferrite shown on the Schaeffler diagram. For the same alloy, approximately 0.7% ferrite was found in the cold-rolled condition. No ferrite was detected for any alloy in the annealed condition.

Figure 19 Schaeffler diagram for UNS S31673 and platinum-containing alloys, 0 - 10wt% (Craig *et al*, 2003)

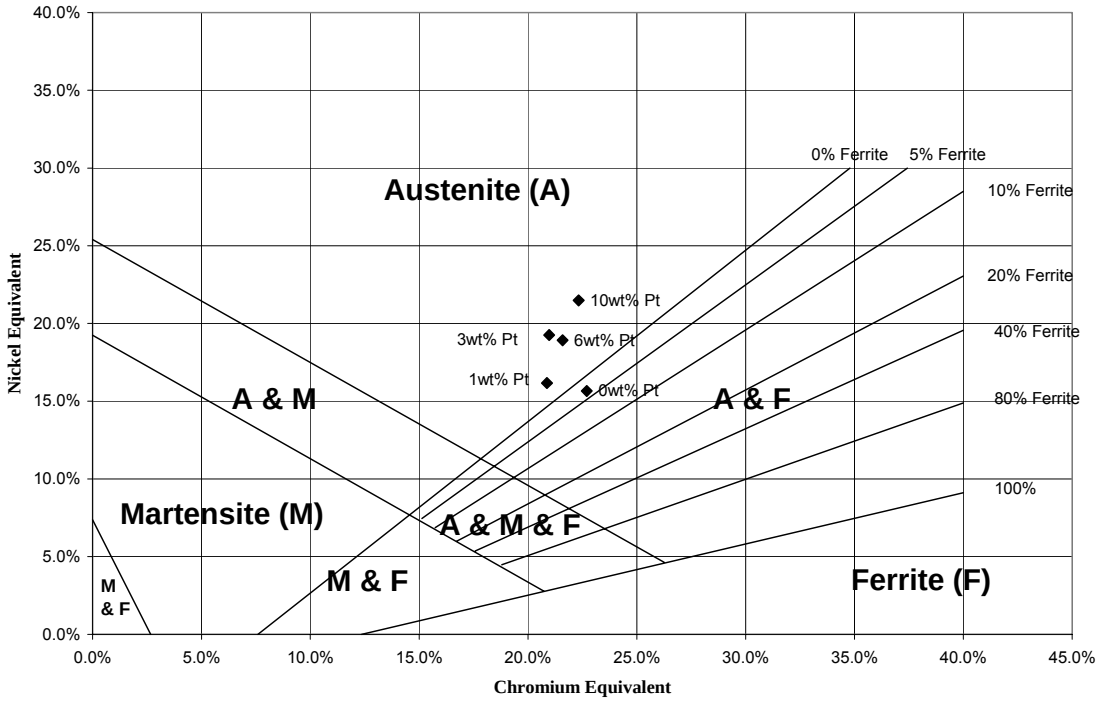

4.3.3.3 New PHACOMP and microscopic analysis

The New PHACOMP results for the 0-10wt% platinum alloys described in Table 21 are shown in Table 22; the Md(crit) is set at 1100°C, some 50°C above the annealing temperature. No sigma-type precipitates are predicted; the Md(avg) of all alloys is well below Md(crit) and becomes more stable with the addition of platinum, as expected since the austenitising effect of platinum is reflected in a lowering of the Md(avg).

Table 23 New PHACOMP results for UNS S31673 and platinum-containing alloys, 0 - 10wt% (Md critical set at 0.920eV, 1100°C)

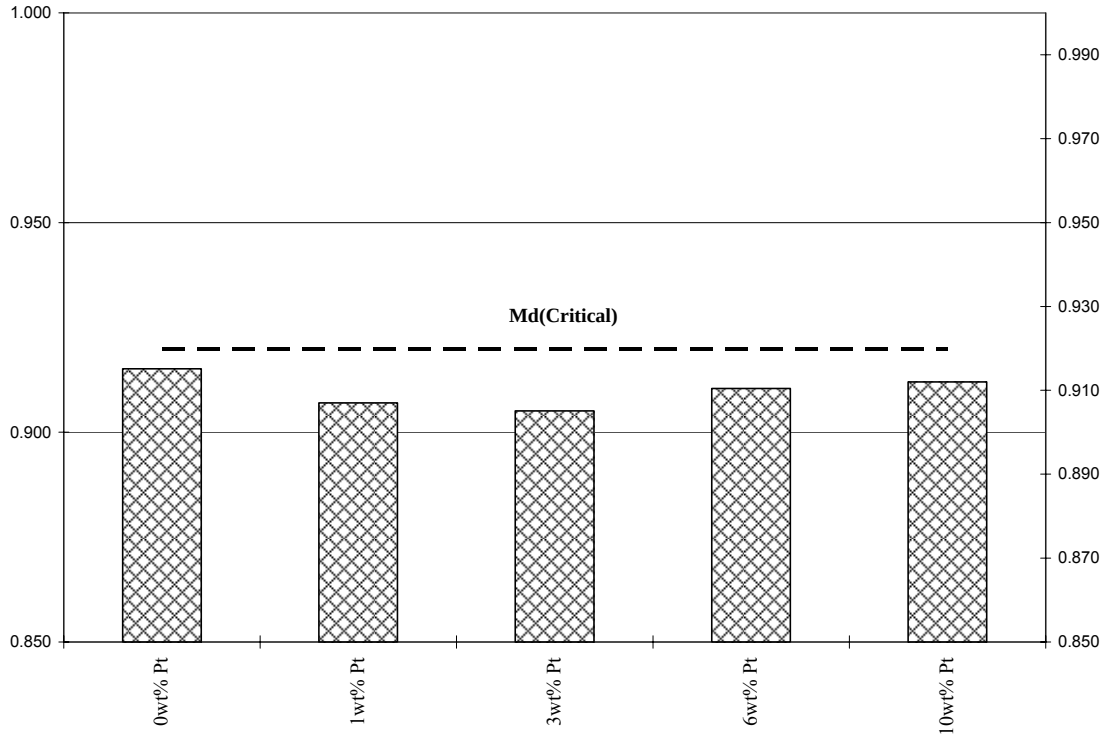

Both optical and transmission electron microscopy results, reported in Craig *et al* (2003), indicate an absence of embrittling phases at the extremes of these five alloys, i.e., in the base alloy and in the 10wt% platinum alloy. Optical micrographs are shown in Figure 20 (0wt% platinum) and Figure 21 (10wt% platinum) for the as-cast structures; bright field micrographs of the annealed structures are shown in Figure 22 (0wt% platinum) and in Figure 23 (10wt% platinum). Other than the expected fine aluminides and silicates typical of stainless steel and allowed by ASTM F139-00, both optical and bright field micrographs indicate the 10wt% platinum alloy contained coarse manganese-chromium oxides; no further investigation of these precipitates was pursued since these are considered typical of the manufacturing process for stainless steel.

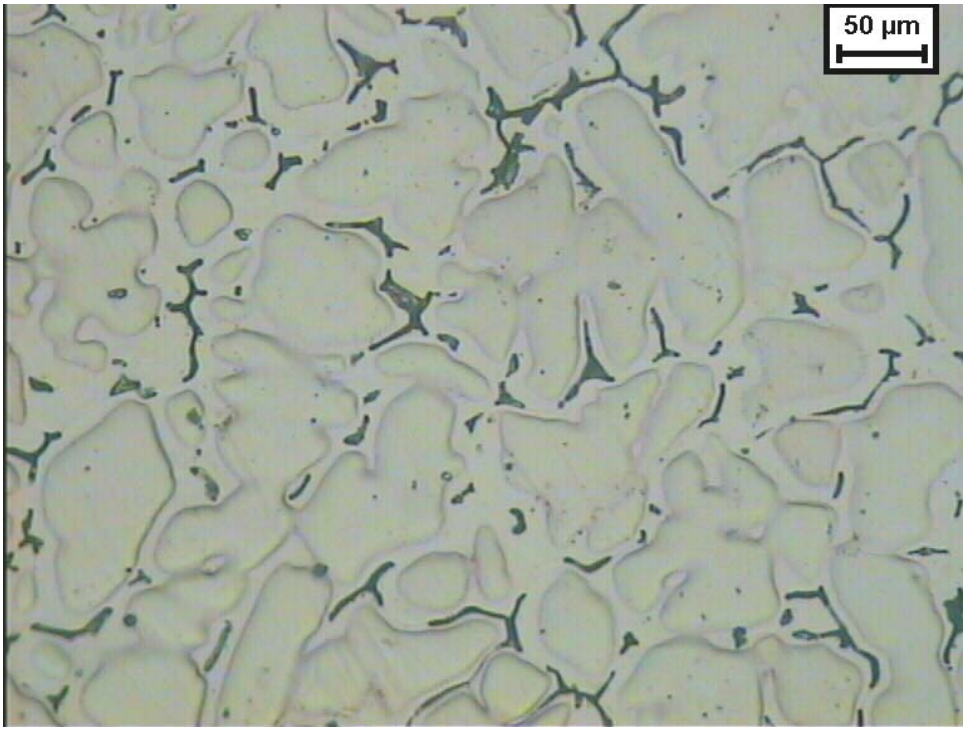

Figure 20 As-cast microstructure of 0wt% platinum showing cellular austenite (light areas) and skeletal ferrite (dark areas). Electrolytically etched in oxalic acid. (Craig *et al*, 2003)

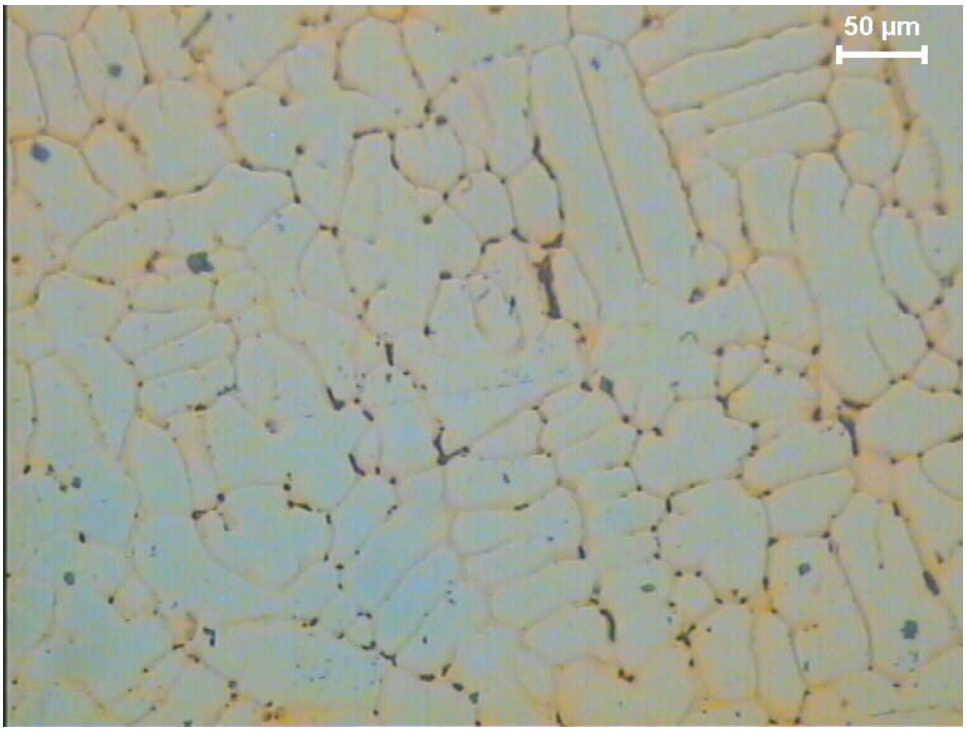

Figure 21 As-cast microstructure of 10wt% platinum showing cellular austenite (light areas) and skeletal ferrite (dark areas). Electrolytically etched in oxalic acid. (Craig *et al*, 2003)

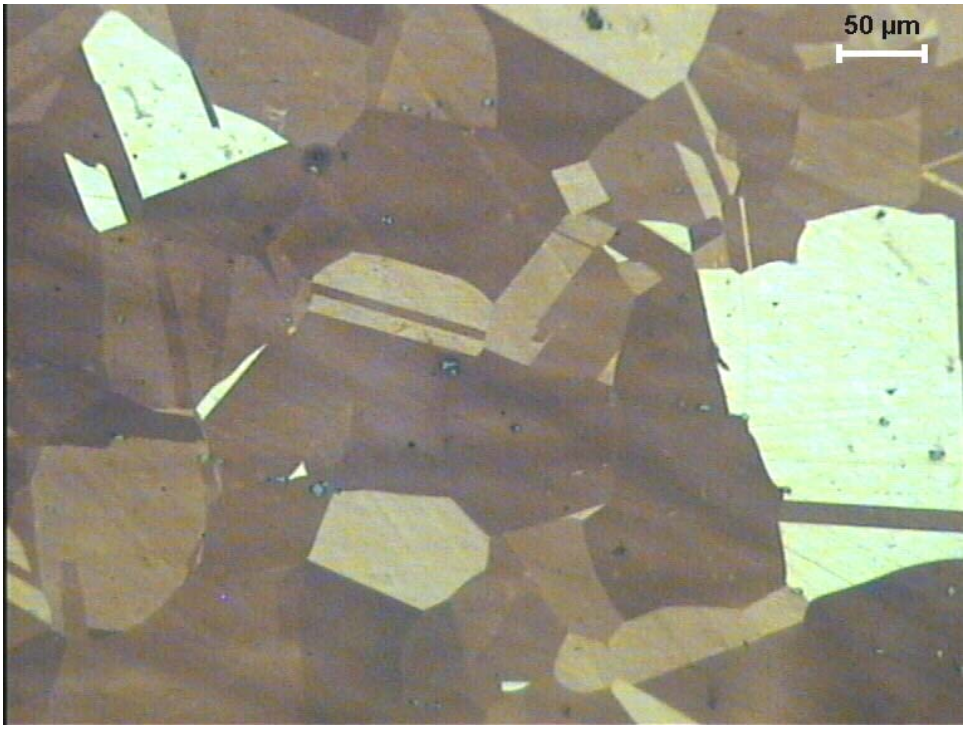

Figure 22 Annealed microstructure of 0wt% platinum sample showing equi-axed grains of austenite. Etched in Behara's No. 3. (Craig *et al,* 2003)

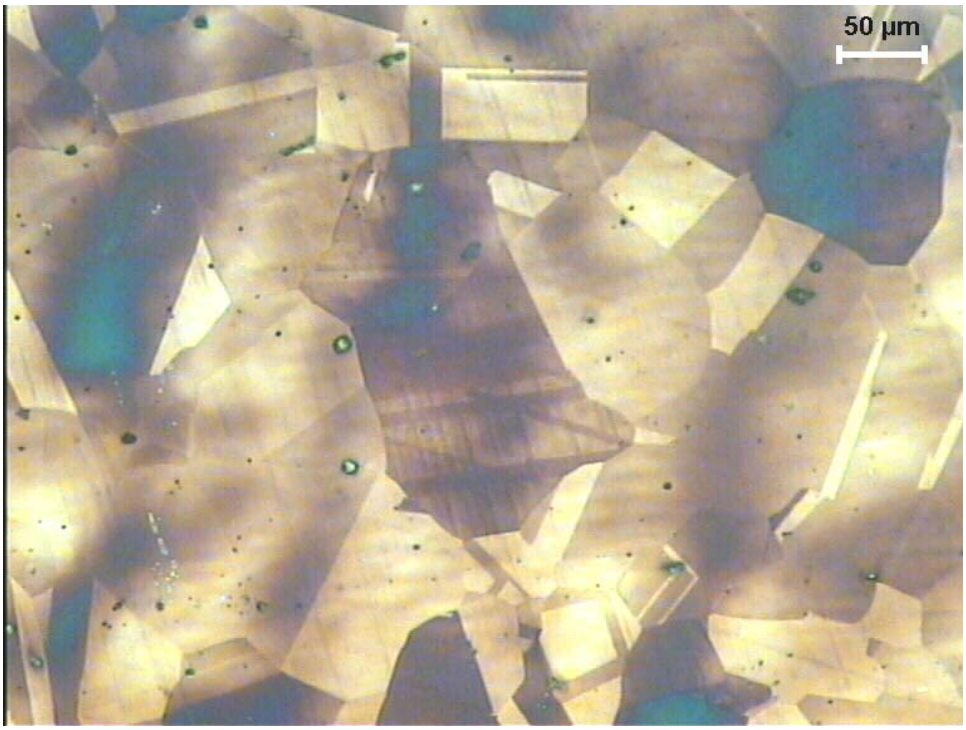

Figure 23 Annealed microstructure of 10wt% platinum sample showing equi-axed grains of austenite. Etched in Behara's No. 3. (Craig *et al,* 2003)

4.3.3.4 Mechanical properties

Calculated and experimental ultimate tensile and yield strengths for the 0-10wt% platinum specimens described in Table 21 are shown in Table 24. The experimental data were obtained in a manner similar to that described in §4.2.3.4; calculations were by application of the Nordberg equations, Equation 10 (tensile) and Equation 11 (yield), using the assumed values as noted in §4.2.3.4, i.e., grain size 0.0449mm and 0% ferrite (since the tensile specimens were all tested in the fully annealed condition). Physical property data are shown in Table 25, along with experimental data shown in Table 24.

Table 24 Strength calculations for UNS S31673 and platinum-containing alloys (0-10wt%)

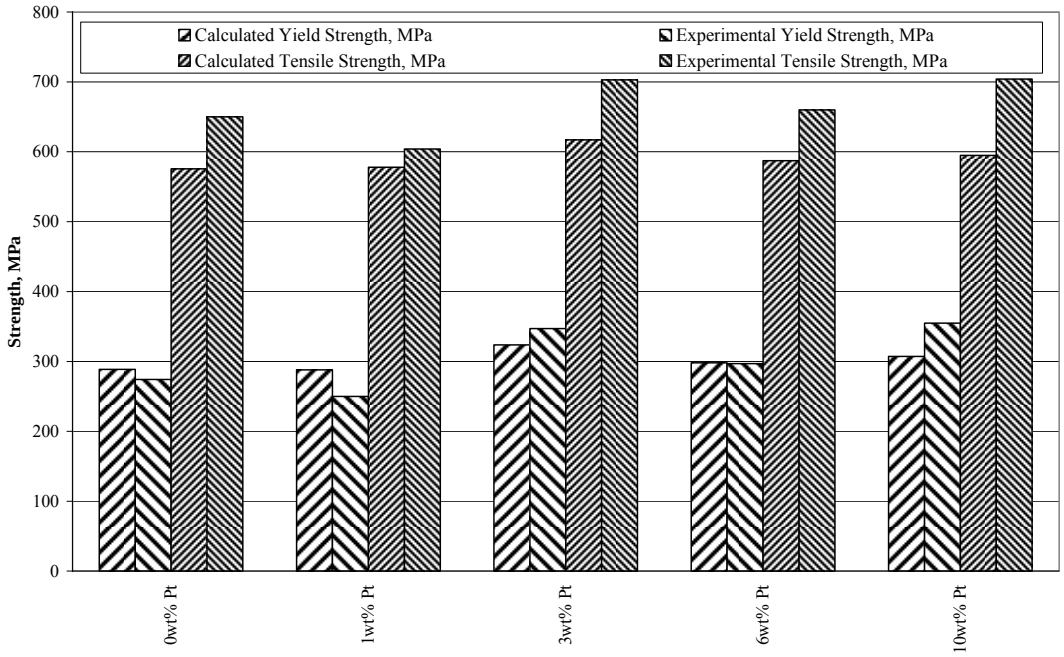

Table 25 Mechanical and physical property data for UNS S31673 and platinum-containing alloys (0-10wt%)(Craig *et al*, 2003)

Sample	ASTM F139-00	0wt% Pt	1wt% Pt	3wt% Pt	6wt%Pt	10wt% Pt
UTS MPa	490	650	604	703	660	704
YS MPa	190	274	250	347	297	355
Elongation %	40 min.	60	55	55	67	52
Hardness Rockwell B	95 max.	62.5	73.5	73.9	70.8	74.2

In Table 24, average calculated yield strength lags experimental yield strength by approximately 1%. The average calculated ultimate tensile strength lags the experimental ultimate tensile strength by 18%. In Table 25, the 10wt% platinum alloy is approximately 8% greater in ultimate tensile strength than the 0wt% platinum alloy (base); yield strength at 10wt% platinum is almost 30% greater than at 0wt% platinum. Discounting the 6wt% platinum hardness reading, which appears anomalous, as does its elongation, a gradual decline in elongation is accompanied by a similar increase in hardness from 0wt% to 10wt% platinum; both accompany the increases in strength.

4.3.3.5 Corrosion

No corrosion testing was completed on these alloys. The calculated pitting resistance equivalent number is as shown in Table 26. All alloys exceeded the ASTM F139-00 requirement of being equal to or greater than 26.

Table 26 Pitting resistance equivalence number calculation for 5-6wt% platinum alloys (top row: IVT 37, second: IVT 38; third: IVT 66; fourth: IVT 78; fifth: IVT 79; bottom: BioDur® 316LS)

Target	Equation 12	Result
0wt% Pt	Σ (19.70wt% Cr + 3.3 (2.62wt% Mo)	PREN = 28.3 (≥ 26 req. by ASTM F139)
1wt% Pt	Σ (18.20wt% Cr + 3.3 (2.55wt% Mo)	PREN = 26.6 (≥ 26 req. by ASTM F139)
3t% Pt	Σ (18.30wt% Cr + 3.3 (2.55wt% Mo)	PREN = 26.7 (≥ 26 req. by ASTM F139)
6t% Pt	Σ (18.40wt% Cr + 3.3 (3.07wt% Mo)	PREN = 28.5 (≥ 26 req. by ASTM F139)
10wt% Pt	Σ (19.20wt% Cr + 3.3 (3.01wt% Mo)	PREN = 29.1 (≥ 26 req. by ASTM F139)

4.3.3.6 Radiopacity

4.3.3.6.1 General

Both calculated and experimental radiopacity data are required because the calculated or 'theoretical' radiopacity data used to predict outcomes is based on single-beam theory, §2.4, rather than the wide-beam (white radiation, or bremsstrahlung) concepts applicable to industrial (and medical) x-ray machines such as are used here. A half-value-layer approach, described below, allows a narrowing of the wide-beam radiation, termed 'hardening' the beam, to better approximate the radiopacity results obtained with single-beam radiation.

As shown in Equation 5, component thickness has a dramatic effect on radiopacity, thus only foil with a thickness comparable to that of a typical tube from which a balloon-expandable coronary stent is made is of value for comparative purposes. To obtain such data, all five of the 0-10wt% platinum alloys were rolled in a jewellers' mill in an attempt to approximate 0.127mm, which is typical of stent tubing wall thickness.

4.3.3.6.2 Methodology

The overall intensity of an x-ray white radiation (bremsstrahlung) spectrum is the area under the spectral curve. Intensity is determined by (a) peak kilovoltage, (b) tube (filament) current, (c) atomic number of the target material, and (d) filtration. Peak kilovoltages used during deployment of coronary stents are typically 80kV to 100kV. Medical x-ray systems typically use three-phase or 'constant potential' generators; the industrial x-ray system used here, the Pantak Model HF 420CP, is such a system and generates a spectrum typical of a medical x-ray system; this system, located in the Radiation Physics Division at United States National Institute of Standards and Technology, in Gaithersburg, Maryland, has the advantage that its spectrum has been well-characterised. A tungsten target is used and x-rays formed at the target exit the tube through a 7.0mm beryllium window, which allows unimpeded flow of the radiation above approximately 10keV and allows the vacuum in the tubehead to be maintained. The inherent filtration of the spectrum is thus defined by the tungsten target and the beryllium window. A second industrial x-ray system, a Philips Model MG 161, also a constant potential generator with a tungsten target and a 1.0mm beryllium window (and, normally, a 3.0mm aluminium inherent filter, which was removed for this work), was used to obtain film data since no film processing capabilities were available at National Institute of Standards and Technology; this system is located in the non-destructive testing facility at United States Naval Surface Warfare Centre, located in Carderock, Maryland, along with a Kodak Model B automatic film processor.

The approach to determine radiopacity that has been used here is that defined in the ASTM International standard for radiopacity of plastics used for medical devices, ASTM F640-79 (reapproved 2000); no comparable standard was found for metals.

Additional inherent filtration of 2.5mm aluminium, UNS A91100 or ISO Al990Cu, is required by ASTM F640 in order to remove the low energy long wavelength radiation that is passed by beryllium windows typical of x-ray tubes. This will shift the intensity peak towards the peak kilovoltage, thus hardening the x-ray spectrum.

With the additional inherent filtration in place on both the Pantak Model HF 420CP and the Philips Model MG 161, the long wavelength spectrum was further hardened by use of additional aluminium of half-value-layer (HVL) thickness. This filtration reduced the intensity by one-half at the point it entered the metal foil samples but also removed additional long-wavelength radiation and made the wide-beam radiation from the x-ray tube better approximate the single-beam radiation used to calculate expected radiopacities in §3.4, which used data from the National Institute of Standards and Technology web site (Hubbell and Seltzer, 1997). Radiation measurements were made at 122cm from the x-ray source with an MDN Model 1015 x-ray monitor instrument and a Radcal ionization chamber. Using a series of aluminium shims, the thickness was increased until the half-value-layer aluminium thickness was determined for both energies (3.2mm at 80kV; 4.1mm at 100kV). The x-ray spectrum for 80kV with and without the half-value layer filtration is shown in Figure 24 (Seltzer, 2003); comparable x-ray spectra for 100kV are shown in Figure 25. The removal of long-wavelength radiation is seen to shift the peak intensity towards the maximum energy level. The characteristic peaks typical of tungsten targets appear at approximately 57.9kV-59.3kV (K-L transition) and at approximately 66.9kV-69.0kV (K-M transition) (Attix, 1986).

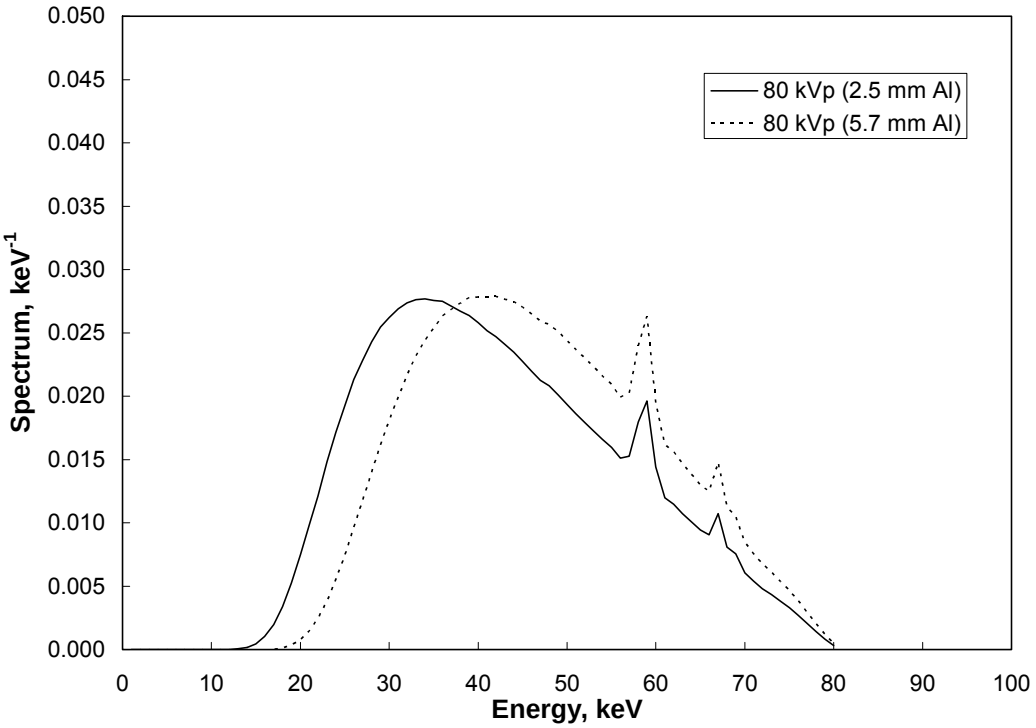

Figure 24 80kV x-ray spectra with and without half-value-layer filters (Seltzer, 2003)

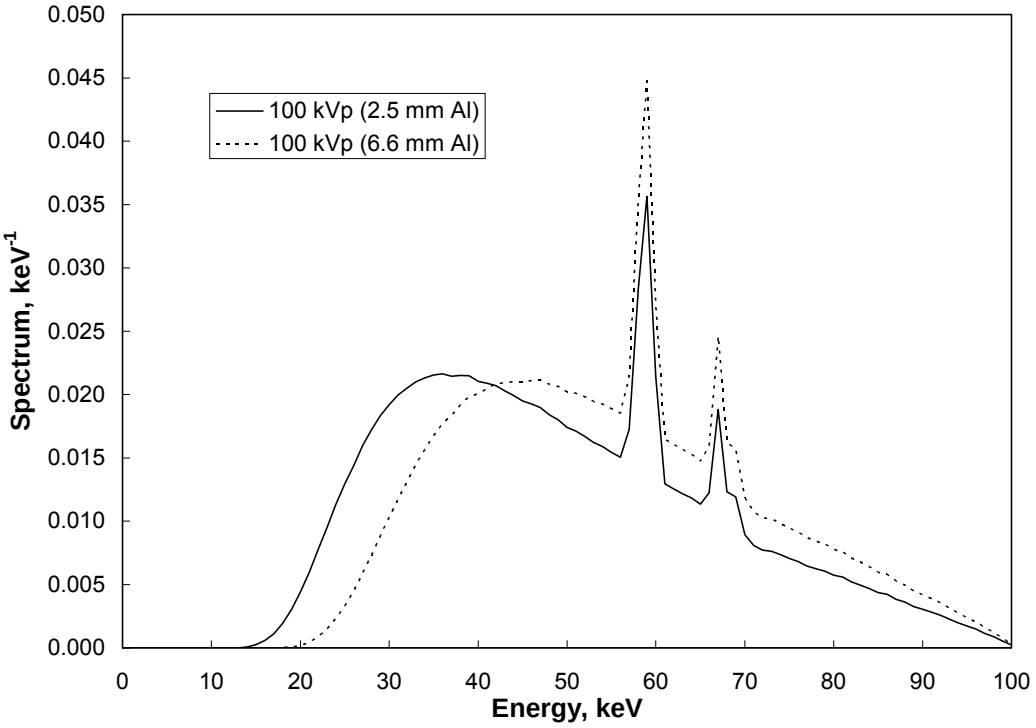

Figure 25 100kV x-ray spectra with and without half-value-layer filters (Seltzer, 2003)

ASTM F640, which has not been modified since 1979, relies on use of transmission film density only to ascertain radiopacity. In Method A, used here, transmission film density (Equation 1) was determined for the metal foil sample and for an area on the film adjacent to the metal foil sample from the processed film; a Macbeth transmission densitometer, Model TD-100A, calibrated using a density strip, Quantalog TD1094A, was used. Kodak Type M film was exposed to the radiation produced by the Philips Model MG 161 with the inherent aluminium filtration removed and replaced with the 2.5mm aluminium filter required by ASTM F640, described above, and additional half-value-layer filtration, also as described above. The source-film distance was 122cm. Since transmission film densities are the common logarithms of the ratios of impinging versus transmitted intensities of light radiation, the characteristic curve for Kodak Type M film processed in a Kodak Model B automatic film processor, Figure 26, was used; processing was conducted at a temperature of 26.6°C and a cycle time of 12 minutes. The log relative exposure corresponding to the density measurement is found and the antilog of that value taken to obtain exposure. The radiopacity of the film, which in ASTM F640 Method A is effectively considered that of the metal sample, is obtained by dividing the exposure found on the fully exposed film adjacent to the metal foil by the exposure of the metal foil sample. Note that inaccuracies in measurement of thickness and in repeating radiopacity measurements are thought to amount to errors in experimentally-determined radiopacity data on the order of plus or minus ten percent. In addition, use of attenuation coefficient data at 80keV unfortunately means there is an inherent error involved due to the overlap with the platinum absorption edge at 80keV.

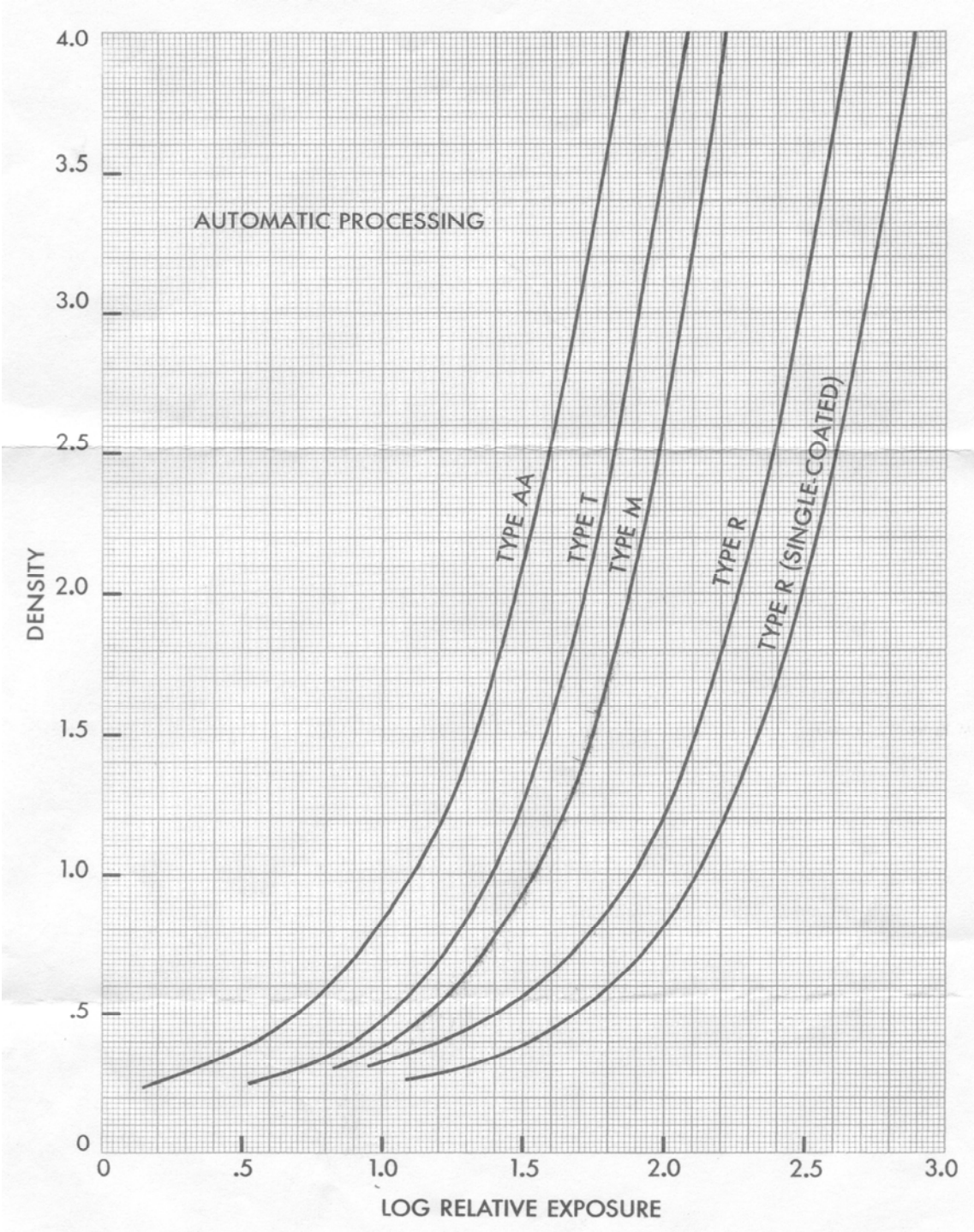

Figure 26 Manufacturer-supplied characteristic curves for industrial and medical film (Eastman Kodak Company, 2003)

The trend since the time ASTM F640 was written in the late 1970's has been towards computed radiography systems, those in which x-ray systems use film-less

techniques. Two systems are described below, including results, which are compared with those obtained from transmission film densities, as described above.

An amorphous silicon flat panel, the dpix FlashScan 30, now marketed by Varian Associates, which is sensitive to visible light rather than x-rays, was used with a gadolinium oxy-sulphide phosphor screen, brand name Kodak Lanex Fine. The digitised output of the dpix panel is in pixels and is converted through a Digitome volumetric image system from a 12-bit to an 8-bit image by dropping the least significant four bits from the image pixel value, resulting in what is termed a linear renormalisation of the data stream by the manufacturer (Digitome Corporation).

The second digital system, used only to obtain data to validate the dpix-Digitome system, is a Science Applications International Corporation (SAIC) Digital Radioscopy System, DRS-2, which has as its imager a proprietary IM-810D charge-coupled device (CCD camera) and phosphor screen. This system is sold principally to security organisations, thus limited technical details were available. The output, as with the dpix-Digitome flat panel system, is a digital image; system output is in pixel values.

In both the dpix-Digitome and SAIC DRS-2 systems, digitised outputs were analysed by a commercial imaging software package, Image-Pro® Plus. The number of pixels from the area that is imaged adjacent to the metal foil is divided by the number of pixels from the metal foil that is imaged simultaneously in order to obtain a non-film equivalent to the ASTM F640 Method A determination of radiopacity. The maximum variation in linearity for the dpix-Digitome system was determined over a 13X range in detector exposure to be within 4 percent; variations in exposure were caused by changing time of exposure. For the SAIC DRS-2 system, the variation over a 6X range in detector exposure, again varying only time, was determined to be within 3 percent.

4.3.3.6.3 Radiopacity results

The wide-beam radiopacities reported by Craig *et al* (2003) were taken earlier, without benefit of either the 2.5mm aluminium required by ASTM F640 or the additional half-value-layer aluminium, thus the results reported there for the 0.127mm samples are from a partially saturated detector. The results are shown in Table 27 and Table 28; these tables also include both the wide-beam and single-beam radiopacities.

Table 27 Wide-beam (80kV) and single-beam (80keV) radiopacities for five alloys

Foil sample 25mm x 25mm	Amor-phous silicon	Type M Film	CCD camera	Amor-phous silicon + Al HVL filter	Type M Film + Al HVL Filter	CCD camera + HVL Filter	Narrow beam (calcu-lated) 80keV
0wt% Pt	1.39	1.43	1.38	1.27	1.34	1.27	1.06
1wt% Pt	1.41	1.45	1.36	1.28	1.38	1.28	1.08
3wt% Pt	1.42	1.46	1.38	1.30	1.34	1.31	1.09
6wt% Pt	1.47	1.55	1.44	1.37	1.41	1.38	1.13
10wt% Pt	1.52	1.59	1.49	1.39	1.45	1.40	1.17

Table 28 Wide-beam (100kV) and single-beam (100keV) radiopacities for five alloys

foil sample 25mm x 25mm	Amor-phous silicon	Type M Film	CCD camera	Amor-phous silicon + Al HVL filter	Type M Film + Al HVL Filter	CCD camera + HVL Filter	Narrow beam (calcu-lated) 100keV
0wt% Pt	1.38	1.28	1.26	1.21	1.18	1.17	1.04
1wt% Pt	1.40	1.32	1.27	1.22	1.19	1.20	1.05
3wt% Pt	1.41	1.29	1.30	1.24	1.19	1.23	1.06
6wt% Pt	1.48	1.36	1.32	1.28	1.27	1.24	1.08
10wt% Pt	1.51	1.41	1.36	1.32	1.33	1.29	1.10

4.3.4 Summary

As in §4.2, platinum was used to demonstrate that the concepts derived from the solubility approach are predictable. In a similar manner, radiopacity is calculated using single-beam radiation and measured using a hardened wide-beam radiation.

Neglecting the 1-6wt% platinum alloys, Table 29 summarises the data at the two extremes of the 0-10wt% platinum experiment (0wt% platinum and 10wt% platinum).

Table 29 Summary of 0wt% platinum and 10wt% platinum data for 0-10wt% alloys

Sample/Parameter	UTS (MPa)	Elon-gation (%)	PREN (pitting resistance)	As-cast ferrite* (%)	Calculated radiopacity: HVL 100keV	Measured radiopacity: HVL 100kV film/avg**
0wt% platinum	650	60	28.3	3.9/4.0	1.04	1.18/1.19
10wt% platinum	704	52	29.1	0.0/0.0	1.10	1.33/1.31

* measured/predicted **average of results from both digitised detector systems

4.4 Non-conforming, high-radiopacity button melts (0-35wt% platinum)

4.4.1 Introduction and approach

The third and final button-furnace stage was designed to extend the radiopacity measurements to just beyond the 32.5wt% platinum limit described in §3.2, Table 8 (80keV) and Table 9 (100keV). The 32.5wt% platinum level was calculated based on allowing a pentanary alloy to achieve a 30% increase in radiopacity. Based on experience with the 0-5wt% platinum alloys (§4.2), which added platinum only to BioDur® 316LS, and the 0-10wt% platinum alloys (§4.3), which created a UNS S31673 alloy from elements, maintaining the required composition while adding platinum, it was determined a more consistent composition could be realised by remelting BioDur® 316LS, adding platinum, chromium, and molybdenum. Nickel was allowed to diminish

naturally in this experiment since platinum has a replacement value on the order of 2:1, as noted in (§3.3), and thus would maintain a minimum equivalency of 13wt% nickel, although the total nickel equivalent (nickel plus half platinum) would quickly exceed the upper specification limit established for these alloys, 15wt% nickel.

To aid in predicting outcomes, particularly when making a number of high-platinum alloys, which are quite costly, Table 30 shows a series of hypothetical or idealised UNS S31673 alloys that rigidly maintain the required elements at the centres of their respective ranges and silicon, manganese, and copper below their maximum values, both required and specified elements being in accordance with the requirements defined in ASTM F139-00. In these alloys, only iron varies as platinum is added, while in the hypothetical alloys of Table 31, nickel also varies, decreasing by 0.85wt% with each 5wt% increase in platinum, an amount taken away from iron content shown in Table 30.

Table 30 Composition of idealised 0-35 wt% platinum alloyed in UNS S31673 (in wt%) (iron diminishes an equal amount with increasing platinum)

alloy/element	Pt	Fe	Cr	Ni	Mo	Si	Mn	Cu
UNS S31673 base	-	63.75	18.00	14.00	2.625	0.375	1.00	0.250
S31673 + 5 Pt	5	58.75	18.00	14.00	2.625	0.375	1.00	0.250
S31673 + 10 Pt	10	53.75	18.00	14.00	2.625	0.375	1.00	0.250
S31673 + 15 Pt	15	48.75	18.00	14.00	2.625	0.375	1.00	0.250
S31673 + 20 Pt	20	43.75	18.00	14.00	2.625	0.375	1.00	0.250
S31673 + 25 Pt	25	38.75	18.00	14.00	2.625	0.375	1.00	0.250
S31673 + 30 Pt	30	33.75	18.00	14.00	2.625	0.375	1.00	0.250
S31673 + 35 Pt	35	28.75	18.00	14.00	2.625	0.375	1.00	0.250

Table 31 Composition of idealised 0-35 wt% platinum alloyed in UNS S31673 (in wt%) (both iron and nickel diminish with increasing platinum)

alloy/element	Pt	Fe	Cr	Ni	Mo	Si	Mn	Cu
UNS S31673 base	-	63.75	18.00	14.00	2.625	0.375	1.00	0.250
S31673 + 5 Pt	5	59.60	18.00	13.15	2.625	0.375	1.00	0.250
S31673 + 10 Pt	10	55.45	18.00	12.30	2.625	0.375	1.00	0.250
S31673 + 15 Pt	15	51.30	18.00	11.45	2.625	0.375	1.00	0.250
S31673 + 20 Pt	20	47.15	18.00	10.60	2.625	0.375	1.00	0.250
S31673 + 25 Pt	25	43.00	18.00	9.75	2.625	0.375	1.00	0.250
S31673 + 30 Pt	30	38.85	18.00	8.90	2.625	0.375	1.00	0.250
S31673 + 35 Pt	35	34.70	18.00	8.05	2.625	0.375	1.00	0.250

When the compositions of the idealised alloys in Table 31 are placed in the New PHACOMP model, it is found, as shown in Table 32, that the Md(avg) for the 35wt% platinum alloy is 0.929eV (1250°C), well in excess of the 0.920eV (1100°C) used in the previous experiments. It is seen that the Md(crit) of 0.920eV intersects between 20wt% platinum (Md = 0.919eV) and 25wt% platinum (Md = 0.921eV) for these hypothetical alloys. As a result, two Md(crit) values are shown in Table 32, with the upper arbitrarily set at 0.929eV, the Md(avg) of the 35wt% platinum alloy.

Table 32 New PHACOMP results for optimised 0-35wt% platinum alloys with iron and nickel diminishing as platinum content increases

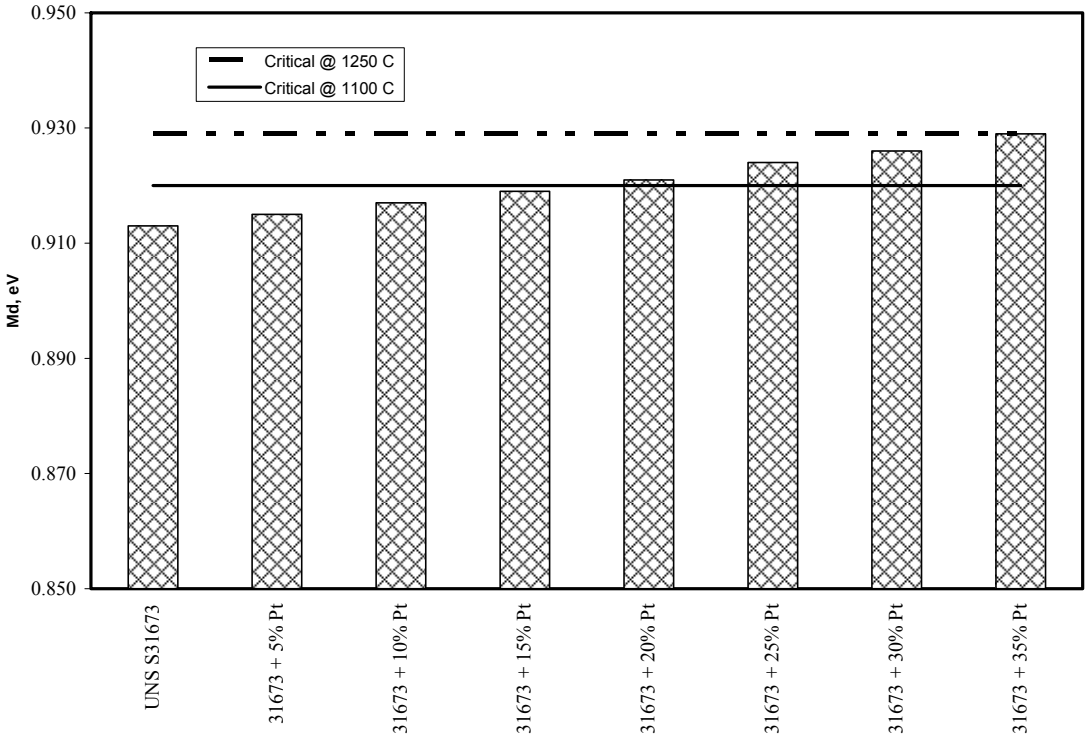

4.4.2 Experiment

Again using the processing approach described in §4.2.2, a large button furnace backfilled with argon was used to prepare the parallel to the eight hypothetical specimens shown in Table 30; these were prepared in 2.5wt% platinum increments up to 15wt% and, after that, in 5wt% platinum increments. As noted in §3.3, platinum has approximately one-half the austenitising effect of nickel, thus no attempt was made to replace nickel as the additions of platinum to the BioDur® 316LS base alloy depleted nickel content. Chromium and molybdenum were added to maintain the pitting resistance equivalent number at equal to or greater than 26, as required by ASTM F139-00. Samples that were rolled and annealed at 1100°C were submitted for x-ray diffraction analysis. Small specimens, approximately 100g, were cold-rolled in a

jeweller's mill to approximately 0.127mm and annealed at both 915°C and 1100°C to be used for analysis using transmission electron microscopy, energy dispersive x-ray spectroscopy, and also as radiopacity specimens.

4.4.3 Results

4.4.3.1 Compositions of matrices and precipitates

The chemical compositions of the eleven specimens as determined by x-ray diffraction (described in §4.2.3.1) and energy dispersive x-ray spectroscopy are shown in Table 33; the latter, as noted above, was based on foil samples of the alloys annealed at both 915°C and 1100°C. In the energy dispersive spectroscopy method, quantitative standardless analysis was performed, employing the Mott/Massy model for the scattering cross-section. The structure of all alloys was found to be fully austenitic at both annealing temperatures. Any residual ferrite in the fully annealed condition, if present, could not be detected against the background radiation.

Table 33 Composition of specimens containing 0-35wt% platinum using x-ray diffraction (top row) and energy dispersive spectroscopy (centre and bottom rows). Top and bottom rows: annealed at 1100°C; centre row: annealed at 915°C.

alloy/element (wt%)	Pt	Fe	Cr	Ni	Mo	Mn
UNS S31673 Base	-	62.8 62.1 60.1	17.5 19.3 20.0	14.6 14.1 13.9	2.8 2.8 3.7	1.8 1.7 1.8
S31673 + 2.5 Pt	2.6 2.9 2.7	60.2 59.6 59.0	17.6 18.9 19.6	14.1 13.5 13.4	3.0 3.6 3.7	1.8 1.7 1.6
S31673 + 5 Pt	5.15 6.3 6.0	58.9 57.1 55.9	17.5 18.9 19.3	13.4 13.1 12.9	2.8 3.1 3.8	1.7 1.6 1.6
S31673 + 7.5 Pt	7.5 9.2 8.9	56.2 55.0 55.6	17.8 18.1 18.3	13.0 12.8 12.4	3.07 3.3 3.3	1.7 1.4 1.5
S31673 + 10 Pt	10.1 11.6 11.6	54.6 54.9 52.6	17.8 16.4 17.8	12.5 12.5 12.3	3.1 3.1 3.7	1.6 1.4 1.5
S31673 + 12.5 Pt	12.6 15.1 14.1	52.4 51.5 51.3	17.8 16.7 17.9	11.9 11.9 11.7	3.0 3.2 3.6	1.5 1.5 1.4
S31673 + 15 Pt	15.04 17.1 17.0	50.7 49.1 48.2	17.8 17.7 17.9	11.5 11.3 11.6	3.1 3.4 3.4	1.5 1.4 1.4
S31673 + 20 Pt	18.8 20.5 22.7	47.1 44.9 45.8	17.8 19.2 17.4	10.8 10.7 10.3	3.0 3.4 3.3	1.4 1.2 -
S31673 + 25 Pt	24.9 25.5 30.5	43.4 43.1 38.3	17.5 17.3 16.6	9.6 10.1 9.6	2.9 3.1 3.4	1.3 1.2 1.2
S31673 + 30 Pt	29.4 29.9 35.2	39.5 40.9 35.1	17.6 15.1 16.2	8.9 9.7 8.9	2.9 3.1 3.2	1.2 1.1 1.0
S31673 + 35 Pt	35.5 37.6 37.5	34.5 34.1 32.9	18.0 16.0 16.9	7.8 8.4 8.1	2.8 2.9 3.3	1.0 0.9 0.9

The New PHACOMP results for the alloys in base through 35wt% platinum alloys, in 5wt% platinum increments, are shown in Table 34. Compositions used are those found with x-ray diffraction (top row in Table 33).

Table 34 New PHACOMP results for 0-35wt% platinum alloys
(jagged line: 1250°C; solid line: 1100°C)

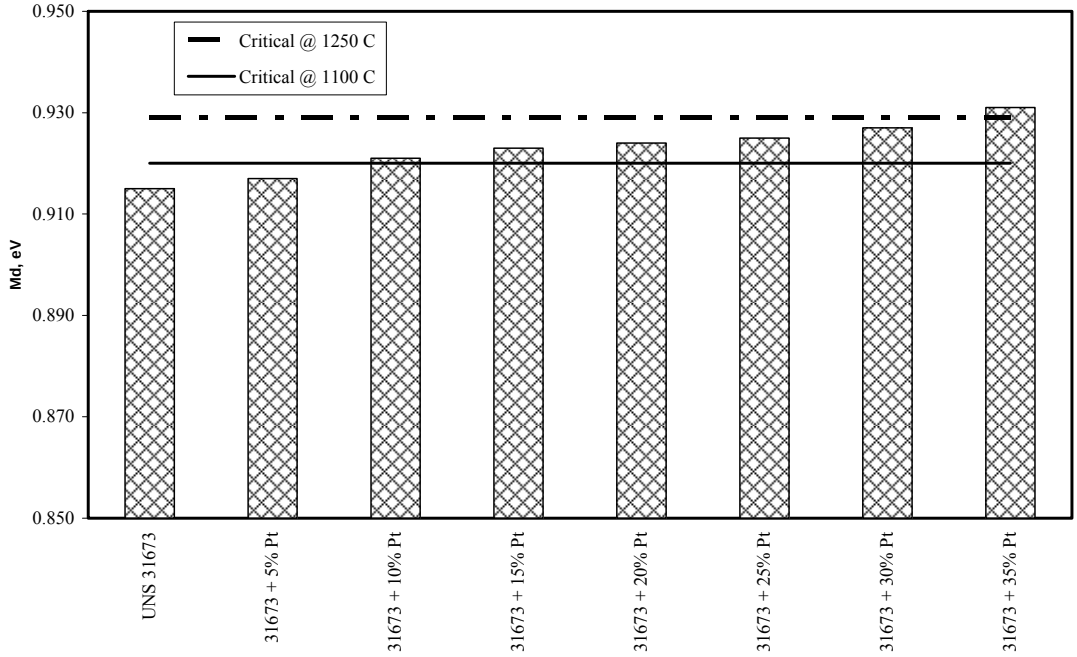

Four distinct precipitates were found in these alloys, using transmission electron microscopy and associated microdiffraction and energy dispersive x-ray spectroscopy. Two types of precipitate (A; B) first appeared in the base alloy and were restricted to alloys containing either up to and including 15wt% platinum (Type A) or up to and including 20wt% platinum (Type B); see Table 35 and Table 36. One type of precipitate (Type C) appeared only in the 25wt% platinum alloy (Table 37); the fourth type of precipitate (Type D) only appeared in the 25-35wt% alloys (Table 38).

For the nominally 12.5wt% platinum alloy, Figure 27 is a bright field image of the matrix at 915°C and the Type A precipitates listed in Table 35, along with microdiffraction patterns for both; Figure 28 shows the energy dispersive spectroscopy spectra of the matrix at 915°C and corresponding the Type A and Type B precipitates. Again for the nominally 12.5wt% platinum alloy, Figure 29 is a bright field image of the matrix at 1100°C and the Type B precipitates listed in Table 36, along with

microdiffraction patterns for both; Figure 30 shows the energy dispersive spectroscopy spectra of the matrix at 1100°C and both Type A and Type B precipitates. The Type A precipitates were found in foils annealed at 915°C but were not found in those annealed at 1100°C. The Type B precipitates were found in both foils annealed at 915°C and those annealed at 1100°C, with the exception of the 20wt% platinum sample, which did not exhibit the Type B precipitate at the lower annealing temperature.

Table 35 Composition of Type A precipitate found in 0-15wt% platinum alloys
(top row: foil annealed at 915°C; bottom row: foil annealed at 1000°C)

alloy/element	Pt	Fe	Cr	Ni	Mo	Mn
UNS S31673	-	17.3	74.8	2.3	4.8	1.1
base	-	-	-	-	-	-
S31673	-	19.1	72.1	3.1	5.1	0.5
+ 2.5 Pt	-	-	-	-	-	-
S31673	-	15.9	75.6	2.4	5.4	0.8
+5 Pt	-	-	-	-	-	-
S31673	2.5	18.1	71.5	2.6	4.9	0.7
+ 7.5 Pt	-	-	-	-	-	-
S31673	1.4	7.7	84.8	0.7	5.2	0.2
+ 10 Pt	-	-	-	-	-	-
S31673	3.2	13.5	75.3	2.1	5.4	0.4
+ 12.5 Pt	-	-	-	-	-	-
S31673	2.2	9.2	81.9	1.0	5.5	0.2
+ 15 Pt	-	-	-	-	-	-

Table 36 Composition of Type B precipitate found in 0-20wt% platinum alloys
(top row: foil annealed at 915°C; bottom row: foil annealed at 1000°C)

alloy/element	Pt	Fe	Cr	Ni	Mo	Mn
UNS S31673	-	11.2	82.1	1.2	5.1	0.6
base	-	11.2	81.6	1.2	5.5	0.6
S31673	-	11.6	81.9	1.2	5.0	0.6
+ 2.5 Pt	-	10.1	82.8	0.8	5.8	0.5
S31673	-	10.7	82.7	1.2	5.0	0.6
+5 Pt	-	10.4	82.8	1.1	5.5	1.0
S31673	1.7	11.4	80.2	1.3	5.2	0.2
+ 7.5 Pt	-	10.2	83.0	1.1	5.5	0.1
S31673	1.4	7.7	84.8	0.7	5.2	0.2
+ 10 Pt	-	8.1	85.6	-	6.1	0.2
S31673	1.6	7.6	85.1	0.8	5.1	0.1
+ 12.5 Pt	-	10.0	83.7	-	6.1	0.3
S31673	2.2	9.2	81.9	1.0	5.5	0.2
+ 15 Pt	-	8.4	84.9	1.0	5.5	0.3
S31673	-	-	-	-	-	-
+ 20 Pt	2.2	7.0	82.9	0.6	6.2	-

Table 37 Composition of Type C precipitate found in 25wt% platinum alloy
(top row: foil annealed at 915°C; bottom row: foil annealed at 1100°C)

alloy/element	Pt	Fe	Cr	Ni	Mo	Mn
UNS S31673	-	-	-	-	-	-
base	-	-	-	-	-	-
S31673	-	-	-	-	-	-
+ 20 Pt	-	-	-	-	-	-
S31673	34.2	25.3	30.0	6.4	3.3	0.8
+ 25 Pt	28.7	34.2	17.2	8.0	6.0	5.9
S31673	-	-	-	-	-	-
+ 30 Pt	-	-	-	-	-	-

Table 38 Composition of Type D precipitates found in 25-35wt% platinum alloys
(top row: foil annealed at 915°C; bottom row: foil annealed at 1100°C)

alloy/element	Pt	Fe	Cr	Ni	Mo	Mn
UNS S31673	-	-	-	-	-	-
base	-	-	-	-	-	-
S31673	47.2	10.8	36.3	2.4	2.7	0.5
+ 25 Pt	-	-	-	-	-	-
S31673	49.5	8.1	37.5	1.8	2.6	0.5
+ 30 Pt	54.0	8.0	32.4	2.0	3.0	0.6
S31673	52.9	6.3	36.7	1.3	2.6	0.2
+ 35 Pt	49.7	6.4	39.2	1.4	2.9	0.3

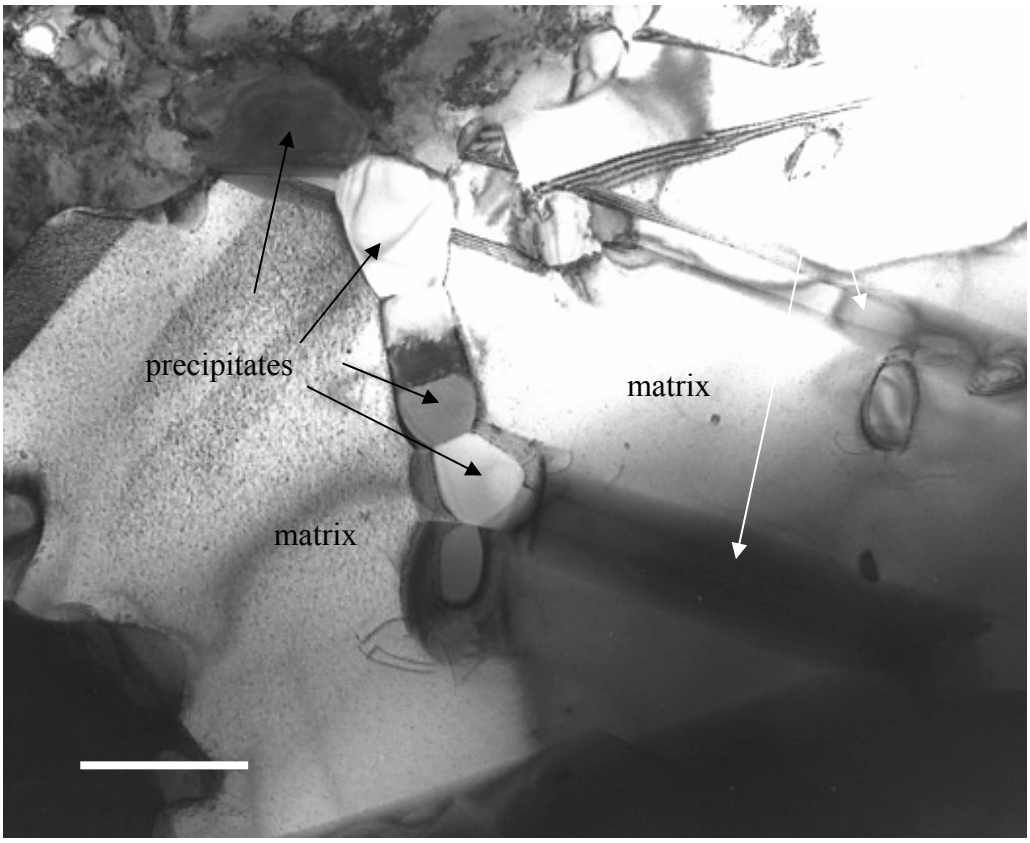

(a)

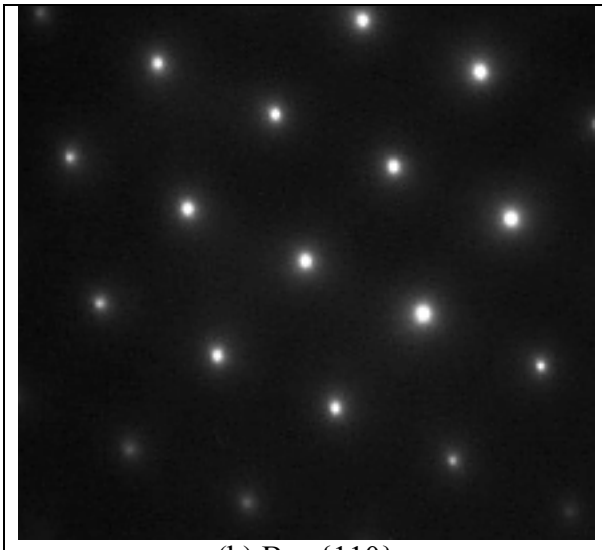

(b) B = {110}

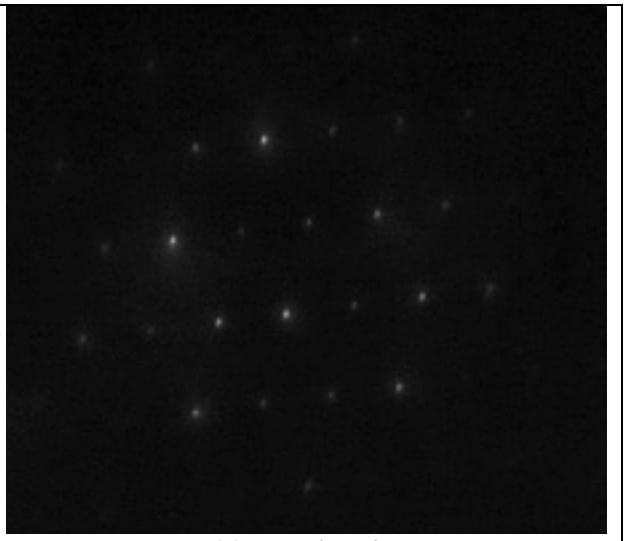

(c) B = {110}?

Figure 27 (a) Bright field image of the 915°C anneal matrix for 12.5wt% platinum alloy (light line is 1 micron), (b) corresponding microdiffraction pattern, and (c) microdiffraction pattern for Type A precipitates

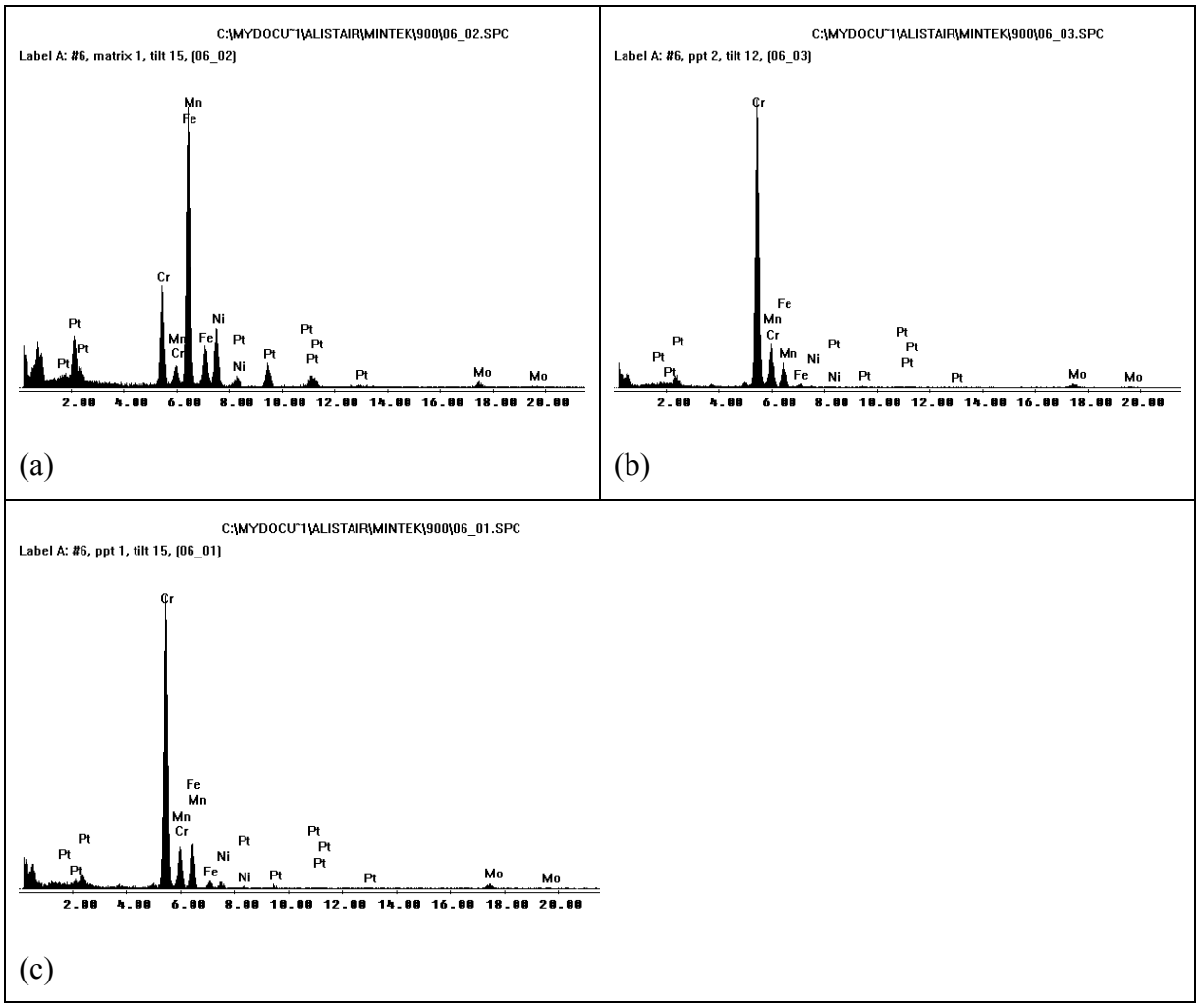

Figure 28 Energy dispersive x-ray spectroscopy spectra for 915°C anneal 12.5wt% platinum alloy. Typical (a) matrix; (b) Type B precipitate, and (c) Type A precipitate

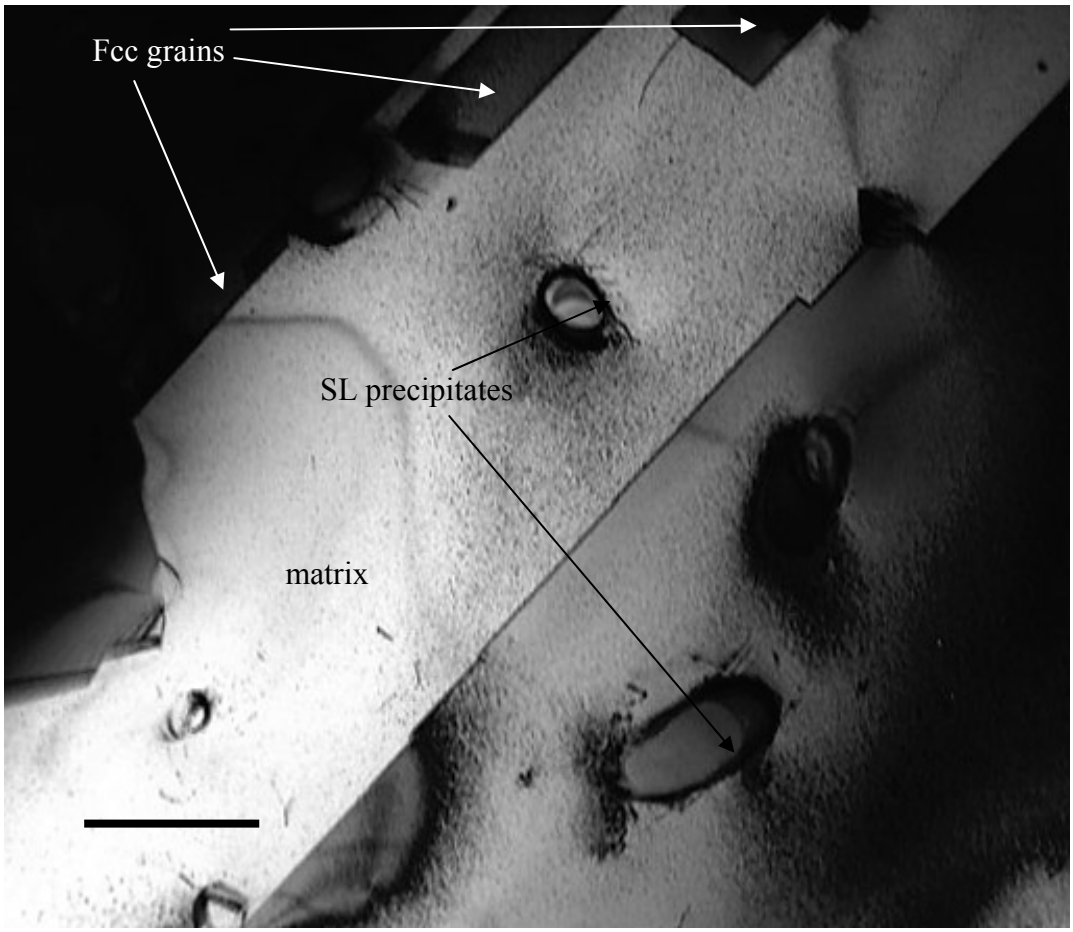

(a)

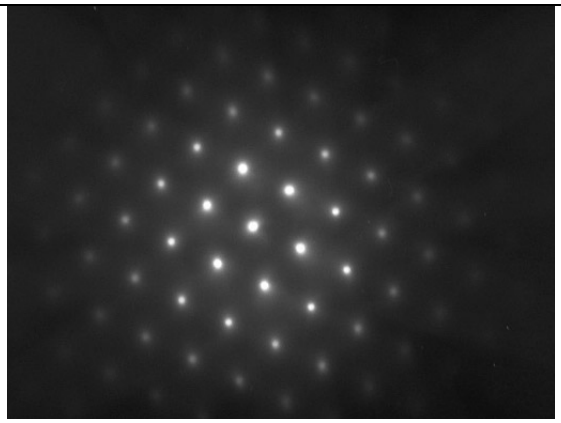

(b) B = {110}

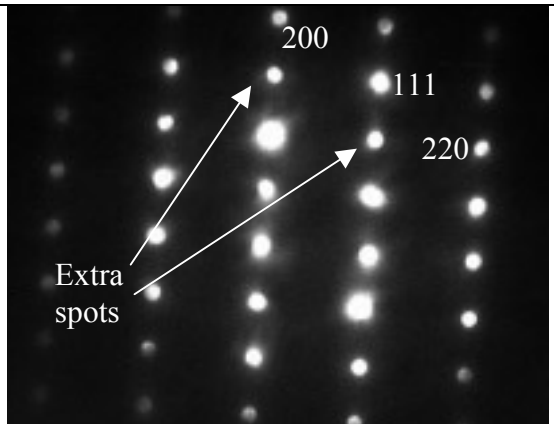

(c) B = {110}?

Figure 29 (a) Bright field image of the 1100°C anneal matrix for 12.5wt% platinum alloy (light line is 1 micron), (b) corresponding microdiffraction pattern, and (c) microdiffraction pattern for Type B precipitates

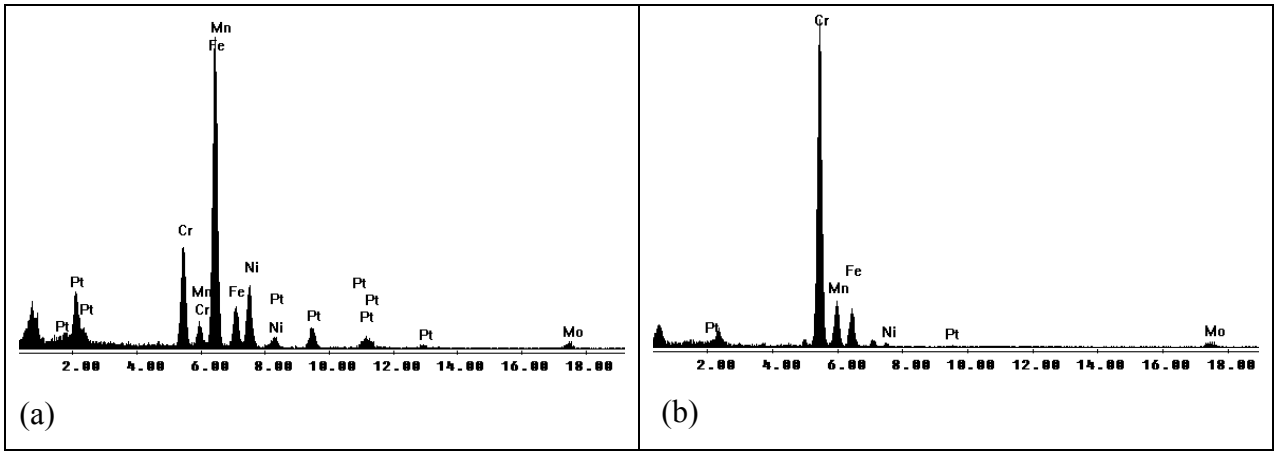

Figure 30 Energy dispersive x-ray spectroscopy spectra for 1100°C anneal 12.5wt% platinum alloy. Typical (a) matrix, and (b) Type B precipitate

For the nominally 25wt% platinum alloy, Figure 31 is a bright field image of the matrix annealed at 915°C and the two types of precipitate found, one rod-like (Type C) and the other (Type D) irregular-shaped (or rounded), along with their corresponding microdiffraction patterns. Figure 32 shows the energy dispersive x-ray spectroscopy spectra for the nominally 25wt% platinum alloy matrix (915°C) and its rod-like and irregular-shaped precipitates.

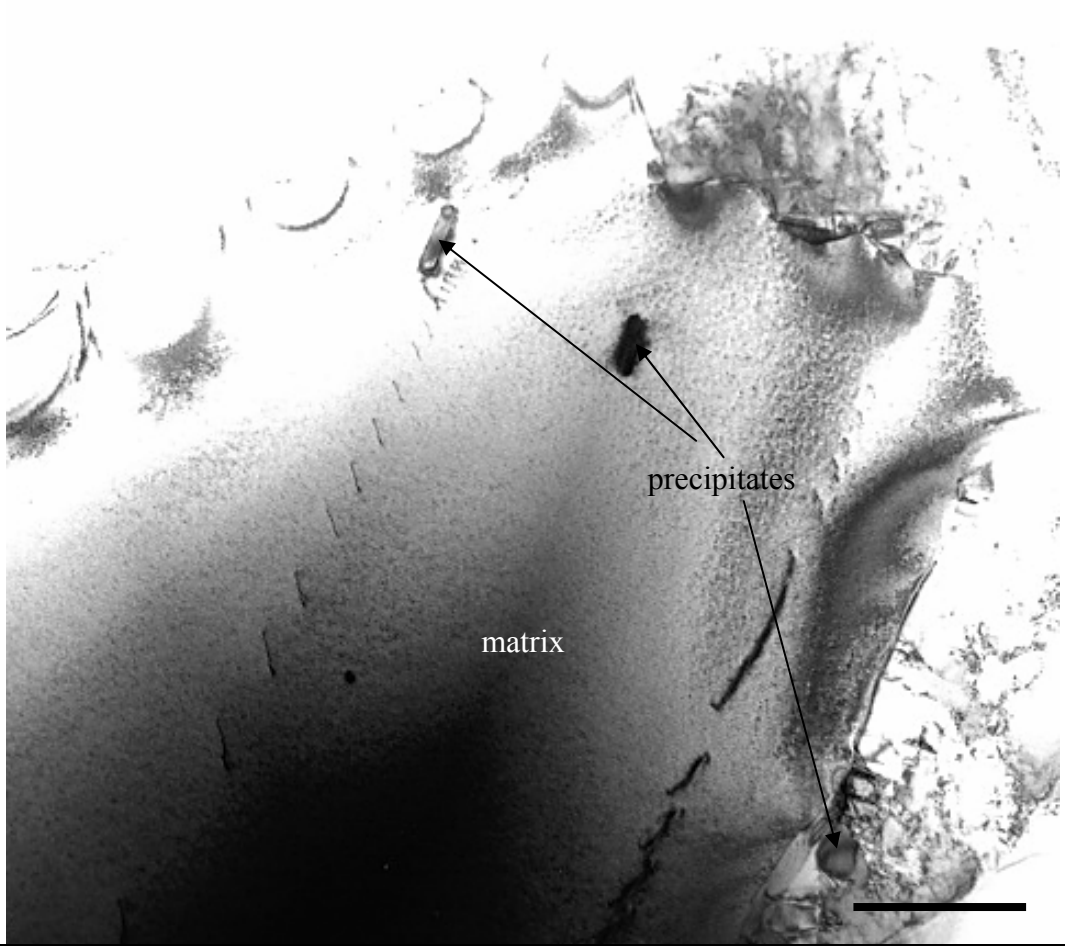

(a)

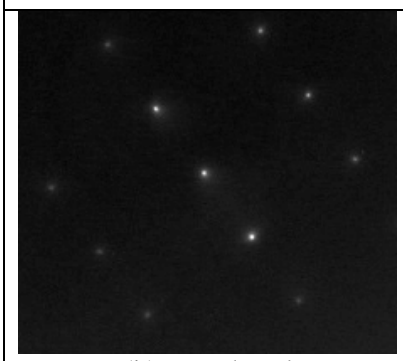

(b) B = {110}

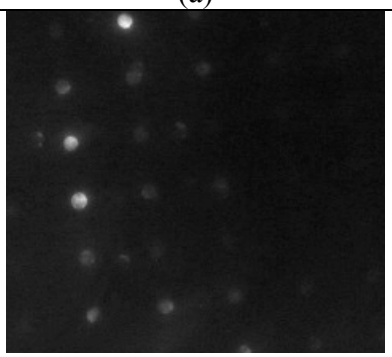

(c) B = {???}, rod

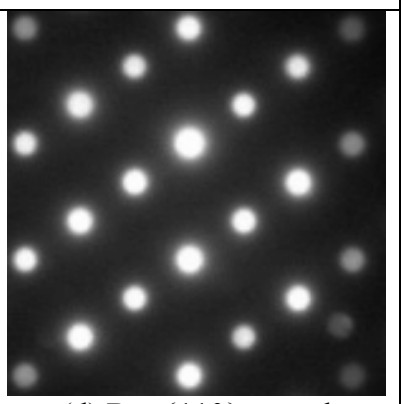

(d) B = {110}, round

Figure 31 (a) Bright field image of Type C (rod-like precipitate at upper left) and Type D (irregular-shaped) precipitates in 25wt% platinum alloy (915°C anneal)(1 micron line); microdiffraction patterns for (b) matrix, (c) Type C and (d) Type D precipitates.

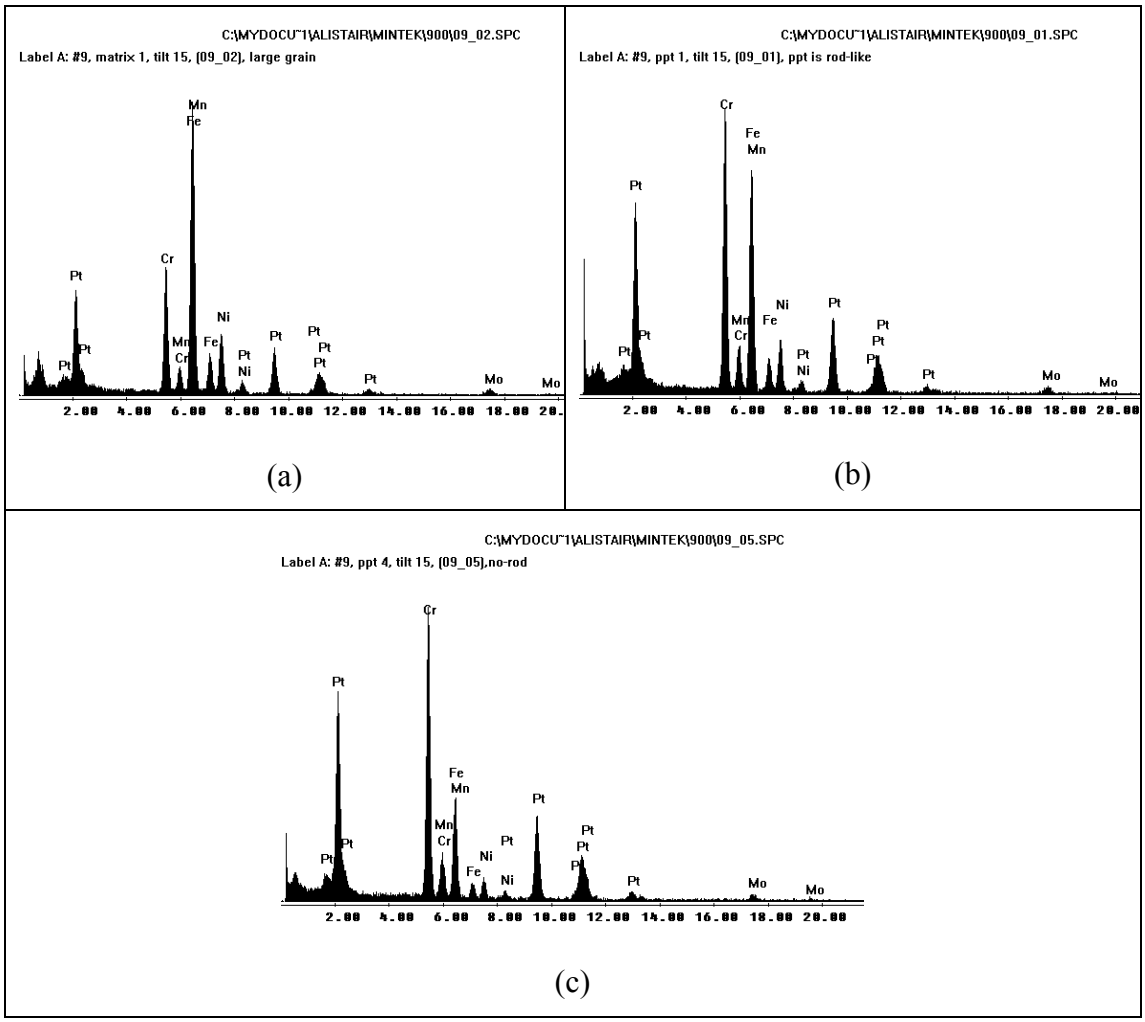

Figure 32 Energy dispersive x-ray spectroscopy spectra for 25wt% platinum in UNS S31673 alloy (915°C anneal). (a) matrix; (b) Type C, and (c) Type D precipitates

Figure 33 shows bright field and dark field images of matrices containing Type D precipitates. Figure 34 shows a typical energy dispersive x-ray spectroscopy spectrum for Type D precipitates.

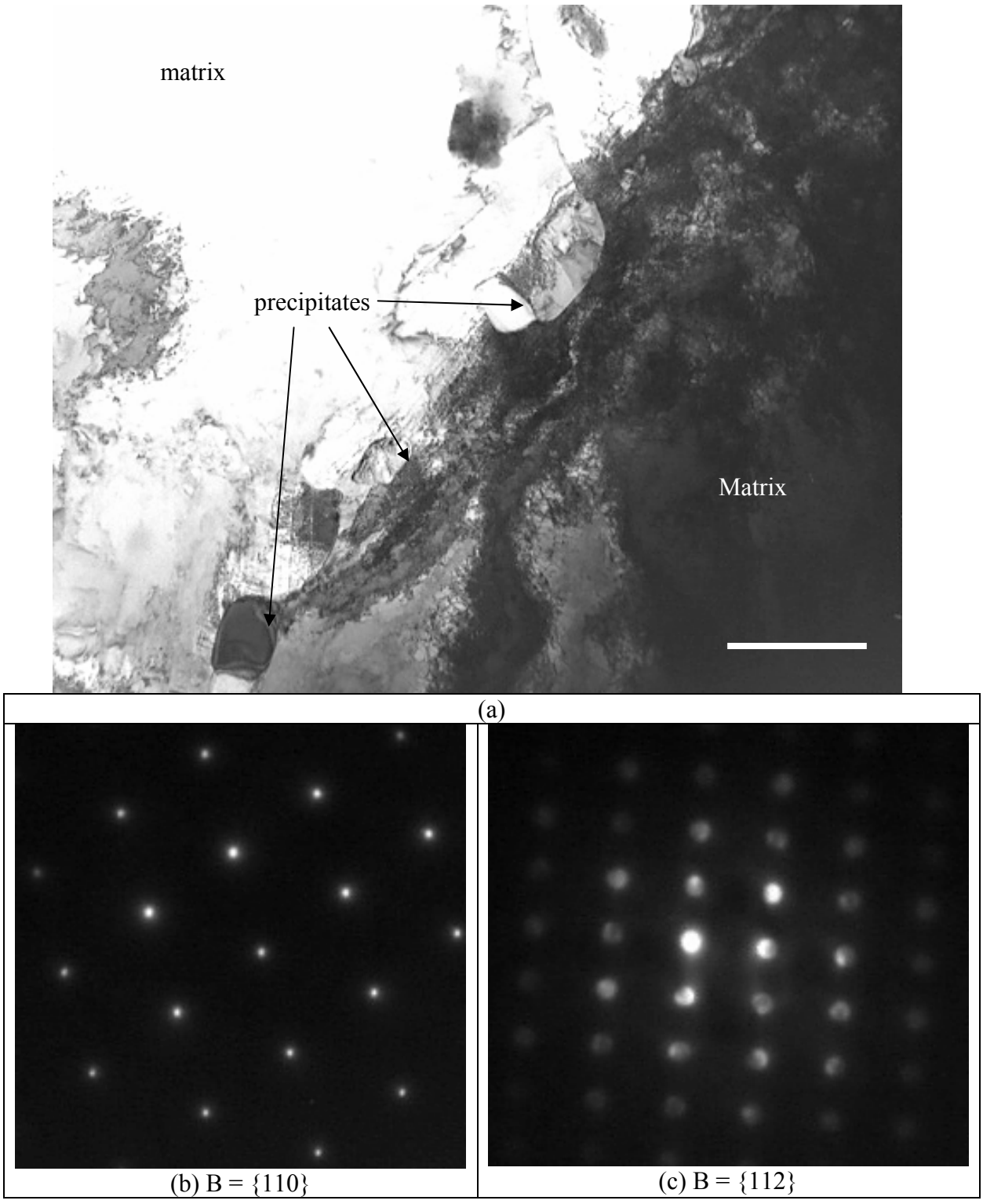

Figure 33 (a) Bright-field image of 915°C matrix and Type D precipitates in 35wt% platinum alloy (bar is 1micron) and corresponding microdiffraction patterns for (b) matrix, and (c) Type D precipitates

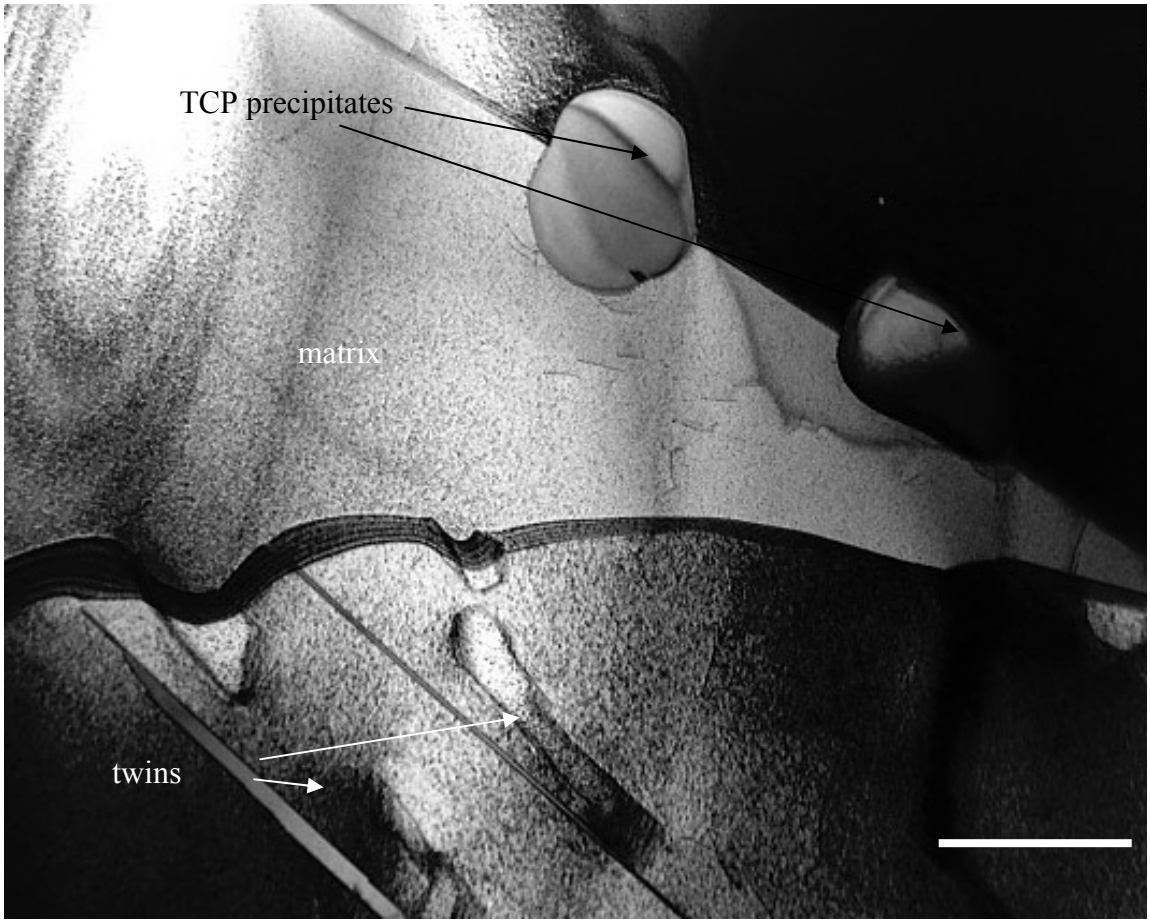

(a)

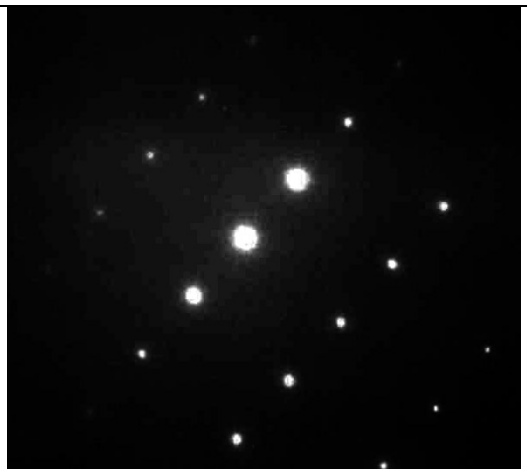

(b) B = {112}

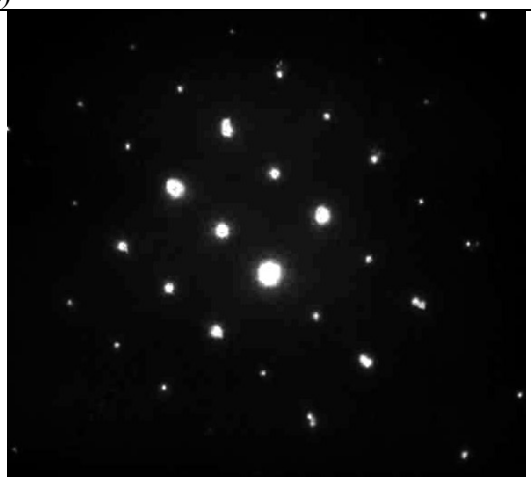

(c) B = {112}

Figure 34 (a) Bright-field image of 1100°C matrix and Type D precipitates in 35wt% platinum alloy (bar is 1micron) and corresponding microdiffraction patterns for (b) matrix, and (c) Type D precipitates

4.4.4 Radiopacity

4.4.4.1 Experiment

Table 31 and Table 33, in the previous section, defined the hypothetical alloys and the actual alloys produced by adding platinum to a UNS S31673 alloy, BioDur® 316LS, along with sufficient chromium and molybdenum to maintain the required pitting resistance equivalent number. Nickel was allowed to diminish naturally since the added platinum more than made up for this in terms of nickel equivalent. Table 39 shows the single-beam radiopacity expected for the hypothetical alloys at 80keV and 100keV, while Table 40 shows the single-beam radiopacity expected for the actual alloys, again at 80keV and 100keV.

Table 39 Single-beam radiopacities for hypothetical 0-35wt% platinum alloys (t = 0.127mm)

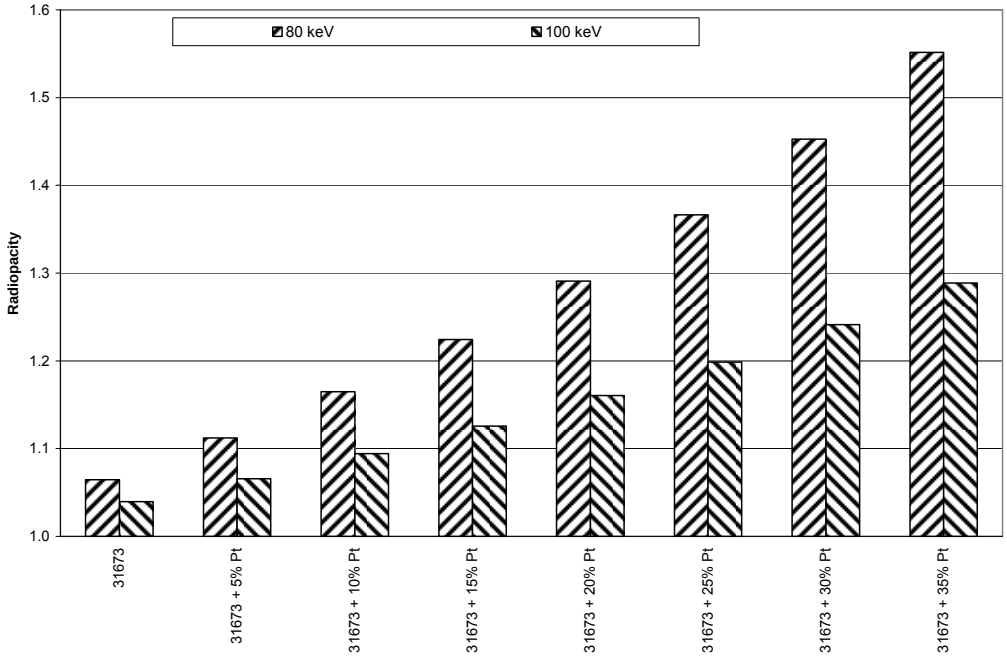

Table 40 Single-beam radiopacities expected for actual 0-35wt% platinum alloys (t = 0.127mm)

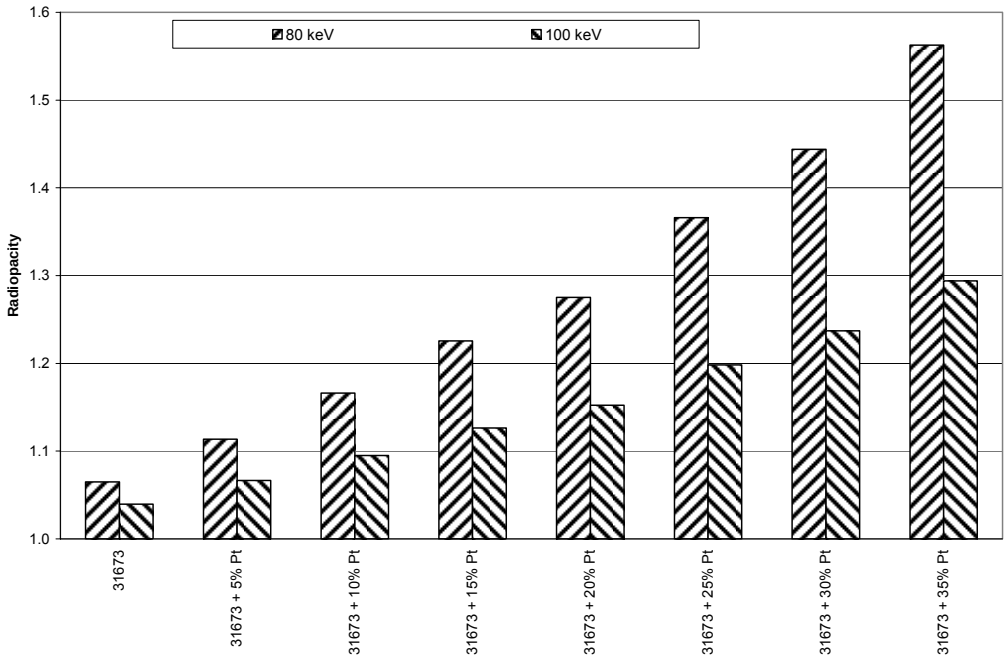

The foil samples of the eight alloys varying in 5wt% increments that were described in the previous section and in Table 33 were x-rayed at 80kV and 100kV using the Pantak Model HF 420CP x-ray system with added aluminium inherent filtration as required by ASTM F640, along with an additional half-value-layer of aluminium, as described in §4.3.3.6.2. The dpix flat panel detector, Kodak phosphor screen, Digitome processor, and Image-Pro® Plus software were used to obtain radiopacity measurements, using the digital analogue to Method A of ASTM F640. No radiographic film was used in these experiments to obtain radiopacity measurements.

Table 41 provides the measured thicknesses of the rolled foil, which varied widely due to the varying densities of the alloys, which also are shown in Table 41.

Table 41 Thickness and density of 0-35wt% platinum specimens

Design Point	Thickness	Density
	mm	g/cc
UNS S31673 base	0.104	7.83
S31673 + 5% Pt	0.135	8.08
S31673 + 10% Pt	0.099	8.35
S31673 + 15% Pt	0.115	8.63
S31673 + 20% Pt	0.135	8.86
S31673 + 25% Pt	0.157	9.25
S31673 + 30% Pt	0.152	9.58
S31673 + 35% Pt	0.152	10.02

4.4.4.2 Radiopacity results

Experimental results are shown in Table 42. Table 42 provides both wide-beam and single-beam radiopacities for the samples, with the single energy (single-beam) radiopacities calculated using Equation 5.

Table 42 Wide-beam (experimental) and single-beam (single-energy) radiopacities

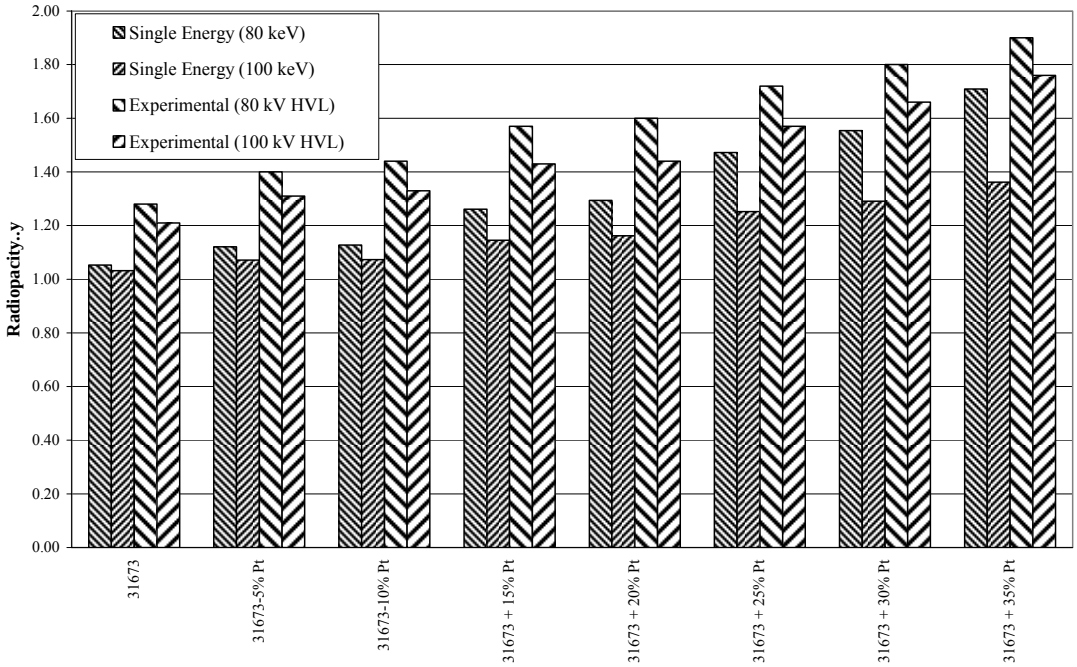

Because of the wide variation in thickness, it was difficult to compare the radiopacities, thus the experimentally determined radiopacity (Table 42), density and

thickness (Table 41) was used in Equation 5 to determine an effective linear absorption coefficient for each alloy. Table 43 shows the 80kV experimental (wide-beam) data from Table 42 normalised to 0.127mm; Table 44 shows the 100kV experimental data normalised to 0.127mm. Averaging results for 30wt% and the 35wt% platinum samples to obtain an approximate 32.5wt% platinum result yielded averaged radiopacities for those two alloys that were found to be 1.67 for 80kV and 1.57 for 100kV. Radiopacity for the base (0wt% platinum) alloy at 80kV was 1.35, thus 1.67/1.35 indicated the increase in radiopacity over the base alloy was approximately 24% at 80kV. At 100kV, the base radiopacity was 1.26, thus the increase in radiopacity at 100kV over the base was 1.57/1.26, again approximately 24%. These results are summarised in Table 45.

Table 43 Experimental results at 80kV normalised to 0.127mm thickness

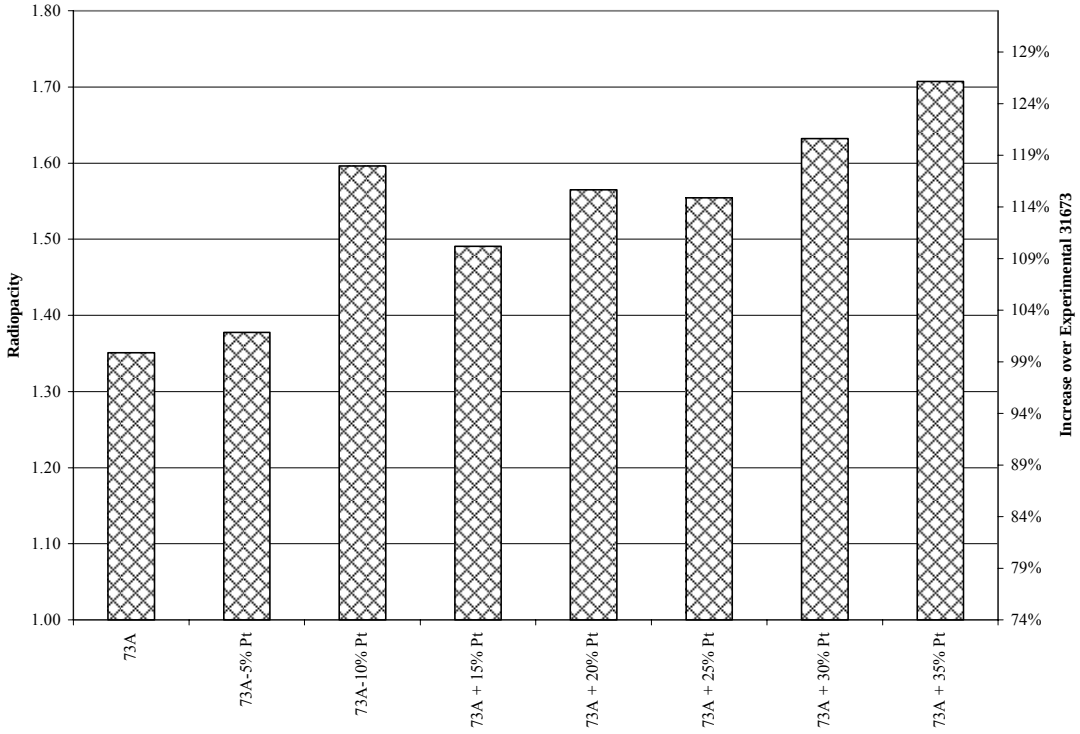

Table 44 Experimental results at 100kV normalised to 0.127mm thickness

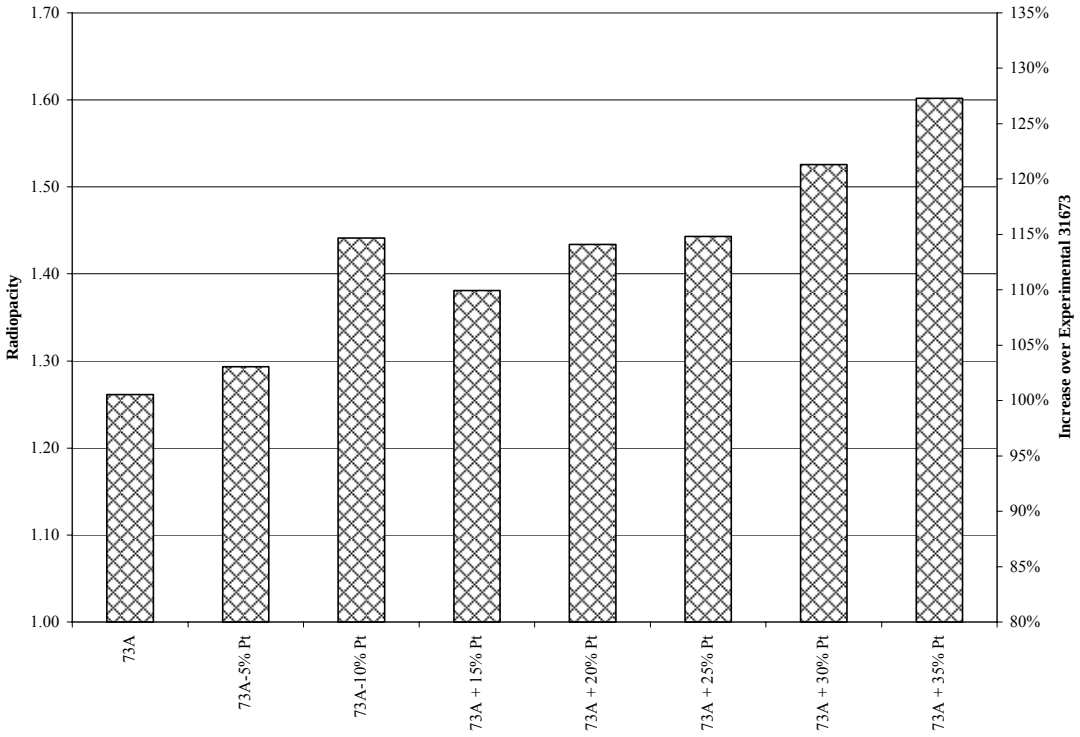

Table 45 Radiopacity of 0-35wt% platinum viewed as percent increase over base alloy

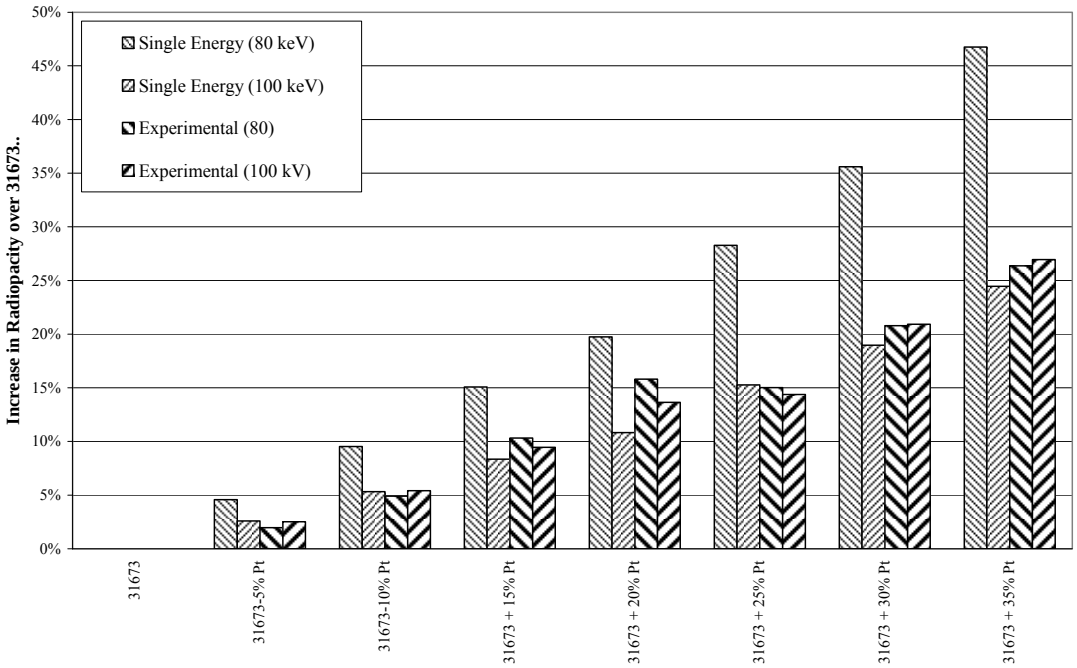

4.4.5 Summary

The experiment in §4.4 was carried out to address the production of alloys containing platinum up to and slightly in excess of that required to achieve the overall goal of a 30% increase in radiopacity over the base alloy whilst maintaining the alloy free of embrittling precipitates and as a stainless steel in accordance with the Unified National Standard, i.e., where iron is the predominant element.

The alloys were found to be fully austenitic when annealed at both 915°C and 1100°C. Two types of precipitate appeared first in the base alloy and, at between 15wt% and 20wt% platinum, disappeared. One type of precipitate was unique to the 25wt% platinum alloy; another was unique to the 25wt% to 35wt% platinum alloy.

Radiopacity, for the equivalent of a 32.5wt% platinum alloy, was found to increase up to approximately 24% at both 80kV and 100kV, using non-film techniques.

4.5 Conforming, low-radiopacity, induction-melted alloys

4.5.1 Introduction and approach

Both the size and the quality of an ingot required for establishing production of tubing to be made into balloon-expandable coronary stents demand use of furnaces typical of commercial stainless steel-making practice; button furnaces are not suited to such production. The commercial suppliers of implant-grade austenitic stainless steel typically make ingots that are a minimum of 125kg, an amount that would make sufficient tubing for a manufacturer of stents that might last for several years. In order to justify its investment in the costs for producing ingots of such demanding quality, the supplier might envision selling the product to a number of stent manufacturers; this in turn could potentially take away the incentive of the stent manufacturer to invest in research and development because the marketing edge normally attributable to such

efforts would be lost. These considerations led to the determination to (a) develop the manufacturing processes on a more modest scale than would be typical of or practical for commercial endeavours, limiting the ingot size to 50kg, and (b) retain control of the proprietary technology that ensued.

A further consideration that applied initially was that the coronary stents being produced were manufactured by a photo-etch process; it was not clear to those who had developed the etching process that it could be easily modified to accommodate the change from UNS S31673 alloys to a variant of those containing 32.5wt% platinum. As a result, a more cautious approach was taken: to develop the required manufacturing processes based on a modest increase in both platinum content and radiopacity. This in turn led to process development of 5-6wt% platinum alloys through a programme at the United States Department of Energy metallurgical laboratory, Albany Research Centre.

4.5.2 Experiment

Alloys containing nominally 5-6wt% platinum were produced by adding platinum to Carpenter Technology's BioDur® 316LS, a UNS S31673 alloy, supplied in bar form and certified to meet the requirements of ASTM F138-00 (rod and bar). Additions of chromium and molybdenum were made to maintain the pitting resistance equivalent number at least equal to 26 (Equation 12).

The manufacturing process to make foil in preparation for making tubing for stents is shown in Figure 35 and was described by Dennis, Craig *et al* (2003).

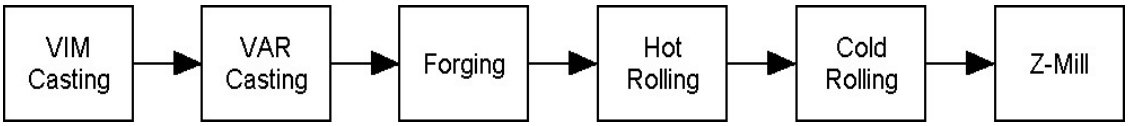

Figure 35 Block diagram of optimum alloy-foil production process

The vacuum induction melting (VIM) process shown in Figure 35 began with accurately weighing the material for the melt, comprised of BioDur® 316LS bar cut to fit inside a melting crucible capable of holding sufficient material for a 50kg ingot. The pieces of bar were placed inside the melting crucible and the platinum, chromium, and molybdenum were placed inside a small container just above the crucible from which the contents could be tipped into it after the pieces of bar were melted. The furnace was closed and brought to a vacuum of approximately 0.02kPa. Power was applied, bringing the power to the induction coils slowly to approximately 100kw over the course of one hour and the vacuum to approximately 0.13kPa whilst noting the condition of the rods through a sight glass. Power was maintained at 100kw for approximately five minutes after it was seen the rods were fully melted in order to ensure melting and promote mixing, then reduced to 70kw. The additional elements were then tipped into the melt. After another five minutes at this power level, the power was reduced to nought and the alloy was tipped from the melting crucible into the receiving crucible. After approximately three hours cooling under vacuum, air was admitted and the ingot was claimed.

A typical ingot made in this manner is shown in Figure 36; these ingots were approximately 15cm diameter by 30cm long and weighed approximately 50kg on being removed from the receiving crucible. After the ingot was cropped and cleaned, approximately 75% of the total weight was available for further processing; scrap material was periodically sent to a precious metals reprocessing centre where up to 95% of the platinum was recovered, at minimal expense.

Figure 36 Typical vacuum induction melting furnace stainless steel ingot and crucible (United States Department of Energy, Albany Research Centre, Albany, Oregon)

A further refinement of the ingot-making process was use of a vacuum arc remelt (VAR) furnace, a stage that follows the vacuum induction melting furnace, as shown in Figure 35. Ingots processed in such a furnace are identified as VAR-produced; those ingots processed in only the vacuum induction furnace are identified as VIM-produced. The basis for using the vacuum arc remelt process was that an alloy with fewer of the naturally-occurring inclusions (oxides, sulphides, aluminides, and silicates) typical of the vacuum induction melting process could be realised. Commercially available implant alloys such as BioDur® 316LS were advertised as triple vacuum arc remelted.

When VIM-produced ingots were made, the mechanically cleaned VIM-produced ingots were quartered, lengthwise, and those pieces were welded together under vacuum and used as consumable electrodes in the vacuum arc remelt process. A typical process started with 0.004kPa vacuum, 26V, and 2400A, and these latter were quickly increased

to approximately 32V and 3900A. As before, a cylindrical ingot of approximately 15cm diameter was produced with length dimensions dependant upon the amount of good-quality alloy obtained from the VIM-produced ingot. Before the VAR-produced ingot was further processed it was either radiographed or subjected to ultrasonic testing to determine its fitness for rolling, as it was not uncommon to find large shrink holes, requiring further remelt processing to obtain a sufficiently large, discontinuity-free ingot to continue the manufacturing process to the forge and rolling mills. Following the vacuum induction and vacuum arc remelt processes, a typical VIM-produced ingot had a composition as shown in the top row below for IVT 65 in Table 46; that ingot, subjected to vacuum arc remelt, had a composition as shown in Table 46, bottom row.

Table 46 Nominally 6wt% platinum enhanced radiopaque austenitic stainless steel before (top) and after (bottom) vacuum arc remelting (in wt%; n.d. = not determined)

Pt	Fe	Cr	Ni	Mo	Mn	Cu	Si	C	N	O
5.83	58.3	17.6	13.6	2.9	1.2	0.1	0.4	n.d.	n.d.	n.d.
5.81	58.4	17.6	13.6	2.9	1.1	0.1	0.4	0.004	0.02	0.02

After casting, whether by vacuum induction melting alone or as a VAR-produced ingot, the mechanically cleaned ingot was sometimes hot upset in a forge, Figure 20, after bringing it to a hot-rolling temperature (typically 1230°C) in an open furnace. Hot-rolling took place in the rolling mill, Figure 19, configured as a two-high mill; the larger rolls of the two-high configuration provided the capability for approximately 15% reductions. Reheating took place at 15-minute intervals to maintain the minimum temperature considered sufficiently high for hot-rolling (1040°C). After a final anneal at 1040°C, the plate was prepared for cold-rolling; the two-high mill was re-configured as a four-high mill since better dimensional control was obtained with smaller rolls, although reductions were smaller. Periodic anneals at 1040°C were made during cold-

rolling operations to maintain ductility and to minimise martensitic transformations. Final cold-rolling thickness was on the order of 1.0mm (sheet).

Rolling of sheet to foil suitable for producing welded tubing for stent fabrication, described by Dennis, Craig, *et al* and shown in Figure 35 as using a Sendzimir® rolling mill, is not further described here since only plate or sheet from the two-high/four-high rolling mill, Figure 16, was subjected to testing here.

4.5.3 ASTM F139 tests and results

The initial ingots were made by vacuum induction melting only and paralleled the original 5wt% platinum alloy made by button furnace processing, as described in §4.2 and shown in Table 16. These alloys are shown in Table 47 as ingots IVT 37 and IVT 38, along with a sample of the BioDur® 316LS base material.

Table 47 Composition of ingot IVT 37 and ingot IVT 38 (Covino, Craig *et al*, 2003)
(top row: IVT 37; second: IVT 38; third: BioDur® 316LS base; bottom: ASTM F139)

Pt	Fe	Cr	Ni	Mo	Mn	Cu	Si	C	N	O
4.95	Balance	17.5	13.6	2.87	1.71	0.07	0.48	-	-	-
4.78	Balance	17.5	14.2	2.89	.096	0.08	0.47	0.027	0.056	0.04
-	Balance	17.6	14.8	2.81	1.80	0.09	0.45	0.018	0.025	0.01
-	Balance	17-19	13-15	2.25-3	2max	0.5max	0.75max	0.03max	0.1max	-

Second-generation alloys (VAR-produced ingots), nominally 6wt% platinum alloys that were subjected to both vacuum induction melting and vacuum arc remelting, are shown in Table 48 for ingot IVT 66 and in Table 49 for ingot IVT 78 and ingot IVT 79.

Table 48 Composition of ingot IVT 66
(top row: IVT 66; second: BioDur® 316LS base; bottom: ASTM F139)

Pt	Fe	Cr	Ni	Mo	Mn	Cu	Si	C	N	O
6.04	Balance	17.7	13.5	2.84	0.99	0.09	0.39	0.004	0.018	0.02
-	Balance	17.6	14.8	2.81	1.80	0.09	0.45	0.018	0.025	0.01
-	Balance	17-19	13-15	2.25-3	2max	0.5max	0.75max	0.03max	0.1max	-

Table 49 Composition of ingot IVT 78 and ingot IVT 79
(top row: IVT 78; second: IVT 79; third: BioDur® 316LS; bottom: ASTM F139)

Pt	Fe	Cr	Ni	Mo	Mn	Cu	Si	C	N	O
6.20	Balance	18.5	13.5	3.07	1.33	0.09	0.48	0.027	0.015	0.02
6.51	Balance	17.9	12.9	3.15	1.35	0.07	0.57	0.023	0.035	0.02
-	Balance	17.6	14.8	2.81	1.80	0.09	0.45	0.018	0.025	0.01
-	Balance	17-19	13-15	2.25-3	2max	0.5max	0.75max	0.03max	0.1max	-

Pitting resistance equivalent numbers for the above alloys are shown in Table 50.

Table 50 Pitting resistance equivalence number calculation for 5-6wt% platinum alloys
(top row: IVT 37, second: IVT 38; third: IVT 66; fourth: IVT 78; fifth: IVT 79; bottom: BioDur® 316LS)

Σ (17.5wt% Cr + 3.3 (2.9wt% Mo)	PREN = 27.1 (≥ 26 req. by ASTM F139)
Σ (17.5wt% Cr + 3.3 (2.9wt% Mo)	PREN = 27.1 (≥ 26 req. by ASTM F139)
Σ (18.0wt% Cr + 3.3 (2.9wt% Mo)	PREN = 27.6 (≥ 26 req. by ASTM F139)
Σ (18.2wt% Cr + 3.3 (2.9wt% Mo)	PREN = 27.8 (≥ 26 req. by ASTM F139)
Σ (18.5wt% Cr + 3.3 (3.1wt% Mo)	PREN = 28.7 (≥ 26 req. by ASTM F139)
Σ (17.6wt% Cr + 3.3 (2.8wt% Mo)	PREN = 26.8 (≥ 26 req. by ASTM F139)

As reported in Covino, Craig *et al* (2003), ingot IVT 37 and ingot IVT 38 were both tested in accordance with Practice E of ASTM A262, as required by ASTM F139-00. Practice E of ASTM A262 was intended to determine susceptibility to intergranular corrosion associated with the precipitation of chromium-rich carbides. The test according to this practice was comprised of (a) embedding the sample in copper granules and then being exposed for 24 hours to a boiling solution of 100g/L hydrated copper sulphate and 100 mL/L of concentrated sulphuric acid, and (b) bending the

exposed samples 180° over a mandrel with a diameter equal to the thickness of the samples and visually inspecting them for evidence of cracking at 20X magnification. Two plate samples from each heat were ground to a 120-grit finish; one of each heat was annealed at 1040°C and one of each heat was sensitised via a one-hour heat treatment at 675°C followed by air cooling. No evidence of cracking was found at 20X magnification in the annealed or the sensitised samples for either heat.

Tensile specimens were made in accordance with ASTM E8M-01 for sheet and plate specimens, Code F3; tensile tests were completed on a universal test machine in accordance with ASTM E8M-01 requirements. Figure 37 shows the stress-strain curve found in the longitudinal direction on ingot IVT 66 and on the BioDur® 316LS base, both annealed at 1050°C and water quenched.

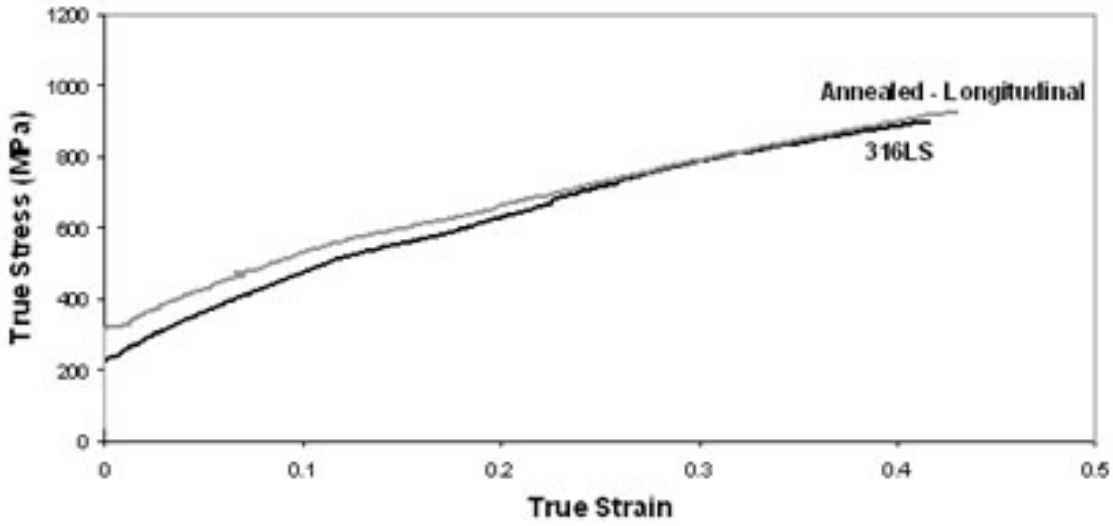

Figure 37 Stress-strain curve for ingot IVT 66 (annealed at 1050°C); and BioDur® 316LS base (annealed at 1050°C and water quenched)

Mechanical properties of ingot IVT 79, annealed at 1050°C and water quenched, were obtained in the same manner as ingot IVT 66 and are shown in Table 51.

Table 51 Mechanical properties for ingot IVT 79 cold-rolled and annealed at 1050°C

Requirement	ASTM F139-00	Experimental results
Ultimate tensile strength	490 MPa (min.)	629 ± 1 MPa
Yield strength (0.2% offset)	190 MPa (min.)	352 ± 19 MPa
Elongation	40% (min.)	67 ± 2%
Hardness	95 Rockwell B (max.)	88 Rockwell B

Metallurgical properties for ingot IVT 79 are shown in Table 52.

Table 52 Metallurgical properties for ingot IVT 79 cold-rolled and annealed at 1050°C

Requirement	ASTM F139-00	Experimental results
Grain Size (ASTM E112)	5 (min.)	10
Ferrite Content	None @ 100X	0.0%
Microcleanliness (ASTM E45**A**)**:**		
• Sulphides	1.5 (max.)/1.5 (max.)	0.0/0.0
• Alumina	1.5 (max.)/1.0 (max.)	0.0/0.0
• Silicates	1.5 (max.)/1.5 (max.)	0.5/0.0
• Globular oxides	1.5 (max.)/1.0 (max.)	0.5/0.0

4.5.4 Summary

The development of low-radiopacity alloys containing nominally 5-6wt% platinum by manufacturing processes comparable to those of commercial suppliers of implant-grade UNS S31673 alloys was undertaken.

For nominally 5-6wt% platinum alloys, the addition of platinum prohibited them from being considered as compliant alloys in accordance with ASTM F139-00. The alloys were initially produced by vacuum induction melting only and the production process was subsequently refined to include vacuum arc remelting.

The composition of the alloys was found to be well within specification limits, with the exception of added platinum, as shown for VIM-produced ingots IVT 37 and IVT 38 in Table 47 and for VAR-produced ingots IVT 65 (Table 46), IVT 66 (Table 48), and

ingots IVT 78 and IVT 79 (Table 49). These ingots all met the pitting corrosion resistance compositional requirements of ASTM F139-00, as shown in Table 50.

As described in Covino, Craig *et al* (2003), ingot IVT 37 and ingot IVT 38 were both subjected to and passed the intergranular stress corrosion cracking tests described in Practice E of ASTM A262.

Ingot IVT 79 was subjected to the mechanical and metallurgical tests of ASTM F139-00 and exhibited properties that were acceptable in accordance with the standard.

4.6 Conforming, high-radiopacity, induction-melted alloy

4.6.1 Introduction and approach

The ideal capstone experiment would have entailed preparing a VAR-produced 50kg ingot that was subject to and successfully completed all ASTM F139-00 requirements. The somewhat less-than-ideal experiment entailed remelting a VIM-produced 30wt% platinum alloy in a button furnace to add nickel, then subjecting that alloy (BSC 83A) to the full set of ASTM F139-00 requirements. Radiopacity experiments were not made.

4.6.2 Experiment

A nominally 30wt% platinum, VIM-produced ingot, BSC 83, was produced as described in §4.5.2, then a 200g ingot was prepared by adding nickel in a button furnace (§4.2.2) to produce BSC 83A, a compositionally compliant alloy in accordance with ASTM F139-00, again recognising that adding platinum invalidated full compliance with the standard. After hot-rolling and cold-rolling, the resulting sheet was annealed at 1100°C and water quenched.

4.6.3 ASTM F139-00 tests and results

Table 53 shows the chemical composition of BSC 83A, BioDur® 316LS, and ASTM F139-00 requirements; Table 54 shows the pitting resistance equivalent number calculated for BSC 83A and BioDur® 316LS.

Table 53 Composition of ingot BSC 83A, BioDur® 316LS, and ASTM F139-00
(top row: BSC 83A; middle: BioDur® 316LS; bottom: ASTM F139-00)

Pt	Fe	Cr	Ni	Mo	Mn	Cu	Si	C	N	O
29.3	33.27	18.4	14.1	3.06	1.28	0.17	0.51	0.030	0.12	-
-	Balance	17.6	14.8	2.81	1.80	0.09	0.45	0.018	0.025	0.01
-	Balance	17-19	13-15	2.25-3	2max	0.5max	0.75max	0.03max	0.1max	-

Table 54 Pitting resistance equivalent number for BSC 83A and BioDur® 316LS

Σ (18.4wt% Cr + 3.3 (3.1wt% Mo)	PREN = 28.6 (≥ 26 req. by ASTM F139)
Σ (17.6wt% Cr + 3.3 (2.8wt% Mo)	PREN = 26.8 (≥ 26 req. by ASTM F139)

Table 55 shows the results from conducting Practice E of ASTM A262 for intergranular corrosion susceptibility, as described in §4.5.3, while Figure 38 shows a typical surface condition after the corrosion susceptibility test.

Table 55 Intergranular corrosion susceptibility test results for BSC 83A
(annealing at 1100°C and annealing and sensitising at 650°C; water quench)

Condition	Mass loss (mg/cm2)	180° Bend Test
Annealed	0.00	No Cracks
Annealed and Sensitised at 650°C	0.16	No Cracks

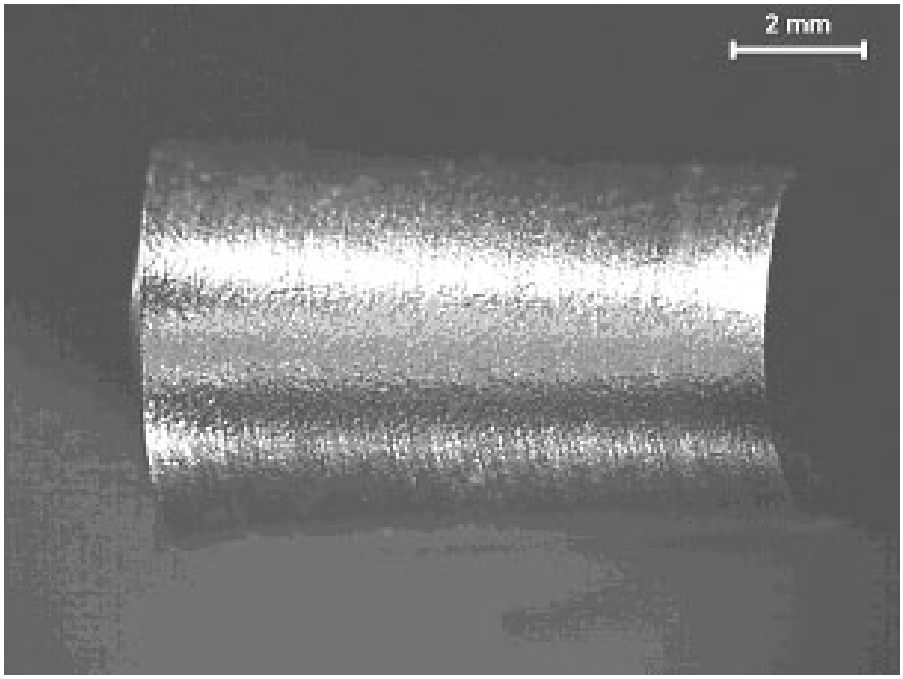

Figure 38 Typical surface of BSC 83A after corrosion susceptibility tests

Tensile specimens prepared as described in §4.5.3 were prepared from BSC 83A sheet, annealed at 1100°C and water quenched. The stress-strain curves for BSC 83A and BioDur® 316LS are shown in Figure 39. Mechanical property data for BSC 83A was determined and is shown in Table 56.

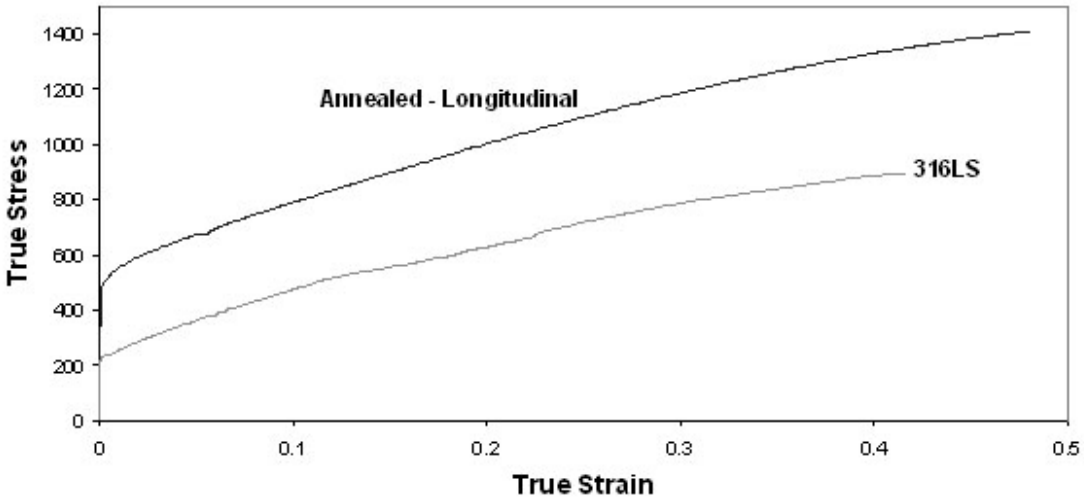

Figure 39 Stress-strain curves for BSC 83A and BioDur® 316LS

Table 56 Mechanical properties of ASTM F139-00 compared to BSC 83A (annealed at 1100°C and water quenched)

Requirement	ASTM F139-00 Limits	Annealed (Longitudinal)
Ultimate Tensile Strength	490 MPa (min.)	954 MPa
Yield Strength (0.2% offset)	190 MPa (min.)	499 MPa
Elongation	40% (min.)	46%
Hardness	95 Rockwell B (max.)	96 Rockwell B

Table 57 shows BSC 83A passed all metallurgical requirements of ASTM F139-00 in terms of grain size, ferrite content, and microcleanliness.

Table 57 Metallurgical properties of ASTM F139-00 compared to BSC 83A

Requirement	ASTM F139-00	Experimental results
Grain Size (ASTM E112)	5 (min.)	
Ferrite Content	None @ 100X	0.0%
Microcleanliness (ASTM E45) • Sulphides • Alumina • Silicates • Globular oxides	Thin/Heavy 1.5 (max.)/1.5 (max.) 1.5 (max.)/1.0 (max.) 1.5 (max.)/1.5 (max.) 1.5 (max.)/1.0 (max.)	Thin/Heavy 0.0/0.0 0.0/0.0 0.0/0.5 1.5/1.0

4.6.4 Additional tests not required by ASTM F139-00

The composition of the matrix of nominally 30wt% platinum ingot BSC 83A was obtained using both x-ray fluorescence and standardless energy dispersive x-ray spectroscopy (§4.4.3.1); the results are shown in Table 58. Figure 40 shows the energy dispersive spectroscopy spectra for the matrix of ingot BSC 83A.

Table 58 BSC 83A elements as determined for the matrix by x-ray fluorescence (XRF) and energy dispersive x-ray spectroscopy (EDS)

Element	Cr	Ni	Mo	Fe	Mn	Pt
	Specified					
ASTM F139 Minimum	17	13	2.25	~33	0.0	-
ASTM F139 Maximum	19	15	3	balance	2.0	-
BSC 83A base (XRF)	18.4	14.1	3.1	33.3	1.3	29.3
BSC 83A matrix (EDS)	16.6	14.1	2.6	33.6	1.2	32.1

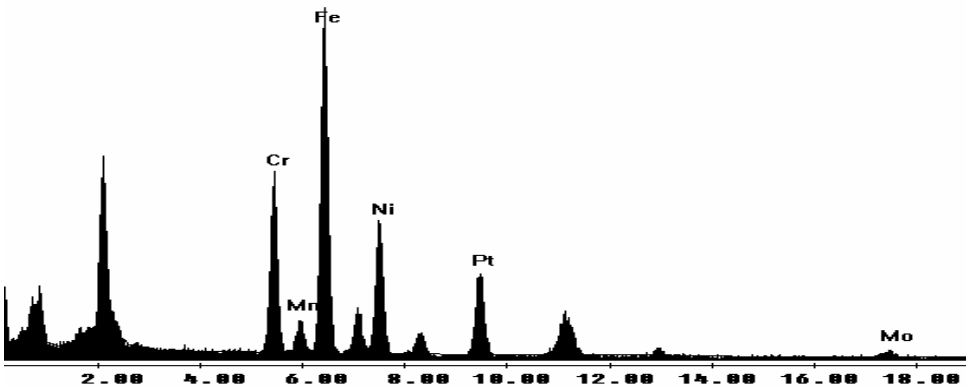

Figure 40 Energy dispersive spectroscopy spectra for ingot BSC 83A matrix

Only one type of precipitate was found in BSC 83A. Five different precipitates found in ingot BSC 83A were analysed with energy dispersive spectroscopy in order to get an average value for their compositions; the average value is shown in Table 59. Figure 41 shows a typical energy dispersive x-ray spectroscopy spectrum for BSC 83A.

Table 59 Average values of elements found in ingot BSC 83A precipitates

Element	Cr	Ni	Mo	Fe	Mn	Pt
BSC 83A precipitates (EDS)	39.2	2.6	2.1	6.5	0	49.7

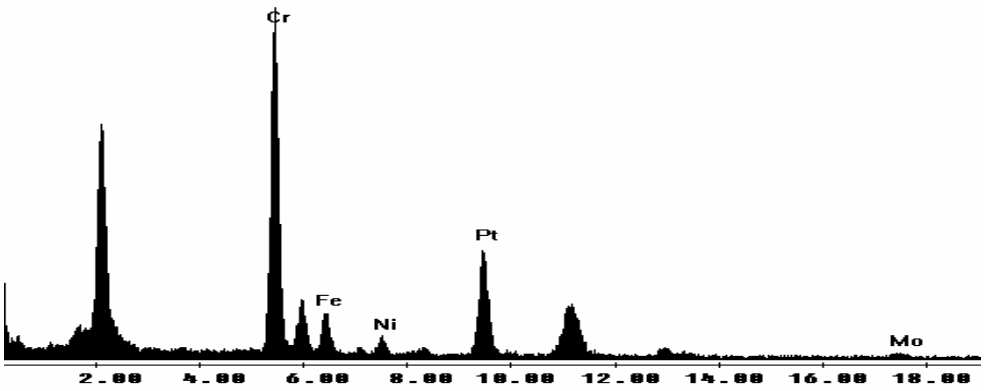

Figure 41 Energy dispersive x-ray spectroscopy spectra for ingot BSC 83A precipitates

4.6.5 Summary

A small compliant ingot containing nominally 30wt% platinum was subjected to the full range of tests required by ASTM F139-00. The alloy, with the exception of having added platinum, fully complied with all the requirements of the ASTM International standard that describes implant-grade UNS S31673 alloys. The only precipitates found in this alloy contained approximately 50wt% platinum and 40wt% chromium.

4.7 References

Attix, FA. (1986). *Introduction to radiological physics and radiation dosimetry*. Page 206. Chichester: John Wiley & Sons. ISBN: 0471011460

Covino, BS. Jr. (2003), Craig, CH., Cramer, SD., Bullard, SJ., Ziomek-Moroz, M., Jablonski, PD., Turner, PC., Radisch, HR., Jr., Gokcen, NA., Friend, CM., and Edwards, MR. Corrosion behaviour of platinum-enhanced radiopaque stainless steel (PERSS®) for dilation-balloon expandable coronary stents. In: Winters, G.L., and Nutt, M.J., *Stainless steels for medical and surgical applications*, *ASTM STP 1438*. Winters, GL., and Nutt, MJ. (eds). Pages 176-193. West Conshohocken, PA.: ASTM International. ISBN: 0803134592

Craig, CH. (2003), Friend, CM., Edwards, MR., Cornish, LA., and Gokcen, NA. Mechanical properties and microstructure of platinum-enhanced radiopaque stainless steel (PERSS®) alloys (JALCOM 9926). *Journal of Alloys and Compounds.* In press.

Dennis, JZ. (2003), Craig, CH., Radisch, HR., Jr., Pannek, EJ., Jr.,Turner, PC., Hicks, AG., Jenusaitis, M., Gokcen, NA., Friend, CM., and Edwards, MR. Processing platinum enhanced radiopaque stainless steels (PERSS®) for use as balloon-expandable coronary stents. In: Winters, G.L., and Nutt, M.J. (eds). *Stainless steels for medical*

and surgical applications, *ASTM STP 1438*. Pages 61-71. West Conshohocken, PA.: ASTM International

Eastman Kodak Company (2003). Sensitometric characteristics of X-ray films. *Radiography in modern industry (on-line version).* Rochester, NY: Eastman Kodak. http://wwwnl.kodak.com/US/en/government/industrial/ndt/literature/radiography

Hubbell, JH. (1997) and Seltzer, SM. *Tables of X-Ray Mass Attenuation Coefficients and Mass Energy-Absorption Coefficients* (version 1.03). Gaithersburg, MD: National Institute of Standards and Technology. URL: http://physics.nist.gov/xaamdi [Accessed 15 April 2003]

International Centre for Diffraction Data® (ICDD). (2000). *Powder Diffraction File.* Newtown Square, Pennsylvania. [http://www.icdd.com]

Seltzer, S. (2003). Private communication.

Chapter 5

DISCUSSION OF RESULTS

In this chapter, the results from the experimental chapters, both design (Chapter 3) and implementation (Chapter 4), will be discussed. In addressing these results, there is a need to revisit the source and context of the problem, the administrative and economic concerns, and the objectives that were established to point towards solutions.

To compete in a newly-emerged technological arena such as balloon-expandable coronary stents, a strategic advantage was required. Austenitic stainless steel was well-known as an engineering solution for this application. However, it had the second lowest radiopacity of any material being used, the nickel-titanium shape-memory alloy having the lowest. To maintain the advantages of having a non-composite material for an application that typically requires plastic deformation during deployment, it was determined that increasing the radiopacity of stents made from the alloy required addition of one or more compatible elements that would increase the radiopacity by the desired amount. Composite materials, whether fabricated by drawing, e.g., a cobalt alloy tube over a platinum wire, or coating the stainless steel struts of a stent with gold, may encounter problems based on differences in elastic modulus and/or yield strength between the two or more elements of the composite when it is plastically deformed. It was further determined that, initially, addition of a single, substitutional element solution would be pursued and the limit of radiopacity increase that could be achieved by such an addition would be governed by one principal constraint: that the resulting alloy would remain, under ASTM E527 (Unified National Standard) guidelines, steel. For this to be so, the iron content (in weight per cent) should be higher than the content

of any other single alloying element. In addition to merely remaining classifiable as steel, the resulting alloy would meet all requirements of an implant-grade austenitic stainless steel utilised internationally for such applications, with the sole exception of having an unspecified additional element. Minor differences between Composition D of ISO 5832-1 and its companion, BS 7252-1, and ASTM F138 and its companion, ASTM F139, did not detract from those goals.

To maximise radiopacity of the alloy within the constraints described meant that the specification chosen to adhere to, ASTM F139-00, had established boundary conditions that must be met, above and beyond the requirement for having iron as the principal element, as required by ASTM E527. Those requirements were that (a) the chromium content of the resulting alloy must be between 17wt% and 19wt%, (b) nickel content must be between 13wt% and 15wt%, and molybdenum content must be between 2.25wt% and 3wt%. With iron, these required elements formed a quaternary alloy; diminishing iron to its minimum and adding a single element meant to increase radiopacity of stents fabricated from the alloy created a pentanary alloy. The basis of the argument to stay within the context of ASTM F139-00 was that, based on experience with the largely government-led committees of ASTM International's F04 committee on medical devices and materials, changes to the documents would likely be accepted into practice if it could be shown that the criteria of acceptance had not changed upon addition of a single element not previously on the list of specified optional elements, e.g., manganese, copper, etc. In turn, the government agency (United States Food and Drug Administration) would likely be more convinced of the acceptability of allowing the previously unspecified additional element if the community it regulates had been involved throughout the proceedings required by

ASTM International for changing standards and, once the committee members had approved such an addition as both reasoned and safe, the change was balloted and approved by the entire voting membership. The alternative, developing a new stent alloy, was not considered achievable within the context of the emergent requirements.

With the framework established of a pentanary alloy, and restricting the choices to a non-allotropic d-block element, the candidate elements were determined to be tantalum, tungsten, rhenium, osmium, iridium, platinum, and gold.

Tantalum and tungsten were eliminated primarily because, as body-centred cubic elements, the fragile balance of the face-centred cubic 'austenite' structure required to minimise ferromagnetism was lost. The minimal size of the gamma loop in the binary with iron of both elements was used to predict this result. At 100keV, both elements had failed to predict radiopacity increases of 130% or more that of the quaternary alloy.

Gold also was found to exhibit a minimal peritectic and eutectoid reaction with iron, indicating low solubility in iron. Gold is known to exhibit high radiopacity when used, e.g., as radiopaque markers. At the typical stent strut thickness utilised, 0.127mm, gold exhibited sufficient radiopacity increases at both 80keV (164%) and 100keV (134%).

The hexagonal close packed elements rhenium and osmium, in a binary alloy with iron, exhibited large gamma phase fields that predicted sufficient solubility to allow a 130% increase in radiopacity at the two energy levels being utilised, 80keV and 100keV. The New PHACOMP modelling tool, however, eliminated these elements based on their Md(avg) exceeding Md(crit) at 1100˚C, i.e., a tendency to form σ phase.

Iridium, a face-centred cubic element, with an open field in its binary with iron, initially appeared suitable as a candidate fifth element in the pentanary, largely due to

its predicted radiopacity when used as a radiopaque stent. However, using New PHACOMP modelling, iridium exhibited a slight tendency to form σ phase.

Platinum, also a face-centred cubic element, was found to have an open field in its binary with iron, like iridium. Platinum, like gold and tantalum, has been used as a radiopaque marker on dilation balloons used to deploy balloon-expandable stents. Platinum has found wide application as an implant material, including use in a composite with a cobalt alloy for fabricating coronary stents. New PHACOMP modelling predicted platinum would fall well below the Md(crit) for σ phase (Table 14). At 32.5wt% platinum, the resulting pentanary at 80keV predicted a 167% increase in radiopacity for a 0.127mm thickness (Table 8), while at 100keV a 135% increase was predicted (Table 9). In addition, based on nickel equivalencies determined by Moema and Paton (2002), the Schaeffler diagram (Figure 13) predicted an increasingly stable austenite structure, contributing to the programme goal of minimising ferrite content.

Platinum was chosen as the candidate alloying element for subsequent experimental use. It was the only element that offered both increased austenite stability and sufficient radiopacity to meet programme goals.

Moving from the concept of a pentanary alloy to the concept of staying within the framework of the international specification limits, with the exception of adding platinum to increase the overall radiopacity of stents made from the revised alloy, a proof-of-concept experiment with alloys containing 0-5wt% platinum was carried out. This was followed by experiments that used low-radiopacity alloys containing 0-10wt% platinum. All these ingots were made in a button furnace. X-ray diffraction results for both the 0-5wt% platinum alloys and the 0-10wt% platinum alloys indicated that up to 10wt% platinum was easily accepted into solution and no new precipitates were formed.

Ferrite content was measured for the 0-10wt% platinum alloys and, in all except the base alloy, which had no added platinum, no ferrite was found, as had also been found to be the case when using x-ray diffraction. Optical microscopy showed some minimal amount of skeletal ferrite in the as-cast structure (Figure 21), as compared to the base alloy (Figure 20), which exhibited somewhat more skeletal ferrite. Annealed microstructures of both the base alloy and the 10wt% platinum alloy correlated well with both x-ray diffraction results and ferrite measurements of annealed specimens. In the lower-radiopacity alloys, it was found that both yield and ultimate tensile strength increased as platinum content increased; hardness in these alloys increased slightly and ductility decreased slightly (Table 25).

With the higher-radiopacity (0-35wt% platinum) button furnace alloys, the composition of the four types of precipitates that were found in these alloys was determined. Two of the precipitate types, described as Type A and Type B, were found in the UNS S31673 base alloy. Type A was only found in alloys containing up to 15wt% platinum and annealed at 915˚C; Type A precipitates had average chromium and iron contents of approximately 77wt% and 14%, respectively (Table 35). Type B was found in alloys containing up to 20wt% platinum; Type B precipitates were found in alloys subjected to a low-temperature (915˚C) anneal up to 15wt% platinum and also were found in alloys subjected to a high-temperature (1000˚C) anneal, up to 20wt% platinum. Type B precipitates, like the Type A precipitates, were determined to be principally chromium (average 83wt%) and iron (average 10wt%)(Table 36). In both precipitates, molybdenum was consistently present at approximately 5wt%. Beginning at 7.5wt%, a small amount of platinum was found, up to approximately 3wt%, in both

Type A and Type B precipitates. The principal features of Type A and Type B precipitates are shown in Table 60.

Table 60 Composition of precipitates found in base alloy

Type/Element	Chromium	Iron	Molybdenum
Type A	77wt%	14wt%	5wt%
Type B	83wt%	10wt%	5wt%

Type C precipitates were only found in the 25wt% platinum alloy. This precipitate was found at both the 915˚C and the 1100˚C anneals (Table 37). Platinum averaged 31wt% in Type C precipitates, followed by iron (30wt%), chromium (24wt%), nickel (7wt%), and molybdenum (5wt%); manganese occurred at the 915˚C anneal at approximately 1wt% but occurred at approximately 6wt% for the same alloy at the 1100˚C anneal. The principal features of Type C precipitates are shown in Table 61.

Table 61 Composition of Type C precipitates found only in 25wt% platinum alloy

Platinum	Iron	Chromium	Nickel	Molybdenum
31wt%	30wt%	24wt%	7wt%	5wt%
10at%	35at%	30at%	8at%	13at%

Type D precipitates first were found beginning in the 915˚C anneal of the 25wt% platinum alloy and in both heat treatments of the 30wt% and 35wt% platinum button melt furnace alloys (Table 33). Type D precipitates were also found in BSC 83A, a 30wt% platinum alloy containing 14wt% nickel; BSC 83A was made from an induction

furnace ingot (BSC 83) that did not have nickel added to the melt when it was melted in an induction furnace; nickel was later added in a button furnace to lower the Md(avg). BSC 83A was annealed at 1100˚C. In the 25wt% to 35wt% alloys (Table 38), platinum averaged 51wt%, followed by chromium (36wt%) and iron, which diminished from a high of 10.8wt% (25wt% platinum) to a low of 6.3wt% (35wt% platinum)(both with 915˚C anneal). Small amounts of nickel (up to 2.4wt%) and molybdenum (up to 3wt%) were also found in these precipitates. In ingot BSC 83A, the Type D precipitate contained 49.7wt% platinum (compared to an average of 51wt%, as above), followed by chromium at 39.2wt% (compared to an average of 36wt%), iron at 6.5wt% (compared to an average of 8wt%), with nickel and molybdenum contents at levels comparable with the non-conforming 25wt% to 35wt% platinum button melt alloys. The principal features of Type D precipitates are shown in Table 62.

Table 62 Composition of Type D precipitates found only in 25-35wt% platinum alloys

Type/Element	Platinum	Chromium	Iron
Non-conforming alloys 25wt% - 35wt%	~51wt% avg. (25at%)	~36wt% avg. (61at%)	~8wt% avg. (15at%)
Conforming alloy 30wt%	~50wt% (23at%)	~39wt% (63at%)	~7wt% (14at%)

The significance of these precipitates was not evaluated in the 0-35wt% platinum button melt alloys since those were being used to study radiopacity and to determine whether precipitates were present. However, the presence of both Type A and Type B

precipitates in the base alloy clearly indicated these precipitates were not the result of adding platinum. The presence of the Type C precipitate in only the 25wt% platinum alloy was of interest but there was no opportunity to make another button to determine whether this was an artefact of the processing route or was truly unique to this alloy.

The presence of the Type D precipitate in the conforming 30wt% platinum alloy, as well as the non-conforming 25-35wt% platinum alloys, is also of interest. In the 30wt% platinum conforming alloy, BSC 83A, hardness was just over the limit (96 versus 95 Rockwell B), elongation was near the minimum (46% versus 40%), and both ultimate tensile strength and yield strength were extremely high (Table 56), i.e., 955MPa versus 490Mpa minimum for ultimate and 499MPa versus 190MPa minimum for yield. The Type D precipitate did not appear to manifest itself as deleterious in this tensile test. Similarly, in the corrosion susceptibility tests, both annealed and sensitised, there was no apparent effect of these precipitates since the alloy passed both 180° bend tests. No annealing temperature greater than 1100°C was attempted to determine whether the precipitates would go into solution at greater annealing temperatures. Processing of the 30wt% platinum alloys was not considered a part of this research programme since this effort was taken over by a stent production organisation in anticipation of its use there; the 30wt% platinum alloys being investigated for production use are being made commercially at this writing, with plans to complete transmission electron microscopy and energy dispersive x-ray spectroscopy analysis of the ingot and the seamless tubing that is to be made from the ingot to determine whether Type D precipitates are present.

BSC 83A was subjected to and passed all tests required to comply with ASTM F139-00. The composition of the matrix and the calculated pitting resistance equivalent number were within specification, again with the exception of having an unspecified

added element, platinum (Table 53; Table 54). The intergranular corrosion susceptibility test was passed in both the annealed and sensitised conditions (Table 55), as noted above. Measured grain size and ferrite content in the annealed condition were acceptable, as were the inclusion contents of sulphides, aluminides, silicates, and globular oxides. Yield and ultimate tensile strengths, again as noted above, were found to be quite high and hardness was found to be slightly in excess of the maximum but within ASTM F139-00 tolerances; elongation was determined to be 46%, just above the minimum required of 40%.

By comparison with the above, low-radiopacity, conforming, pre-production alloys made in the vacuum induction furnace were subjected to the same series of F139-00 tests and, for ingot IVT 79, a nominally 6wt% alloy, yield and ultimate tensile strength were 352MPa and 629MPa, versus 499MPa and 954MPa, respectively, with BSC 83A. Hardness was 88HRB for IVT 79 versus 96HRB for BSC 83A; elongation for IVT 79 was 67% (Table 51). Grain size for ingot IVT 79, after pre-production hot- and cold-rolling, was ASTM E112 size 10 (fine). Ingot BSC 83A exhibited an ASTM E112 grain size of 5 (minimum). Ingot (button) BSC 83A was rolled in a small mill. The annealing temperature for ingot IVT 79 was 1050˚C and, for ingot BSC 83A, 1100˚C. These key parameters are summarised below in Table 63.

Table 63 Comparison of conforming alloys at 6wt% and 30wt% platinum

Alloy/Property	Hardness (Rockwell B)	Elongation	Ultimate tensile strength	Yield strength
BSC 83A (30wt%)	96	46%	954MPa	499MPa
IVT 79 (6wt%)	88	67%	629MPa	352MPa
ASTM F139	95 (max.)	40% (min.)	490MPa (min.)	190MPa (min.)

As noted above, radiopacity determination was primarily addressed through the 0-35wt% platinum button melt alloys (Table 40). Using x-ray diffraction data from Table 33, which closely parallels the design set in Table 31, excellent agreement was found between single energy radiopacities (Table 39 compared to 40). At 20wt% platinum, where only the Type B precipitates were found, the radiopacity increase at 80kV and 100kV over the base alloy was approximately 16% and 13.5%, respectively. At 30wt% platinum and 35wt% platinum, for an equivalent to a 32.5wt% platinum alloy, these increases averaged approximately 24% for both 80kV and 100kV. Thus for the maximum 32.5wt% platinum alloy that maintained the definition of these alloys as steel these lower values would be the maximum experimentally determined radiopacity increase, rather than the 64% and 34% increases that were found using narrow beam calculations for the pentanary alloy at those same energy levels. These data are summarised in Table 64.

Table 64 Radiopacity increases for 20wt% and (equivalent) 32.5wt% platinum alloys

Alloy / Radiopacity increase	80kV / 80keV (wide-beam / single-beam)	100kV / 100keV (wide-beam / single-beam)
20wt% platinum alloy	16% / 20%	14% / 11%
32.5wt% platinum alloy (avg 30 & 35wt% data)	24% / 42%	24% / 22%

As was shown in Table 45, summarised in Table 64 for the 20wt% platinum alloy and the average of the 30wt% and 35wt% platinum alloys, the increases in radiopacity for calculated (single-beam) versus experimental (wide-beam) were determined to be more dramatic for the 80keV versus 80kV than for the 100keV versus 100kV energies. Those differences are explained by noting that the single-beam calculations take into account the K-alpha of platinum, which is at 80keV, thus causing the calculated radiopacity at 80keV to be quite high and to increase with platinum content, as shown in Table 45. At 20wt% platinum, the increase in single-beam radiopacity over the base alloy is 19% and the experimental increase over the base alloy is 16%. At the averaged values of 30wt% platinum and 35wt% platinum, the equivalent 32.5wt% platinum alloy indicates a 42% increase over the base alloy for narrow beam radiopacity and only a 24% increase over the base alloy for wide-beam radiopacity. The explanation for this large differential lies, in addition to the greater weight percent platinum (at 32.5wt% versus 20wt%), in the hardened 80kV beam, which averages radiopacities both above and below the K-alpha into a single numeric value, which is substantially less than the peak found at the K-alpha. With the 100keV data, there is less of a difference between the single-beam and the wide-beam radiopacities because this energy is well above the peak found at the platinum K-alpha.

Chapter 6

CONCLUSIONS AND RECOMMENDATIONS

Conclusions

1. The New PHACOMP method, with its Md(avg) for individual alloys and with an experimentally determined Md(crit), provides a means to predict and to compare the propensity of alloys to develop deleterious phases (c.f., Table 32).
2. Schaeffler plots can be modified by adding nickel or chromium equivalents (e.g., 0.5 platinum for nickel) to predict ferromagnetic phases (c.f., Figure 13).
3. Radiopacities of alloy foil determined by single-beam calculations compare well with radiopacities of alloy foil determined experimentally by wide-beam methods when (a) the large difference in intensity between the two methods is recognised, and (b) ratios are used rather than absolute numbers (c.f., Table 8, Table 9 for single-beam calculations; c.f., Table 43, Table 44 for wide-beam).
4. Nordberg formulae for predicting strength are useful for zero platinum alloys but must be modified to be useful for alloys containing platinum (c.f., §3.4).
5. Alloys containing up to 35wt% platinum are shown from Schaeffler to be free from ferrite and martensite and this is confirmed experimentally (c.f., §4.4.3).
6. Alloys containing up to 20wt% platinum are shown from New PHACOMP to be free from precipitates which are not in the base alloy and this is confirmed experimentally (c.f., Table 32, §4.4.3).

7. Alloys containing greater than 20wt% platinum are shown from New PHACOMP to contain precipitates high in platinum and chromium that are not in the base alloy and this is confirmed experimentally (c.f., Table 32, §4.4.3).
8. Both a nominally 6wt% platinum induction melted alloy (IVT 79) and a nominally 30wt% platinum button furnace melted alloy (BSC 83A) passed all ASTM F139-00 tests, thus a 20wt% platinum induction furnace alloy subjected to these tests should pass all these tests, as well (c.f., §4.5.4, §4.6.5).
9. Increases in strength and hardness at the 20wt% platinum level are expected to be well above the base alloy but not as high as those found with the 30wt% platinum alloy (BSC 83A) that was subjected to and passed ASTM F139 tests.
10. The average experimentally determined increase in radiopacity for a 20wt% platinum alloy at 80kV and 100kV was 16% (the programme goal was 15%); the average experimentally determined increase in radiopacity for a 32.5wt% platinum alloy is expected to be 24% (less than programme goal of 30%).
11. Based on the above, a base alloy containing 20wt% platinum would provide sufficient radiopacity increase and should pass required ASTM F139-00 tests.

Recommendations for further work

1. Computational thermochemistry should be used, if an appropriate database containing platinum can be found or developed, to provide a phase diagram that brings out the precipitate compositions as well as the austenite solubility limits.
2. The source of the precipitate found beginning in the 25wt% platinum alloy and continuing through the 35wt% platinum alloy needs to be carefully analysed and characterised prior to adopting an alloy in this range for stent fabrication; the phase diagram obtained in (1) above should be used in such an analysis.
3. The source of the precipitate at 25wt% platinum needs to be determined; if this is determined to be an artefact or anomalous finding, it may be possible to increase platinum content somewhat higher than the 20wt% referred to above.